UNIVERSITY OF CALIFORNIA, BERKELEY
Department of Materials Sciences and Mineral Engineering

Final Report
to
U.S. Office of Naval Research
on

MICROMECHANISMS OF CYCLIC AND ENVIRONMENTALLY-ASSISTED SUBCRITICAL CRACK GROWTH IN CERAMIC-MATRIX COMPOSITES

Grant N00014-89-J-1094
for period 1 October 1988 to 30 September 1991

by
R. H. Dauskardt and R. O. Ritchie

November 1991

Report No. UCB/R/91/N1076

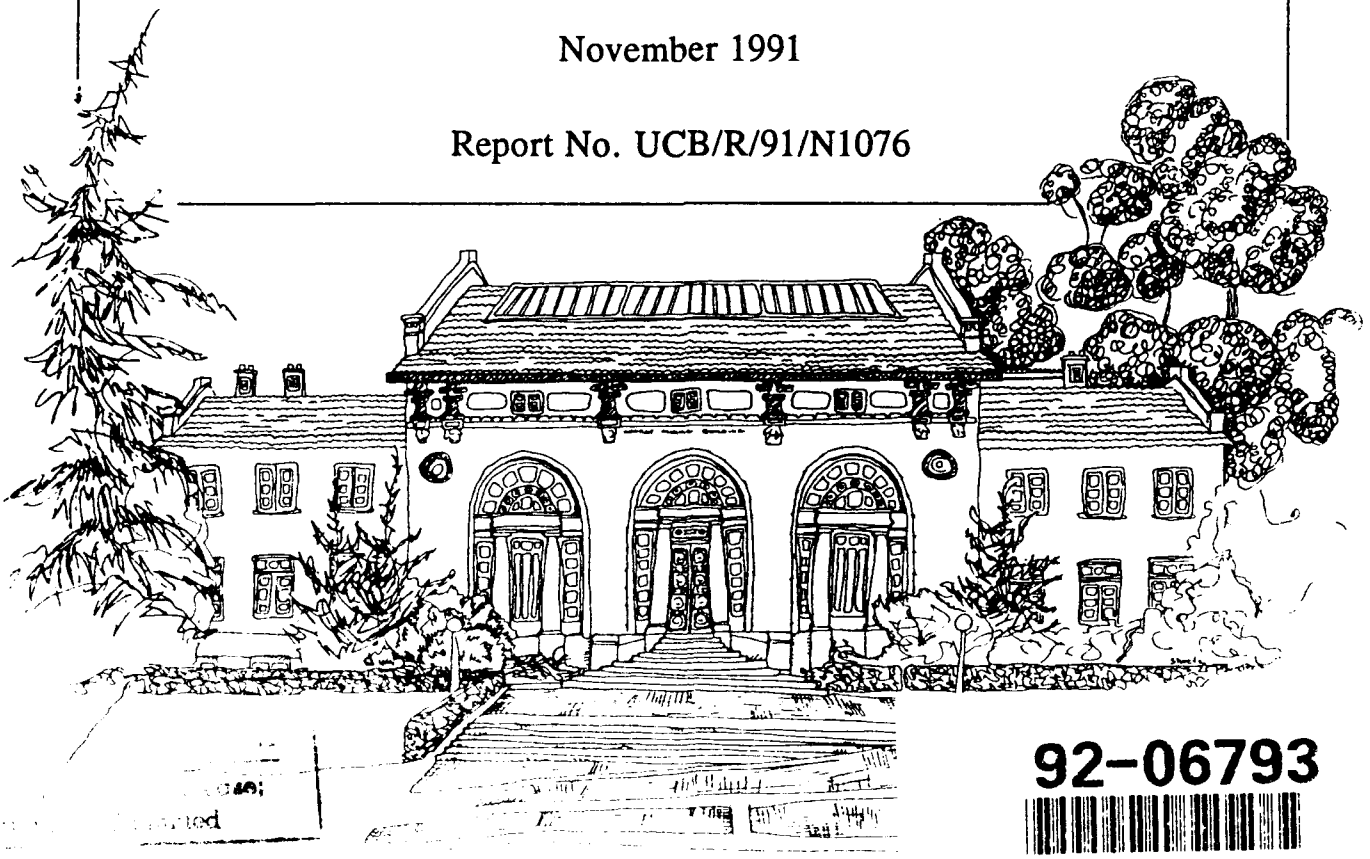

Hearst Mining Building, Berkeley, CA 94720

REPORT DOCUMENTATION PAGE

1a. REPORT SECURITY CLASSIFICATION Unclassified	1b. RESTRICTIVE MARKINGS None
2a. SECURITY CLASSIFICATION AUTHORITY Not Applicable	3. DISTRIBUTION / AVAILABILITY OF REPORT Not Applicable
2b. DECLASSIFICATION / DOWNGRADING SCHEDULE Not Applicable	
4. PERFORMING ORGANIZATION REPORT NUMBER(S) UCB/R/91/N1076	5. MONITORING ORGANIZATION REPORT NUMBER(S)
6a. NAME OF PERFORMING ORGANIZATION Robert O. Ritchie, Dept. of Mat. Sci. & Mineral Eng. 6b. OFFICE SYMBOL (If applicable)	7a. NAME OF MONITORING ORGANIZATION Office of Naval Research ONR
6c. ADDRESS (City, State, and ZIP Code) University of California Hearst Mining Building Berkeley, California 94720	7b. ADDRESS (City, State, and ZIP Code) 800 N. Quincy Street Arlington, VA 22217-5000 ATTN: Dr. S. G. Fishman
8a. NAME OF FUNDING / SPONSORING ORGANIZATION 8b. OFFICE SYMBOL (If applicable)	9. PROCUREMENT INSTRUMENT IDENTIFICATION NUMBER N00014-89-J-1094
8c. ADDRESS (City, State, and ZIP Code)	10. SOURCE OF FUNDING NUMBERS PROGRAM ELEMENT NO. / PROJECT NO. 431330 / TASK NO. A1 / WORK UNIT ACCESSION NO.

11. TITLE (Include Security Classification)
MICROMECHANISMS OF CYCLIC AND ENVIRONMENTALLY-ASSISTED SUBCRITICAL CRACK GROWTH IN CERAMIC-MATRIX COMPOSITES (Unclassified)

12. PERSONAL AUTHOR(S)
DAUSKARDT, R. H. and RITCHIE, R. O.

13a. TYPE OF REPORT	13b. TIME COVERED	14. DATE OF REPORT (Year, Month, Day)	15. PAGE COUNT
Final	FROM 88/10/1 TO 91/9/30	1991 November 1	105

16. SUPPLEMENTARY NOTATION

17. COSATI CODES			18 SUBJECT TERMS (Continue on reverse if necessary and identify by block number)
FIELD	GROUP	SUB-GROUP	Cyclic Fatigue; Fracture Toughness; Subcritical Crack Growth; Ceramic Matrix Composites; Small Cracks

19. ABSTRACT (Continue on reverse if necessary and identify by block number)

The future use of ceramics for advanced structural applications represents an important precursor to potential major improvements in design performance for high temperature, corrosion and wear resistance applications. The limited use of such brittle materials to date has primarily been attributed to their inherently low toughness and lack of defect tolerance. Scientific research in the last decade, however, has resulted in major advances in the toughening of ceramics by such mechanisms as whisker reinforcement, transformation and microcrack toughening. However, very recent work has shown that such toughened ceramics and composites, contrary to conventional wisdom, may become susceptible to cyclic fatigue.

...Continued

20 DISTRIBUTION / AVAILABILITY OF ABSTRACT ☒ UNCLASSIFIED/UNLIMITED ☐ SAME AS RPT ☐ DTIC USERS	21 ABSTRACT SECURITY CLASSIFICATION Unclassified
22a NAME OF RESPONSIBLE INDIVIDUAL Robert O. Ritchie	22b TELEPHONE (Include Area Code) (510) 642-0417 22c OFFICE SYMBOL

The intent of this program was to study and model the physics and fundamental micromechanisms of environmentally-assisted and principally cyclic fatigue crack-growth processes in several classes of ceramic-matrix composites, chosen to reflect different primary toughening mechanisms. Based on initial studies, the central hypothesis of this work is that the mechanisms of crack-tip shielding, used to enhance fracture toughness, can lead to degradation in crack-growth resistance under cyclic loading. By focusing on the microstructural aspects of the local failure processes, the approach will be to identify the mechanisms responsible for cyclic crack advance in each class of material in terms of their intrinsic and extrinsic components, to define and model the origin of such fatigue failure in terms of the characteristic microstructural features, to document the implications of such fatigue mechanisms to material behavior in general, and ultimately to utilize the models obtained to provide guidelines for the design of new composite ceramic microstructures with superior toughness and fatigue resistance.

This report is centered on characterizing fatigue-crack propagation behavior in Nicalon fiber-reinforced LAS glass ceramics and SiC reinforced-alumina ceramic composites, specifically with whisker reinforcement or uni- or bi-directional continuous fiber reinforcement. The approach is to characterize cyclic fatigue-crack growth behavior, specifically involving such factors as the role of load ratio, crack size, nature of the reinforcement, etc., in terms of the fundamental mechanisms of crack advance and crack-tip shielding.

Report No. UCB/R/91/N1076

Final Report
to
U.S. Office of Naval Research

on

MICROMECHANISMS OF CYCLIC AND ENVIRONMENTALLY-ASSISTED SUBCRITICAL CRACK GROWTH IN CERAMIC-MATRIX COMPOSITES

Grant No. N0014-89-J-1094

for period 1 October 1988 to 30 September 1991

submitted to

U.S. Office of Naval Research
800 N. Quincy Street
Arlington, VA 22217-5000
Attention: Dr. S. G. Fishman

submitted by

R. H. Dauskardt and R. O. Ritchie
Department of Materials Science and Mineral Engineering
University of California
Berkeley, California 94720

November 1991

TABLE OF CONTENTS

		Page
	FORWARD	iv
	ABSTRACT	v
1.	INTRODUCTION	1
2.	CYCLIC FATIGUE OF CERAMICS	6
3.	FATIGUE IN CONTINUOUS SiC FIBER REINFORCED Al_2O_3 COMPOSITES	48
4.	CYCLIC FATIGUE IN SiC-REINFORCED LAS GLASS-CERAMIC COMPOSITE	57
5.	CYCLIC FATIGUE IN SiC WHISKER-REINFORCED ALUMINA	72
6.	ACKNOWLEDGEMENTS	101
7.	PROGRAM ORGANIZATION AND PERSONNEL	101
8.	PUBLICATIONS	101

MICROMECHANISMS OF CYCLIC AND ENVIRONMENTALLY-ASSISTED SUBCRITICAL CRACK GROWTH IN CERAMIC-MATRIX COMPOSITES

R. H. Dauskardt, R. M. Petrany and R. O. Ritchie

(Grant No. N00014-89-J-1049)

FORWARD

This manuscript constitutes the Final Report on Grant No. N00014-89-J-1049, administered by the U.S. Office of Naval Research, with Dr. Steven G. Fishman as Program Manager. The work, covering the period October 1, 1988, through September 30, 1991, was performed under the direction of Dr. R. O. Ritchie, Professor of Materials Science, University of California at Berkeley, with Dr. R. H. Dauskardt as Research Engineer, R. M. Petrany as a graduate student research assistant, and F. J. Pennisi as an undergraduate engineering aide.

ABSTRACT

The future use of ceramics for advanced structural applications represents an important precursor to potential major improvements in design performance for high temperature, corrosion and wear resistance applications. The limited use of such brittle materials to date has primarily been attributed to their inherently low toughness and lack of defect tolerance. Scientific research in the last decade, however, has resulted in major advances in the toughening of ceramics by such mechanisms as whisker reinforcement, transformation and microcrack toughening. However, very recent work has shown that such toughened ceramics and composites, contrary to conventional wisdom, may become susceptible to cyclic fatigue.

The intent of this program was to study and model the physics and fundamental micromechanisms of environmentally-assisted and principally cyclic fatigue crack-growth processes in several classes of ceramic-matrix composites, chosen to reflect different primary toughening mechanisms. Based on initial studies, the central hypothesis of this work is that the mechanisms of crack-tip shielding, used to enhance fracture toughness, can lead to degradation in crack-growth resistance under cyclic loading. By focusing on the microstructural aspects of the local failure processes, the approach will be to identify the mechanisms responsible for cyclic crack advance in each class of material in terms of their intrinsic and extrinsic components, to define and model the origin of such fatigue failure in terms of the characteristic microstructural features, to document the implications of such fatigue mechanisms to material behavior in general, and ultimately to utilize the models obtained to provide guidelines for the design of new composite ceramic microstructures with superior toughness and fatigue resistance.

This report is centered on characterizing fatigue-crack propagation behavior in Nicalon fiber-reinforced LAS glass ceramics and SiC reinforced-alumina ceramic composites, specifically with whisker reinforcement or uni- or bi-directional continuous fiber reinforcement. The approach is to characterize cyclic fatigue-crack growth behavior, specifically involving such factors as the role of load ratio, crack size, nature of the reinforcement, etc., in terms of the fundamental mechanisms of crack advance and crack-tip shielding.

1. INTRODUCTION

The last decade has witnessed major improvements in the microstructural design and processing techniques of ceramics, which has provided a versatile class of materials offering exceptional properties in the areas of mechanical strength, extreme hardness and the creep resistance. In combination with other properties such as dimensional stability, corrosion and wear resistance, and retention of strength with time at temperature, recent advances in the development of enhanced toughness has resulted in the potential of ceramics to perform functions structurally not possible with other more traditional engineering materials. As a result, ambitious predictions have been made for the application of ceramics in numerous engineering markets where their low density and unique set of properties may be exploited.

Of particular interest in the aerospace and defense industries are reinforced ceramic-matrix composites for use in gas turbine and other advanced heat engine applications. Although the particular material property requirements for gas turbine and reciprocating engines differ, in both cases increased operating temperatures and faster rotational speeeds may provide impressive improvements in efficiency, power/weight ratios and fuel consumption. In gas turbine applications, blades, rotors, vanes, shrouds, combuster, combuster liners, and other parts are all candidates for ceramic materials. Here much effort has been directed towards the development of high performance reinforced ceramic-matrix composites capable of operating at higher temperatures and higher operating stresses [1,2]. While the high temperature properties have received most attention for heat-engine applications, these materials are also being developed for 'stationary' products such as heat exchangers, recuperators, tubes, exhaust systems and similar high-temperature operating equipment [3]. Conversely, requirements for reciprocating heat engines stress the need for thermally insulating and wear and abrasion resistant materials [4,5]. For example, in addition to hostile environmental conditions, the precombustion chamber in diesel engines must survive both mechanical and thermal stressing which is often cyclic in nature. Large temperature gradients are present and mechanical stresses may be exacerbated by thermal expansion mismatch between the chamber and cylinder-head materials [6]. Advantages of ceramic components include improved combustion performance due to higher running temperatures, reduction of idle noise, and easier starting.

Life prediction is naturally crucial to permit the reliable design and use of ceramic composite materials. Accordingly, extensive research has been undertaken to improve the toughness of ceramics which ultimately translates into improved reliability. In particular, extensive research has been undertaken in the development of materials toughened by the addition of dispersed zirconia particles, whisker/fiber reinforced ceramic-matrix composites, microcrack toughening, and more recently the addition of ductile particle dispersions [7,8]. In

most of the cases, the mode of toughening results in resistance-curve behavior where the fracture resistance increases with crack extension. A number of the more significant composite materials, together with their primary toughening mechanism and maximum toughness, are summarized in Table 1.1.

Table 1.1
Typical Reinforced Ceramic-Matrix Composite Materials Indicating Present Toughness and Toughening Mechanisms (from [8])

Material	Toughening Mechanism	Maximum Toughness
LAS/SiC	Fiber Reinforced	>20 MPa$\sqrt{m}$
Glass/C		>20
SiC/SiC		>20
Al_2O_3/SiC (20%)	Whisker Reinforced	10
Si_3N_4/SiC (20%)		14
Al_2O_3/Al (20%)	Ductile Dispersion	>12
B_4C/Al (20%)		>14
WC/Co (20%)		20

Despite the impact of the potential widespread use of ceramic-matrix composites in the aerospace and defense industries, it is perhaps surprising that relatively few systematic studies of a fundamental nature have been performed to relate mechanistically, and ultimately model, the role of the composite microstructure in controlling *subcritical* crack-growth resistance in these materials. This may be particularly important where crack propagation occurs under cyclic loading conditions. Indeed, it has long been the perception that ceramics do not suffer significant degradation by fatigue [9-11]. Accordingly, other mechanisms of subcritical crack growth, primarily involving environmentally-assisted cracking processes under sustained loading, have received far more attention [12-15]. Recently, however, there has been increased interest in possible mechanisms of cyclic crack propagation as viable modes of subcritical crack extension in brittle materials [16-22]. As most of the more significant applications of ceramics for components in gas turbine and reciprocating heat engine applications entail substantial cyclic loading and thermal shock conditions, a detailed characterization and more fundamental understanding of any fatigue processes must be considered essential.

The refuted existence of true cyclic crack-propagation effects in conventional monolithic ceramics has been based primarily on the very limited crack tip plasticity apparent in

these materials [9]. However, where local inelastic deformation normally associated with many of the toughening mechanisms previal, or where unloading induces additional fracture phenomena, the notion of fatigue in ceramics and more particularly, in reinforced ceramic-matrix composites, clearly becomes realistic. However, comparatively few mechanisms for tension-tension and tension-compression loading have been reported in the literature [9,16,20,21]. Experimental evidence for fatigue cracking in polycrystalline alumina has recently been reported under far-field cyclic compression loading [19,20]. In addition, the existence of cyclic mechanical fatigue effects has also been observed in a number of ceramics and reinforced ceramic composites tested in bending under tension-tension loading [23-29]. Based on these data, non-conservative estimates of subcritical crack extension and serious overestimates of life may result if damage-tolerant predictions are based solely on sustained-load cracking and toughness data.

Accordingly, the principal thesis of this study is to identify and characterize the salient micromechanisms of subcritical crack propagation processes in reinforced ceramic-matrix composites.

In this report, a review is presented first on the current literature on the cyclic fatigue behavior of ceramics and ceramic composite materials. The next section is focused on the behavior of the LAS/SiC_f glass ceramic system, which is principally toughened by fiber bridging across the crack; experiments were specifically centered on the role of microstructurally-small cracks on cyclic fatigue behavior in light of this bridging. It was found that such glass-ceramic composites do indeed suffer degradation from cyclic fatigue. In fact, fatigue-crack growth rates, over the range 10^{-6} to 10^{-11} m/cycle, for crack sizes of between 20 and 300 μm, were found to show a negative power-law dependency on the nominal (applied) maximum stress intensity, K_{max}, analogous to short-crack behavior in metals. Frictional-slip models of crack bridging by unbroken fibers in the crack wake were used to estimate a shielding stress intensity in the LAS/SiC_f system; by accounting for such shielding in the computation of an effective (near-tip) stress intensity, the expected positive power-law dependency of growth rates on stress intensity was obtained, with an exponent of over 50. In view of these results, we conclude that non-conservative estimates of the life of ceramic components are very possible from fracture-mechanics (da/dN vs. K) damage-tolerant predictions, due to the growth of short cracks below the fatigue threshold ΔK_{TH}.

Subsequent chapters deal with SiC reinforced alumina-matrix composites, reinforced either with SiC whiskers or bidirectional continuous Nicalon fibers, which again rely on crack bridging as a primary toughening mechanism. With the whisker reinforced composites, collaborative work with the Rockwell Science Center centered on a comparison of long and small-crack fatigue-crack growth results and in documenting the mechanistic role of crack

bridging in promoting the critical crack-size effect. In the continuous fiber reinforced composite, research was directed to a characterization of the effect of crack bridging during monotonic and cyclic crack growth.

1.1 References

1. A. Bennett, *Mater. Sci. Technol.*, **2** (1986) 891.
2. D. W. Richerson, *Am. Ceram. Soc. Bull.*, **64** (1985) 282.
3. L. M. Sheppard, *Adv. Mater. Pro.*, **1** (1985) 39.
4. D. A. Parker, *Mater. Sci. Technol.*, **9** (1986) 900.
5. M. E. Woods, W. F. Mandler and T. L. Scofield, *Am. Ceram. Soc. Bull.*, **64** (1985) 287.
6. L. M. Sheppard, *Adv. Mater. Pro.*, **2** (1986) 35.

   F. L. Riley, S. J. Milsom, *Mater. Sci. Technol.*, **9** (1986) 891.
8. A. G. Evans, pp. 267-91 in *Fracture Mechanics: Perspectives and Directions*, ASTM STP 1020, R. P. Wei and R. P. Gangloff, eds., American Society for Testing and Materials, Philadelphia, PA (1989).
9. A. G. Evans, *Int. J. Fract.*, **16** (1980) 485.
10. A. G. Evans and M. Linzer, *ibid.*, **12** (1976) 217.
11. A. G. Evans and E. R. Fuller, *Metall. Trans.*, **5** (1974) 27.
12. S. M. Wiederhorn, E. R. Fuller and R. Thomson, *Met. Sci.*, **14** (1980) 450.
13. Li-Shing Li and R. F. Pabst, *J. Mater. Sci.*, **15** (1980) 2861.
14. P. F. Becher, *J. Mater. Sci.*, **21** (1986) 297.
15. P. F. Becher, *J. Am. Ceram. Soc.*, **66** (1983) 485.
16. D. A. Krohn and D. P. H Hasselman, *J. Am. Ceram. Soc.*, **55** (1972) 208.
17. F. Guiu, *J. Mater. Sci.*, **13** (1978) 1357.
18. H. N. Ko, *J. Mater. Sci. Lett.*, **5** (1986) 464.
19. L. Ewart and S. Suresh, *ibid.*, **5** (1986) 774.
20. L. Ewart and S. Suresh, *J. Mater. Sci.*, **22** (1987) 1173.
21. R. W. Rice, *J. Phys. Chem. Solids*, **45** (1984) 1033.

22. L. S. Williams, Chapter 18 in *Mechanical Properties in Engineering Ceramics*, W. W. Kriegel and H. Palmour, III, eds., Interscience Publishers, Inc., New York (1961).

23. R. H. Dauskardt, W. Yu and R. O. Ritchie, *J. Am. Ceram. Soc.*, **70** (1987) C248.

24. M. J. Reece, F. Guiu and M. F. R. Sammul, *J. Am. Ceram. Soc.*, **72** (1989) 348.

25. R. H. Dauskardt and R. O. Ritchie, *Closed Loop*, **17** (1989) 7.

26. L. X. Han and S. Suresh, *J. Am. Ceram. Soc.*, **72** (1989) 1233.

27. R. O. Ritchie, R. H. Dauskardt, W. Yu and A. M. Brendzel, *J. Biomed. Mat. Res.*, **24** (1990) 189.

28. D. C. Cardona and C. J. Beevers, *Scripta Met.*, **23** (1989) 945.

29. S. Lathabai, Y.-W. Mai and B. R. Lawn, *J. Am. Ceram. Soc.*, **72** (1989) 1760.

2. CYCLIC FATIGUE OF CERAMICS: A FRACTURE MECHANICS APPROACH TO SUBCRITICAL CRACK GROWTH AND LIFE PREDICTION

(R. O. Ritchie and R. H. Dauskardt)

2.1 Introduction

The importance of mechanical degradation under cyclic fatigue loading in the design of metallic structures and components is characterized by either a classical stress/life (S/N) approach or using fracture mechanics concepts which incorporate the subcritical growth behavior of both "long" and "small" cracks (Fig. 2.1). Over the past few years, several studies have provided persuasive evidence of a similar susceptibility of ceramic and ceramic-matrix composite materials to cyclic fatigue. In fact, extensive data have now been reported indicating reduced lifetimes during S/N testing under cyclic, compared to sustained (quasi-static), loads, and accelerated cyclic crack-propagation rates at stress intensities less than required for environmentally-enhanced crack growth (static fatigue) during fracture-mechanics testing; results exist for zirconia [1-11], graphite [12], alumina [6,13-24], silicon nitride [16,25-29] and silica glass [30] ceramics and LAS/SiC_f [31] Al_2O_3/SiC [32-34] and laminated graphite/pyrolytic carbon [12] composites.

While the precise micro-mechanisms for such cyclic fatigue are still unclear, behavioral characteristics are in general *qualitatively* similar to those in metallic materials. For example, typical ambient-temperature stress/life data for alumina, TZP, silicon nitride and silicon carbide, taken from the four-point bend (zero-tension) data of Kawakubo *et al.* [6], are shown in Fig. 2.2. It is clear that for lives in excess of $\sim 10^3$ cycles, the time to failure under cyclic loads is less than that under quasi-static loads at the same maximum stress, and further, with the exception of SiC, the cyclic fatigue life is less than that predicted using the static data by integrating over the fatigue cycle. However, the inverse slope, n, of these curves is far higher than that found in metals; values range from 11 in TZP to 132 in SiC.

Alternatively, typical crack-propagation data (long crack), taken from the authors' own ambient-temperature studies [1,4,12,33] on compact-tension specimens, are shown in Fig. 2.3; these results illustrate the dependency of cyclic fatigue-crack growth rates, da/dN, on the applied (far-field) stress-intensity range ($\Delta K = K_{max} - K_{min}$), for three zirconia ceramics, graphite, a pyrolytic-carbon-coated graphite laminate and a SiC-whisker-reinforced alumina (Al_2O_3-SiC_w) composite, and are compared with similar data for steel and aluminum high-strength metallic alloys [35,36]. Similar to metals, the ceramic fatigue data follow a Paris power-law relationship [37] of the form:

$$da/dN = C(\Delta K)^m , \quad (1)$$

where C and m are scaling constants; the exponent, m, however, varies between 12 to over 40, which is far higher than the typical values of between 2 and 4 generally found for metals in this regime.

In addition to such crack-propagation data for "long" cracks (typically longer than ~3 mm), more recent results [7-10,16,26,29] on cracks which are physically small (typically smaller than ~500 μm) or approach the dimensions of the microstructure or local crack-tip inelasticity, have shown radically different growth behavior. Again, similar to behavior widely reported for metals [38], crack-propagation rates for such "small" surface cracks have been observed to far exceed those of "long" cracks at equivalent applied stress-intensity levels, and more importantly to occur at stress intensities *less than* the fatigue threshold, ΔK_{TH}, below which (long) cracks are presumed to be dormant [7-9].

Accordingly, the objective of this review is to survey current understanding of the cyclic fatigue behavior of monolithic and reinforced ceramics, with respect to stress/life and crack-propagation data under both constant and variable-amplitude loading. Long and microstructurally-small crack-growth behavior will be reviewed and possible micro-mechanisms advanced. Finally, the implications for fatigue life prediction and design criteria for ceramic components are discussed.

2.2 Testing Methods

2.2.1 Stress/life testing

In general, stress/life (S/N) cyclic fatigue tests on ceramic materials have been performed in similar fashion to the standard techniques used for metallic materials, although much greater care has been required in the design of the loading grips. Techniques include zero-tension and tension-tension testing in cantilever bend and three- and four-point bending [6,9,25], tension-compression testing in rotary bending [14,18], and uniaxial push-pull, and tension-torsion testing [27]. Typical stress/life results are shown in Fig. 2.2.

2.2.2 Constant-amplitude crack-propagation testing

Cyclic fatigue-crack propagation studies on through-thickness long cracks have been conducted on a variety of pre-cracked fracture mechanics samples; results have been reported for single-edge-notched specimens in three- and four-point bending, single- and double-anvil

configured specimens in bending, tapered double-cantilever beam specimens and compact-tension C(T) specimens. The system used by the current authors, illustrated in Fig. 2.4a, utilizes ~1 to 6 mm thick C(T) specimens which are cycled at various positive load ratios (R = ratio of minimum to maximum loads) at frequencies up to 50 Hz [1,4]. Following crack initiation from a wedge-shaped starter notch [1], crack-growth rates are determined over the range $\sim 10^{-12}$ to 10^{-4} m/cycle using computer-controlled K decreasing and K increasing conditions; applied loads are varied such that the instantaneous values of the crack length, a, and stress-intensity range, ΔK, vary according to the equation:

$$\Delta K = \Delta K_o \exp[C^*(a - a_o)] , \qquad (2)$$

where a_o and ΔK_o are the initial values of a and ΔK, and C^* is the normalized K gradient [(1/K)(dK/da)] set typically to ± 0.08 mm^{-1}. Linear elastic stress-intensity solutions for the various specimen geometries are given in standard handbooks [39].

As an alternative to optical crack-length measurements, electrical-resistance techniques, using ~0.1 μm NiCr films evaporated onto the specimen surface, can be employed to continuously monitor *in situ* the crack length to a resolution of within ± 5 μm [1,4]. In addition, unloading compliance measurements using back-face strain gauges have been utilized [4] to assess the extent of fatigue crack closure caused by premature contact of the crack surfaces during the loading cycle. This is achieved by defining a far-field stress intensity, K_{cl}, at first contact of the crack surfaces during the unloading cycle, i.e., at the highest load where the elastic unloading compliance deviates from linearity [36]. In metal fatigue, the value of the closure stress intensity is often used to compute an effective (near-tip) crack-driving force given by the difference of the maximum stress intensity and K_{cl}, i.e., $\Delta K_{eff} = K_{max} - K_{cl}$ (where $K_{cl} > K_{min}$).

Corresponding fatigue-crack propagation data for small (<250 μm) surface cracks has generally been determined through replication or optical examination of the top surface of cantilever-beam specimens loaded in tension-compression (Fig. 2.4b); depending upon the ease of crack initiation, such specimens are either unnotched or contain stress concentrators such as micro-hardness indents or a notch. Ideally tests are interrupted after ~100 cycles to ascertain damage accumulation during initial loading and then subsequently at 10^2 to 10^3 cycle intervals until failure [8]. Small-crack lengths can be readily quantified, with a resolution better than ± 0.5 μm by digitizing optical micrographs of the specimen surface using an image analyzer, in order to compute growth rates between $\sim 10^{-12}$ to 10^{-6} m/cycle. Stress-intensity factors for such surface cracks can be obtained from linear elastic solutions [40] for three-dimensional semi-elliptical surface cracks in bending (and/or tension) (Fig. 2.2b) in terms of crack depth a, crack

length c, elliptical parametric angle ϕ, shape factor Q, specimen width t, specimen thickness B, and remote (outer surface) bending stress, σ_b:

$$K = H_c \sigma_b (\pi a/Q)^{1/2} F(a/c, a/t, c/B, \phi), \quad (3)$$

where H_c is the bending multiplier and F is a boundary correction factor (Fig. 2.4b).

2.2.3 Variable-amplitude crack-propagation testing

Limited results have also been reported by the authors for cyclic fatigue-crack propagation behavior in ceramic materials during variable-amplitude loading sequences [5,33]. Such tests have been performed on long cracks, specifically in transformation-toughened Mg-PSZ and a SiC-whisker-reinforced alumina, by applying various load excursions during steady-state fatigue-crack growth, and monitoring the transient crack-growth response as a function of crack extension until steady-state growth is re-established. The principal loading spectra that have been used include single tensile overloads and block-loading sequences (both low-high and high-low), comprising selected constant stress-intensity ranges. In addition, growth rates have been examined under constant K_{max}/variable-R conditions, where the maximum stress intensity is held constant as K_{min} is increased; such loading spectra have been used in metal fatigue studies to minimize the influence of crack closure on growth-rate behavior [41].

2.3 Stress-Life Behavior

As noted above, cyclic stress/life (S/N) data for most ceramic materials at ambient temperatures show lifetimes to be less than that to cause failure at the same maximum stress under quasi-static loads, and to be less than that predicted from the static stress/life data assuming only time-dependent (and not cycle-dependent) processes [6,25]. As in metals, the fatigue strength decreases with number of cycles, although the dependence of life on applied stress, i.e., the inverse slope, n, of the S/N curve is far higher; typical values are listed in Table 2.1. In addition, S/N curves appear to be much more sensitive to the load ratio than with metallic materials [10].

S/N curves on *unnotched* cantilever-beam samples of mid-toughness (MS grade) and overaged (pre-transformed) Mg-PSZ, under both zero-tension (R = 0) and tension-compression (R = -1) loading, are shown in Fig. 2.5 [7,8]; corresponding data from Swain *et al.* [2] for MS-grade Mg-PSZ, tested in four-point bend (R = 0) and rotating bend (R = -1), are included for comparison. It is apparent that, similar to behavior in steels, the MS-grade material shows

evidence of a "fatigue limit" of roughly 50% of the single-cycle tensile (or bending) strength, at 10^8 cycles (R = -1). However, not all ceramics have such a distinct knee in the S/N curve above 10^6 cycles; sintered alumina, for example, can fail at lives in excess of 10^8 cycles, with a 10^8-cycle endurance strength some 25 to 40% of the single-cycle strength [18].

Similar to results reported for Si_3N_4 [25,27], the Mg-PSZ data in Fig. 2.5 also indicate that cycling in tension-compression is significantly more damaging than in tension. This is apparent from optical examination [8] of specimen surfaces in MS-grade material at both R-ratios, where quantitative analysis of the crack-size distributions reveals an increased distribution of larger microcracks at R = -1 (Fig. 2.6). Microcracks appear in regions of surface uplift from transformation and their alignment is primarily orthogonal to the stress axis, although some cracks form at angles of $\sim 45°$ to the stress axis at R = -1.

This effect, however, is not general to ceramic fatigue. Unlike results on smooth samples [7,8,26], S/N data derived from results on *micro-indented* cantilever-bend specimens, of a SiC-whisker-reinforced alumina [33], show no such difference between tension-compression and tension-tension cycling (Table 2.2). This may be because fully reversed cyclic loading has a greater effect on *initiating* fatigue damage in the form of microcracks, which in unnotched samples can account for a significant proportion of the life. In fact, it is known that where defects pre-exist (as micro-indents), lifetimes in tension and tension-compression are comparable as *crack-growth rates* are similar (Fig. 2.7) [33].

2.4 Fatigue-Crack Propagation Behavior

2.4.1 Long-crack behavior

The variation in cyclic fatigue-crack propagation rates with the applied stress-intensity range, shown in Fig. 2.1 for long cracks in an range of ceramic materials, illustrates the extremely high dependency of da/dN on ΔK. Similar results are apparent for several transformation-toughened (sub-eutectoid aged) and pre-transformed (overaged) microstructures in Mg-PSZ [4] (Fig. 2.8a), SiC-whisker-reinforced alumina (Fig. 2.9) [33], silicon nitride [29], silica glass [30], and a pyrolytic-carbon coated graphite laminate [12] (Fig. 2.10). As noted above, these data in general conform to a power-law relationship (Eq. 1) over the mid-range of growth rates, with very high exponents (i.e., the slope m of the da/dN vs. ΔK curve). Values of m, listed for several ceramics in Table 2.2, can vary between ~ 10 and over 100; the constant C, on the other hand, appears to scale inversely with the fracture toughness K_c. Fatigue threshold ΔK_{TH} values may be defined at a maximum growth rate of $\sim 10^{-10}$ m/cycle since the

da/dN(ΔK) curves do not always show a sigmoidal shape; these values are typically of the order of 50% of K_c.

In view of past skepticism over the fatigue of ceramics, experiments have been performed to demonstrate unequivocally that crack growth in these instances is cyclically induced and not simply a consequence of stress-corrosion cracking (static fatigue) [4,12]. To achieve this, crack extension has been monitored at constant K_{max} with varying K_{min}, as shown for a pyrolytic-carbon/graphite laminate in Fig. 2.11. It is apparent that, whereas crack extension proceeds readily under cyclic loading conditions (region a), upon removal of the cyclic component by holding at the same K_{max} (region b), crack-growth rates are markedly reduced. Aside from establishing that the crack-growth behavior is a true cyclic fatigue phenomenon, this result illustrates that subcritical crack-growth rates due to cyclic fatigue are far in excess of those due to static fatigue at the same K_{max} [1].

In certain experiments, crack closure has been observed during fatigue-crack growth in ceramics; results are shown in Fig. 2.12 for four microstructures in Mg-PSZ with increasing degrees of transformation toughening [4]. Data are plotted in terms of the far-field closure stress intensity, K_{cl}, normalized by K_{max}, as a function of the applied ΔK. K_{cl} values are measured globally at first contact of the fracture surfaces during the unloading cycle; specifically, values of K_{cl} are calculated from the highest load at which the elastic unloading compliance line deviates from linearity [4]. In metals, such closure primarily results from premature contact between the crack surfaces by fracture-surface asperities, and can have a potent influence in *locally* affecting the "crack-driving force" [42,43]. The degree of closure in ceramics, however, appears to be smaller, and in materials like Mg-PSZ is dwarfed by other mechanisms of crack-tip shielding such as transformation toughening [4]. In fact, resistance to cyclic fatigue-crack extension in Mg-PSZ is observed to increase directly with the degree of crack-tip shielding resulting from increased transformation toughening (Fig. 2.8a). Such crack-growth data can therefore be normalized to a single curve (Fig. 2.8b) by characterizing in terms of the near-tip stress-intensity range, ΔK_{tip}, which allows for the extent of shielding, as outlined below [4].

In Mg-PSZ, the tetragonal phase, which typically consists of approximately 40 vol% of lens-shaped precipitates of maximum size ~300 nm, can undergo a stress-induced martensitic transformation to a monoclinic phase in the high stress field near the crack tip. The resultant dilatant transformation zone in the wake of the crack exerts compressive tractions on the crack surfaces which shield the crack tip from the applied (far-field) stresses [44-46]. The crack-tip stress intensity, K_{tip}, is therefore reduced from the applied (far-field) K by a shielding stress intensity, K_s, which is dependent upon the volume fraction, f, of the transforming phase within the zone, the width of the zone w, and the dilatational component of the transformation strain

ϵ^T, Young's modulus E, Poisson's ratio ν, and a constant A dependent on the frontal zone shape [47,48]:

$$K_{tip} = K - K_s \ , \tag{4}$$

$$K_s = A\,(E/1 - \nu^2)\epsilon^T f w^{1/2} \ . \tag{5}$$

Under cyclic loading, shielding from transformation far exceeds that due to crack closure; accordingly, the *local* near-tip stress-intensity range can be expressed by [4]:

$$\Delta K_{tip} = K_{max} - K_s \ , \tag{6}$$

By computing K_s using the integrated form of Eq. 5 and Raman spectroscopy measurements of the transformation-zone size [4,5,49,50], growth rates can be characterized in terms of ΔK_{tip}, thereby accounting for the differing fatigue resistance of the four microstructures (Fig. 2.8b). An equivalent result can be achieved by normalizing the crack-growth data in terms of $\Delta K/K_c$ [4].

Fractographically, little discernible difference is generally apparent between monotonic and fatigue fracture surfaces in ceramics; this is in marked contrast to metals where clear distinction is generally observed between striation growth under cyclic loads and microvoid coalescence or cleavage, for instance, under quasi-static loads [35]. Fatigue and fracture surfaces in silicon carbide, graphite, pyrolytic carbon, and Mg-PSZ are essentially identical [4,51]; in Mg-PSZ, for example, surfaces are primarily transgranular with crack paths showing evidence of crack deflection, branching, and uncracked-ligament bridging behind the crack tip. In certain ceramics, however, the fractography of the resulting cyclic and monotonic fracture surfaces do show some distinction. An example of this is Al_2O_3-SiC_w [33]. Fatigue fracture surfaces appear to be more textured and rougher with a higher degree of SiC whisker pull out than monotonic fracture surfaces. At higher magnification, crack paths formed under monotonic loading can be seen to be predominantly transgranular, with a high incidence of cleavage steps (indicated by arrows on the micrograph) and a flatter appearance (Fig. 2.13a,b). The increased roughness of the fatigue surfaces, conversely, appears to be associated with an increasing degree of intergranular fracture (Fig. 2.13c,d).

2.4.2 Small-crack behavior

The question of small cracks is undoubtedly of special importance to ceramics simply because the majority of ceramic components in service will not be able to tolerate the presence

of physically long cracks. In metal fatigue, it is known that where crack sizes approach the dimensions of the microstructure or the extent of local crack-tip plasticity, or where cracks are simply physically small (typically $\lesssim$250 μm), the similitude of crack-tip field characterization can break down (see, for example ref. 38). Specifically, small-crack growth rates are often far in excess of those of corresponding long cracks at the same applied ΔK levels; moreover, small-crack growth can occur at stress intensities well below the (long-crack) threshold ΔK_{TH}. Although such apparently anomalous behavior can be attributed to a number of factors [38], the primary reason is that the extent of crack-tip shielding (in metals, principally from crack-closure phenomena) is generally diminished in small flaws by virtue of their limited wake [36]. In fact, a more precise definition of a small crack is one whose length is small relative to the size of the shielding zone. Since crack-tip shielding, from phase transformation, microcracking, crack bridging etc., plays a pivotal role in the toughening of many monolithic and composite ceramics, it is to be expected that such small-crack effects may also be prevalent in ceramic fatigue behavior.

Results on small fatigue cracks in ceramics, however, are very limited [7-10,29,33]. Typical crack-growth data for Mg-PSZ, monitored from unnotched cantilever-beam S/N samples and characterized in terms of the applied K_{max}, are compared to corresponding long-cracks data in Fig. 2.14a [7,8]. In sharp contrast to long-crack results, the small cracks grow at progressively decreasing growth rates with increase in size, until finally linking together as the density of cracks across the specimen surface increases; the specimen then fails. Small-crack propagation rates display a negative, non-unique dependency on stress intensity and occur at applied stress-intensity levels well below ΔK_{TH} (specifically at K_{max} levels of 1.6 MPa$\sqrt{m}$, *a factor of seven less than* K_c). Moreover, growth rates are clearly not a unique function of K_{max} and appear to be sensitive to the level of applied stress.

Similar behavior has been reported for ceramic composites [33]. The crack lengths of selected microcracks at similar maximum applied stress levels, emanating from micro-indents in cantilever-beam samples of SiC-whisker-reinforced alumina, are compared as a function of number of cycles at R = 0.05 and -1 in Fig. 2.15. As in monolithic ceramics, the small cracks grow at progressively decreasing growth rates, i.e., when plotted as propagation rates as a function of the applied K_{max} (Fig. 2.9), the crack-growth rate data display a characteristic negative dependency on applied stress intensity.

Such sub-threshold small-crack growth behavior can be explained by analogy to small-crack behavior in metals (e.g., refs. 36,38). Although the nominal (far-field) stress intensity K increases with increase in crack size, the shielding stress intensity K_s is also enhanced as a shielding zone is developed in the crack wake. The near-tip stress intensity (Eq. 6) and hence the crack-growth behavior is thus a result of the mutual competition between these two factors;

initially K_{tip} is diminished with crack extension until a steady-state shielding zone is established, whereupon behavior approaches that of a long crack. In Mg-PSZ, the primary shielding is due to phase transformation, whereas in the Al_2O_3/SiC_w composite, it is presumed to result from crack bridging by unbroken whiskers in the crack wake [33], and from the residual stress field surrounding the micro-indent.

With a detailed knowledge and quantitative modelling of the salient shielding mechanisms, it is possible to normalize long and small crack data by characterizing in terms of the near-tip or net stress intensity, K_{tip}, i.e., after subtracting out the stress intensity due to shielding. Computations of K_s and hence K_{tip} have been achieved for small fatigue cracks in a SiC-fiber-reinforced LAS glass-ceramic, where the predominant shielding resulted from fiber bridging [31], and in Al_2O_3, Si_3N_4 and 3Y-TZP where the effect of the residual stress field associated with the crack-initiating micro-indents was taken into account [10,16,26]. This is illustrated in Fig. 2.16 where small and long crack data in 3Y-TZP are normalized by defining K_{tip} in terms of a superposition of the applied and residual stress fields [10]. In addition, long-crack data in Mg-PSZ has been characterized in terms of K_{tip} in Fig. 2.14b after correcting for transformation shielding [8]; it is apparent that the da/dN ($K_{tip,max}$) curve corresponds closely to that associated with the initial growth of the small cracks. However, whether such analytical procedures to normalize small and long crack data are practical on a regular engineering basis for all ceramic materials in service is clearly questionable.

2.4.3 Variable-amplitude loading

In addition to the cyclic fatigue of ceramics under constant-amplitude loading data described above, limited studies have been performed to examine crack-propagation behavior under variable-amplitude loading. These studies have been focused on the transient crack-growth response to single tensile overload, block loading and constant-K_{max}/variable-R (increasing K_{min}) sequences during steady-state fatigue-crack growth, specifically in MS-grade Mg-PSZ [5] and a SiC-whisker-reinforced Al_2O_3 composite [33].

Behavior in Mg-PSZ, shown for MS- and TS-grades in Fig. 2.17 [5], is similar to that widely reported in metals (e.g., ref. 52). In Fig. 2.17a, a high-low block overload, from a ΔK of 5.48 to 5.30 MPa$\sqrt{m}$, is first applied to an MS-grade sample; on reducing the cyclic loads, an immediate transient retardation is seen followed by a gradual increase in growth rates until the (new) steady-state velocity is achieved. Similarly, by subsequently increasing the cyclic loads so that ΔK = 5.60 MPa$\sqrt{m}$ (low-high block overload), growth rates show a transient acceleration before decaying to the steady-state velocity. The increment of crack growth over which the transient behavior occurs is ~700 μm, approximately five times the measured [5,49]

transformed-zone width of ~150 μm. This is consistent with zone-shielding calculations which compute the maximum steady-state shielding to be achieved after crack extensions of approximately five times the zone width [47,48]. In fact, relatively accurate predictions of the post load-change transient crack-growth behavior have been obtained (dotted line in Fig. 2.17a) by computing the extent of crack-tip shielding in the changing transformation zone following the load changes [5]. The changing size of the crack-tip transformation zone can be readily mapped using spatially-resolved Raman spectroscopy techniques [49]. For example, zone sizes for the block-loading sequence on TS-grade material shown in Fig. 2.17b are illustrated in Fig. 2.18 [5]. In general, the significant variation in growth rates with small changes in ΔK is consistent with the steep slope of the da/dN-ΔK curves (Eq. 1) found in ceramics.

In contrast, variable-amplitude loading in the Al_2O_3-SiC_w composite is quite different (Fig. 2.19) [33]. Over the first ~1.2 mm of crack advance, the crack-growth rate remains approximately constant at a baseline ΔK of 3.6 MPa$\sqrt{m}$. On reducing the cyclic loads so that ΔK = 3.2 MPa$\sqrt{m}$ (high-low block overload), crack-growth rates decrease by a ~1.5 orders of magnitude; by subsequently increasing the cyclic loads to a ΔK of 3.6 MPa$\sqrt{m}$ (low-high block overload), growth rates increase to previous baseline levels. Unlike Mg-PSZ where marked transient growth-rate effects result from transformation-zone shielding, the Al_2O_3-SiC_w composite, which is presumed to undergo crack bridging by intact whiskers spanning the crack, does not show such transient behavior; the scatter in growth rates, however, is large.

The precise role of variable-amplitude loading on cyclic crack growth in the various ceramic systems is still uncertain. It is known that in metals and phase-transforming ceramics, an overload cycle creates an enlarged crack-tip plastic or transformation zone which then promotes crack-growth retardation by reducing the near-tip stress intensity by residual compressive stress and resulting crack-closure effects in metals or by transformation shielding in the ceramics [5,52]. However, in the non-transforming ceramics, such as Al_2O_3/SiC_w which may rely on shielding by crack bridging, the overload cycle may enhance shielding by increasing the extent of the bridging zone in the crack wake, or conversely diminish shielding by causing the failure of more bridges. Resolution of this effect must await more detailed bridging calculations and experimental measurements of the bridging-zone sizes following various loading sequences.

2.4.4 High temperature fatigue

Despite the anticipated high-temperature use of ceramics in service applications, studies on the cyclic fatigue of monolithic and composite ceramics at elevated temperatures are extremely limited [2,11,22,32,34,53]. However, studies on the S/N behavior of MS- and TS-

grade Mg-PSZ using 100 Hz rotational flexture (R = -1) tests at moderately high temperatures up to 400°C in air clearly show a progressive decrease in fatigue resistance with increase in temperature, concurrent with a general increase in the inverse slope, e.g., the exponent, n, varies from 34 at 20°C to 116 at 200°C in TS-grade material [2]. Resistance to cyclic fatigue-crack propagation rates is similarly diminished in Mg-PSZ at these temperatures; in TS-grade material, ΔK_{TH} thresholds have been reported to drop from 3.5 MPa$\sqrt{m}$ at 20°C to 3.0 MPa$\sqrt{m}$ at 650°C, with the exponent, m, increasing from 25 to 70 over the same temperature range [11].

At high homologous temperatures in the creep regime, however, cyclic fatigue mechanisms in ceramics do not appear to be as damaging as static fatigue or creep mechanisms. For example, S/N uniaxial tensile fatigue studies on alumina at 1200°C reveal the lives of samples loaded in cyclic fatigue (R = 0.1) in general to exceed those loaded quasi-statically at the same maximum stress (Fig. 2.20) [22]. Cyclic fatigue lifetimes were found to be dependent upon the frequency and cyclic waveform, specifically to the duration of the application of the maximum stress. In fact, assuming only time- (and not cycle-) dependent processes, cyclic lifetimes predicted from the static fatigue data were in general less than measured lifetimes, in sharp contrast to behavior at ambient temperatures (Fig. 2.2a). Similar results have been reported for hot pressed Si_3N_4 at 1200°C [53]. Corroborating evidence from crack-propagation studies in alumina at 1050°C and SiC-whisker-reinforced alumina at 1400°C (frequency = 2 Hz, R ~ 0.1) show the cyclic crack-growth rates to be less than those measured under static loading at the same applied maximum stress intensity (Fig. 2.21) [32]. In these cases, the improved cyclic fatigue resistance has been attributed, at least in part, to the bridging of crack surfaces by the glassy phase, present in grain boundaries or formed *in situ* by the oxidation of the SiC whiskers.

2.5 Mechanisms of Ceramic Fatigue

In metals, mechanisms of cyclic fatigue have been based primarily on crack-tip dislocation activity leading to crack advance via such processes as alternating blunting and resharpening of the crack tip [54]. Accordingly, the refuted existence of a true fatigue effect in ceramics has been based in the past on the very limited crack-tip plasticity in these materials. However, it is now apparent that other inelastic deformation mechanisms may prevail; these mechanisms include microcracking and transformation "plasticity" in monolithic materials, the frictional sliding or controlled debonding between the reinforcement phase and ceramic matrix in brittle fiber or whisker reinforced composites, and the plastic deformation of a metallic or intermetallic phase itself in ductile-particle toughened composites. In fact, these factors are the

prime reason for marked resistance-curve (R-curve) fracture-toughness properties of ceramic composites [55], as such crack-tip shielding mechanisms develop progressively (until steady state) with increasing initial crack extension. Such deformation processes, like dislocation activity in metals, can similarly contribute to fatigue damage due to their nonlinear irreversible nature, although the precise micromechanisms of crack advance are presently unknown.

Despite the uncertainty in the mechanistic nature of ceramic fatigue, two general classes of mechanisms can be identified (where failure is associated with a dominant crack), specifically involving either *intrinsic* or *extrinsic* mechanisms [4,12]; these are illustrated schematically in Fig. 2.22. Intrinsic mechanisms involve the actual creation of a fatigue-damaged microstructure ahead of the crack tip, and thus result in a crack-advance mechanism unique to cyclic fatigue. This could entail crack extension via alternating crack-tip blunting and re-sharpening, as in metals where the consequent striation fracture morphology is distinct from monotonic fracture modes, or through the formation of shear or tensile cracking at the tip due to contact between the mating fracture surfaces on unloading. In fact, fatigue striations have been reported for cyclic failure in zirconia ceramics [10,11]. Another example is the high temperature fatigue of SiC-whisker-reinforced alumina; cyclic fractures show clear evidence of whisker breakage, whereas under quasi-static loads the majority of whiskers oxidize to form glass pockets [32].

Extrinsic mechanisms, conversely, do not necessarily involve a change in crack-advance mechanism compared to monotonic fracture; here, the role of the unloading cycle is to affect the magnitude of the *near-tip* stress intensity by diminishing the effect of crack-tip shielding. Several mechanisms are feasible. These include reduced shielding through an enhanced forward transformation zone in transforming ceramics, although careful Raman spectroscopy measurements have not revealed any change in zone size in Mg-PSZ for cyclic and quasi-static conditions at the same K_{max} [4,50]. An alternative mechanism is the reduction in crack-tip bridging via the cyclic induced failure of the bridges in the crack wake, where several possible processes exist. In ductile-particle toughened composites, cyclic loading may simply cause fatigue cracking in the ductile phase, which would otherwise remain intact under quasi-static loads and act as a crack bridge. An example of this is in γ-TiAl intermetallics reinforced with TiNb particles [56]. Under monotonic loading, bridging zones of uncracked TiNb particles in excess of 3 mm are formed in the crack wake leading to an elevation in the fracture toughness K_c from 8 MPa$\sqrt{m}$ in unreinforced γ-TiAl to over 25 MPa$\sqrt{m}$ in the composite; under cyclic loading, conversely, the TiNb particles suffer fatigue failure to within ~ 150 μm of the crack tip, such that the ductile-particle bridging mechanism essentially is obliterated. Also it is feasible that brittle fibers or whiskers in specific composites may similarly fracture and/or buckle due to the unloading cycle, again diminishing shielding by

crack bridging under cyclic loads. Finally, in certain monotonic ceramics, such as coarse-grained alumina, where toughening is achieved (primarily for intergranular fracture) by grain bridging or the interlocking of fracture-surface asperities between the crack faces [57,58], in cyclic fatigue, the unloading cycle may cause cracking and/or crushing of the asperities, or may degrade the grain-bridging mechanism through progressive wear of the sliding interfaces. In fact, evidence for the latter mechanism has recently been obtained in alumina using *in situ* scanning electron microscopy [59].

Indirect evidence for the extrinsic mechanism for cyclic fatigue-crack advance by the suppression of shielding can also be found from studies on small cracks in alumina and silicon nitride [19,29]. In a comparison of cyclic and quasi-static behavior, small surface cracks, which because of their limited wake would have developed only minimal shielding, were found to show no acceleration under cyclic loading; long cracks, conversely, were found to be significantly accelerated by the cyclic loads, consistent with their higher shielding levels [29].

2.6 Design Considerations

For structural design where failure results from the propagation of a single dominant crack, cyclic fatigue in ceramic materials presents unique problems. In safety-critical applications involving metallic structures, damage-tolerant design and life-prediction procedures generally rely on the integration of crack velocity/stress intensity (v/K) curves (e.g., Eq. 1) to estimate the time or number of cycles for a presumed initial defect to grow to critical size. Although such data are now available for many ceramic materials, the approach may prove difficult to utilize in practice because of the large power-law dependence of growth rates on stress intensity, which implies that the projected life will be proportional to the reciprocal of the applied stress raised to a large power [8].

For example, for a cracked structure subjected to an alternating stress $\Delta\sigma$, where the applied (far-field) stress-intensity factor K can be defined in terms of an applied stress σ and a geometry factor Q' as:

$$K = Q' \sigma\sqrt{(\pi a)} \ , \tag{7}$$

the projected number of cycles N_f to grow a crack from some initial size a_o to a critical size a_c is given by:

$$N_f = \frac{2}{(m-2)\, C(Q'\Delta\sigma)^m\, \pi^{(m/2)}} \left[a_o^{-\{(m-2)/2\}} - a_c^{-\{(m-2)/2\}}\right] \ , \tag{8}$$

assuming a crack-growth relationship of the form of Eq. 1 (for $m \neq 2$). For metallic structures where the exponent m is of the order of 2 to 4, a factor of two increase in the applied stress reduces the projected life by roughly an order of magnitude; in ceramic structures, conversely, where m values generally exceed 20 (and can be as high as 50 to 100), this same factor of two increase in stress reduces the projected life by some six to thirty orders of magnitude!

Thus, conventional damage-tolerant criteria for ceramics imply that marginal differences in the assumption of the component in-service stresses will lead to significant variations in projected life. Furthermore, any fluctuation of the applied stress and possible overloads frequently encountered in service may also result in highly non-conservative design lives. Two additional features of the approach provide further complication. First, in many practical applications, acceptable projected component life may only be guaranteed by restricting the initial defect size to extremely small sizes, often below the resolution of non-destructive evaluation techniques. Expensive and time consuming on-line scanning electron microscopy or proof testing at elevated loads of individual components are therefore required; in fact, these procedures are currently in use in quality control procedures for pyrolytic-carbon prosthetic heart-valve devices. Second, and perhaps most important, the approach generally does not consider, and in this case cannot easily be modified to include, small-crack effects such as those described above.

An alternative procedure is to redefine the critical crack size in terms of the fatigue threshold, ΔK_{TH}, below which crack growth is presumed dormant; this in essence is a crack-initiation criterion where ΔK_{TH} is taken as the effective toughness, rather than the fracture toughness K_c. This procedure, in addition to sharing similar problems associated with defining a minimum detectable defect size, also does not address small-crack effects which may arise at loads considerably below those required for the growth of long-cracks. As a result, although data on the small-crack effect in ceramic fatigue are very limited, the observed sub-threshold crack-growth behavior implies that conventional damage-tolerant design criteria may be again highly non-conservative for ceramics.

Like many high strength metallic materials, however, crack-initiation effects may involve a very significant portion of lifetime under alternating loads. Having referred to a number of potential limitations of a fracture-mechanics approach to ensure component reliability, it is important to note that these approaches are typically highly conservative in the sense that they assume crack growth from the first loading cycle. Although the degree of this conservatism is difficult to quantify, due in part to the paucity of data from crack-initiation studies, the disadvantages of the approach may in fact be considerably outweighed by neglecting the cycles required for initiation. Selection of a damage-tolerant approach is,

therefore, at present undertaken on a case by case basis, often affected by the requirements of appropriate regulatory agencies.

The importance of fatigue-crack initiation does, however, suggest an additional design criterion for ceramic components; this more traditional approach is invariably based on stress/life S/N data. In addition to simple consideration of the fatigue limit, a more sophisticated approach might include a damage-mechanics analysis utilizing detailed finite-element stress analyses for components of complex shape and a statistical evaluation of the pre-existing defect population. While this approach has serious limitations in some applications, particularly in large structures where numerous defects may be present and therefore fatigue-crack initiation periods diminished, it might be quite appropriate for small ceramic components. Clearly, more indepth studies of both fatigue-crack initiation and crack-growth behavior, together with improved design criterion are required to enhance the in-service reliability and life prediction of ceramic and ceramic-matrix components subjected to alternating loads.

2.7 Conclusions

1. Results on a wide range of monolithic and composite ceramics clearly indicate a strong susceptibility to mechanical degradation under cyclic loading. Ceramic fatigue is promoted by inelastic deformation mechanisms, such as microcracking and transformation "plasticity" in monolithic ceramics and irreversible deformation in the reinforcement phase or its interface with the matrix in composites.

2. Stress/life (S/N) data show lifetimes to be shorter under cyclic loading compared to corresponding lifetimes under quasi-static (static fatigue) loading at the same maximum stress. In many ceramics, "fatigue limits" at 10^8 cycles ($R = -1$) approach ~50% of the single-cycle tensile (or bending) strength. Data on unnotched samples indicate that cycling in tension-compression ($R = -1$) is generally more damaging that in tension-tension ($R > 0$).

3. With the exception of SiC, cyclic fatigue lifetimes in S/N tests at ambient temperatures are less than those predicted from static fatigue data assuming only time-dependent (and not cycle-dependent) processes; conversely, at high homologous temperatures, results for alumina at 1200°C suggest that the reverse is true.

4. Cyclic fatigue-crack growth rates for long (>3 mm) cracks are found to be power-law dependent on the applied stress intensity (ΔK, K_{max}), with an exponent m much larger than typically observed for metals (i.e., in the range ~10 to over 100). Crack-growth behavior is sensitive to several factors including microstructure, load ratio, environment and crack size. Fatigue threshold stress intensities (ΔK_{TH}), below which long cracks are presumed dormant, approach ~50% of the fracture toughness (K_c).

5. At ambient temperatures, crack-growth rates under cyclic loading generally exceed those by static fatigue (at the same K_{max}) by many orders of magnitude. Conversely, at high homologous temperatures (1000° to 1400°C) in the creep regime, cyclic fatigue-crack growth rates in monolithic and SiC_w-reinforced alumina have been observed to be less than those measured under quasi-static loads.

6. Cyclic fatigue-crack growth rates for small (<250 μm) surface cracks are found to be in excess of corresponding long cracks at the same applied stress intensity, and furthermore to occur at stress intensities significantly smaller than the nominal long-crack threshold, ΔK_{TH}. Similar to metallic materials, small-crack growth rates show a negative dependency on applied stress intensity and appear sensitive to the applied stress level. Such behavior is attributed to diminished crack-tip shielding (e.g., by transformation toughening in Mg-PSZ or crack bridging in whisker- or fiber-reinforced composites) with cracks of limited wake.

7. The fractography of failures by cyclic fatigue is frequently similar and often indistinguishable from corresponding failures under quasi-static loading. Such similarity complicates the post-fracture failure analysis of ceramic components.

8. Although precise micro-mechanisms of cyclic fatigue are currently uncertain, two classes are identified. *Intrinsic* mechanisms involve the creation of an inherent fatigue-damaged microstructure ahead of the crack tip and hence result in a crack-advance mechanism unique to cycle fatigue (as in metals). *Extrinsic* mechanisms involve no change in crack-advance mechanism compared to that under quasi-static loading; here the unloading cycle acts to enhance the near-tip stress intensity by diminishing the role of crack-tip shielding.

9. Cyclic fatigue-crack growth-rate data, particularly pertaining to small cracks, have significant implications for damage-tolerant lifetime prediction and design criteria in ceramic materials. The observed marked dependency of growth rates on the stress intensity implies an excessive dependency of projected lifetime on applied stress; this leads to difficulties in applying conventional damage-tolerant procedures. An indepth understanding of the initiation and growth of microstructurally-small cracks is required to provide more reliable design criteria for safety-critical applications.

2.8 References

1. R. H. Dauskardt, W. Yu and R. O. Ritchie, *J. Am. Ceram. Soc.*, **70** (1987) 248-52.

2. M. V. Swain and V. Zelizko, pp. 595-606 in *Advances in Ceramics, 24B Science and Technology of Zirconia III*, Edited by S. Somioya, N. Yammoto and H. Hanagida, American Ceramic Society, Westerville, OH, 1988.

3. L. A. Sylva and S. Suresh, *J. Mater. Sci.*, **24** (1989) 1729-38.

4. R. H. Dauskardt, D. B. Marshall and R. O. Ritchie, *J. Am. Ceram. Soc.*, **73** (1990) 893-903.

5. R. H. Dauskardt, W. C. Carter, D. K. Veirs and R. O. Ritchie, *Acta Metall. Mater.*, **38** (1990) 2327-36.

6. T. Kawakubo, N. Okabe and T. Mori, pp 717-32 in *Fatigue '90* (Proc. 4th Intl. Conf. on Fatigue and Fatigue Thresholds), Vol. 2, Edited by H. Kitagawa and T. Tanaka, Mat. Comp. Eng. Publ., Ltd., Edgbaston, U.K., 1990.

7. A. A. Steffen, R. H. Dauskardt and R. O. Ritchie, pp. 745-52 in *Fatigue '90* (Proc. 4th Intl. Conf. on Fatigue and Fatigue Thresholds), Vol. 2, Edited by H. Kitagawa and T. Tanaka, Mat. Comp. Eng. Publ., Ltd., Edgbaston, U.K., 1990.

8. A. A. Steffen, R. H. Dauskardt and R. O Ritchie, *J. Am. Ceram. Soc.*, **74** (1991) 1259-68.

9. D. C. Cardona and C. J. Beevers, pp. 1023-29 in *Fatigue '90* (Proc. 4th Intl. Conf. on Fatigue and Fatigue Thresholds), Vol. 2, Edited by H. Kitagawa and T. Tanaka, Mat. Comp. Eng. Publ., Ltd., Edgbaston, U.K., 1990.

10. S.-Y. Liu and I.-W. Chen, *J. Am. Ceram. Soc.*, **74** (1991) 1197-216.

11. D. L. Davidson, J. B. Campbell and J. Lankford, J., *Acta Metall. Mater.*, **39** (1991) 1319-30.

12. R. O. Ritchie, R. H. Dauskardt, W. Yu and A. M. Brendzel, *J. Biomed. Mater. Res.*, **24** (1990) 189-206.

13. F. Guiu, *J. Mater. Sci. Lett.*, **13** (1978) 1357-61.

14. H. N. Ko, *J. Mater. Sci. Lett.*, **5** (1986) 464-66.

15. L. Ewart and S. Suresh, *J. Mater. Sci. Lett.*, **5** (1986) 774-78.

16. T. Hoshide, T. Ohara and T. Yamada, *Int. J. Fracture*, **37** (1988) 47-59.

17. G. Grathwohl and T. Liu, *J. Am. Ceram. Soc.*, **72** (1989) 1988-90.

18. H. N. Ko. *J. Mater. Sci. Lett.*, **8** (1989) 1438-41.

19. S. Lathabai, Y.-W. Mai and B. R. Lawn, *J. Am. Ceram. Soc.*, **72** (1989) 1760-63.

20. M. J. Reece, F. Guiu and M. F. R. Sammur, *J. Am. Ceram. Soc.*, **72** (1989) 348-52.

21. I. Bar-On and J. T. Beals, pp. 793-98 in *Fatigue '90* (Proc. 4th Intl. Conf. on Fatigue and Fatigue Thresholds), Vol. 2, Edited by H. Kitagawa and T. Tanaka, Mat. Comp. Eng. Publ., Ltd., Edgbaston, U.K., 1990..

22. C.-K. J. Lin and D. F. Socie, *J. Am. Ceram. Soc.*, **74** (1991) 1511-18.

23. T. Fett, G. Martin, D. Munz and G. Thun, *J. Mater. Sci.* (1991) 3320-28.

24. T. Fett and D. Munz, Proc. 7th World Ceramics Congress (CIMTEC), Montecatini Therme, Italy, 1990, in press.

25. T. Kawakubo and K. Komeya, *J. Am. Ceram. Soc.*, **70** (1987) 400-05.

26. S. Horibe, *J. Mater. Sci. Lett.*, **7** (1988) 725-27.

27. M. Masuda, T. Soma, M. Matsui and I. Oda, *J. Ceram. Soc. Japan Inter. Ed.*, **96** (1988) 275-80.

28. A. Ueno, H. Kishimoto, H. Kawamoto and M. Asakwa, pp. 733-38 in *Fatigue '90* (Proc. 4th Intl. Conf. on Fatigue and Fatigue Thresholds), Vol. 2, Edited by H. Kitagawa and T. Tanaka, Mat. Comp. Eng. Publ., Ltd., Edgbaston, U.K., 1990.

29. Y. Mutoh, M. Takahashi, T. Oikawa and H. Okamoto, pp. 211-25 in *Fatigue of Advanced Materials*, Edited by R. O. Ritchie, R. H. Dauskardt, and B. N. Cox, Mat. Comp. Eng. Publ., Ltd., Edgbaston, U.K., 1991.

30. S. Lauf, V. Gerold and R. F. Pabst, pp. 775-80 in *Fatigue '90* (Proc. 4th Intl. Conf. on Fatigue and Fatigue Thresholds), Vol. 2, Edited by H. Kitagawa and T. Tanaka, Mat. Comp. Eng. Publ., Ltd., Edgbaston, U.K., 1990.

31. E. H. Luh, R. H. Dauskardt and R. O. Ritchie, *J. Mater. Sci. Lett.*, **9** (1990) 719-25.

32. L. X. Han and S. Suresh, *J. Am. Ceram. Soc.*, **72** (1989) 1233-38.

33. R. H. Dauskardt, M. R. James, J. R. Porter and R. O. Ritchie, *J. Am. Ceram. Soc.*, **74** (1991) in press.

34. J. W. Holmes, *J. Am. Ceram. Soc.*, **74** (1991) 1639-45.

35. R. O. Ritchie, *Int. Met. Rev.*, **20** (1979) 205-30.

36. R. O. Ritchie and W. Yu, pp. 167-89 in *Small Fatigue Cracks*, Edited by R. O. Ritchie and J. Lankford, The Metallurgical Society of the American Institute of Mining, Metallurgical, and Petroleum Engineers, Warrendale, PA, 1986.

37. P. C. Paris and F. Erdogan, *J. Bas. Eng.*, Trans. ASME, **85** (1963) 528-34.

38. S. Suresh and R. O. Ritchie, *Intl. Metals Rev.*, **29** (1984) 445-76.

39. H. Tada, P. C. Paris and G. R. Irwin, *Stress Analysis of Cracks Handbook*, Paris Publications Inc./Del Research Corp., St. Louis, MO, 1985.

40. J. C. Newman, Jr. and I. S. Raju, pp. 312-34 in *Computational Methods in the Mechanics of Fracture*, Chapter 9, Vol. 2, Edited by S. N. Atluri, North Holland, Amsterdam, 1986.

41. R. W. Hertzberg, W. A. Herman and R. O. Ritchie, *Scripta Metall.*, **21** (1987) 1541-46.

42. W. Elber, pp. 230-42 in *Damage Tolerance in Aircraft Structures*, ASTM STP 486, American Society for Testing and Materials, Philadelphia, PA, 1971.

43. S. Suresh and R. O. Ritchie, pp. 227-61 in *Fatigue Crack Growth Threshold Concepts*, Edited by D. L. Davidson and R. O. Ritchie, The Metallurgical Society of the American Institute of Mining, Metallurgical, and Petroleum Engineers, Warrendale, PA, 1984.

44. R. H. J. Hannick and M. V. Swain, *J. Aust. Ceram. Soc.*, **18** (1982) 53-62.

45. R. H. J. Hannick, *J. Mater. Sci.*, **18** (1983) 457-70.

46. D. B. Marshall, *J. Am. Ceram. Soc.*, **69** (1986) 173-88.

47. R. M. McMeeking and A. G. Evans, *J. Am. Ceram. Soc.*, **63** (1982) 242-46.

48. B. Budiansky, J. W. Hutchinson and J. C. Lambropoulos, *Int. J. Solids Struct.*, **19** (1983) 337-55.

49. R. H. Dauskardt, D. K. Veirs and R. O. Ritchie, *J. Am. Ceram. Soc.*, 72 (1989) 1124-30.

50. D. B. Marshall, M. C. Shaw, R. H. Dauskardt, R. O. Ritchie, M. Readey and A. H. Heuer, *J. Am. Ceram. Soc.*, **73** (1990) 2659-66.

51. R. O. Ritchie, R. H. Dauskardt and F. J. Pennisi, *J. Biomed. Mater. Res.*, **25** (1991) in press.

52. R. W. Hertzberg, *Deformation and Fracture Mechanics of Engineering Materials*, 3rd ed., Wiley, New York, NY, 1989.

53. T. Fett, G. Himsolt and D. Munz, *Adv. Ceram. Matls.*, **1** (1986) 179-84.

54. P. Neumann, *Acta Metall.*, **22** (1974) 1155-65.

55. A. G. Evans, pp. 267-91 in *Fracture Mechanics: Perspectives and Directions (Twentieth Symp.)*, ASTM STP 1020, Edited by R. P. Wei and R. P. Gangloff, American Society for Testing and Materials, Philadelphia, PA, 1989.

56. K. T. Venkateswara Rao, G. R. Odette and R. O. Ritchie, *Acta Metall. Mater.*, **39** (1991) in press.

57. P. L. Swanson, C. J. Fairbanks, B. R. Lawn, Y.-W. Mai and B. J. Hockey, *J. Am. Ceram. Soc.*, **70** (1987) 279-89.

58. G. Vekinis, M. F. Ashby and P. W. R. Beaumont, *Acta Metall. Mater.* **38** (1990) 1151-62.

59. S. Lathabai, J. Rödel and B. R. Lawn, *J. Am. Ceram. Soc.*, **74** (1991) 1340-48.

Table 2.1 - Values of Parameters for S/N and Crack-Propagation Fatigue Tests for Ceramic Materials at Ambient Temperatures

	K_c ($MPa\sqrt{m}$)	S/N slope n	Crack Propagation (R = 0) C ($m/c\ (MPa\sqrt{m})^{-m}$) (Eq.1)	Crack Propagation (R = 0) slope m	Crack Propagation (R = 0) ΔK_{TH} ($MPa\sqrt{m}$)	Ref.
alumina	~4.0	12.7-64	-	27-33	2.5-2.7	18,20
Mg-PSZ (TS-grade)*	16.0	34	1.70×10^{-48}	42	7.7	4
(MS-grade)	11.5	36	5.70×10^{-28}	24	5.2	4
(AF-grade)	5.5	-	4.89×10^{-22}	24	3.0	1,4
(overaged)	2.9	-	2.00×10^{-14}	21	1.6	4
silicon nitride	6.0	~30	1.01×10^{-21}	12-18	2.0-4.3	21
3Y-TZP	5.3	~21	4.06×10^{-18}	21	2.4	10
Al_2O_3-SiC_w	4.5	-	3.28×10^{-20}	15	3.1	33
graphite/pyrolytic C	~1.6	-	1.86×10^{-18}	19	~0.7	12

*TS ≡ 7 hr at 1000°C, MS ≡ 3 hr at 1100°C, AF ≡ as fired, overaged ≡ 24 hr at 1100°C.

Table 2.2 - Comparison of Fatigue Lifetimes at Various Load Ratios for Al_2O_3/SiC_w Composite

Load Ratio ($\sigma_{min}/\sigma_{max}$)	σ_{max} (MPa)	Life, N_f (cycles)
0.05	245	60×10^3
0.05	247	140×10^3
0.05	252	150×10^3
-1.0	248	60×10^3
-1.0	255	240×10^3

(1) STRESS/STRAIN-LIFE

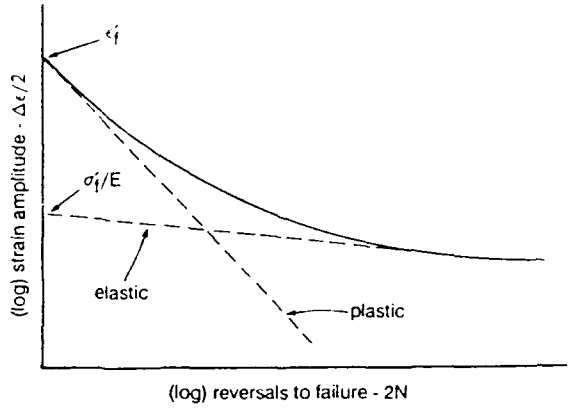

(2) FATIGUE-CRACK GROWTH
(long cracks)

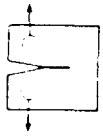

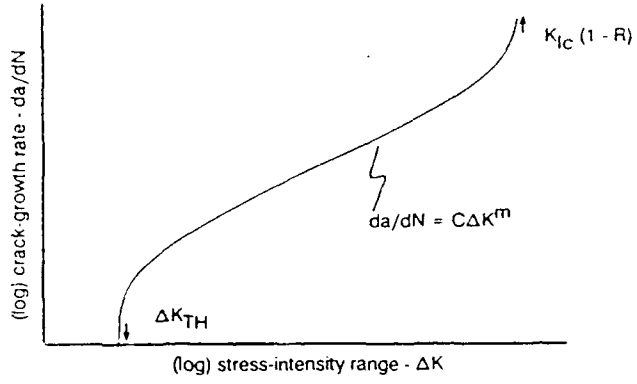

(3) FATIGUE-CRACK GROWTH
(small cracks)

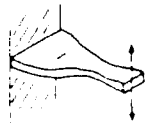

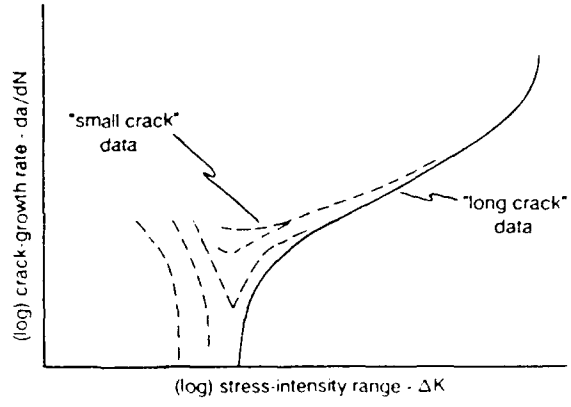

Fig. 2.1. Methodologies for characterizing cyclic fatigue resistance in materials; a) stress or strain/life (S/N) testing, b) fatigue-crack propagation tests on long cracks (typically larger than ~ 3 mm), and c) fatigue-crack propagation testing on small cracks (typically ~ 1 to 250 μm in size).

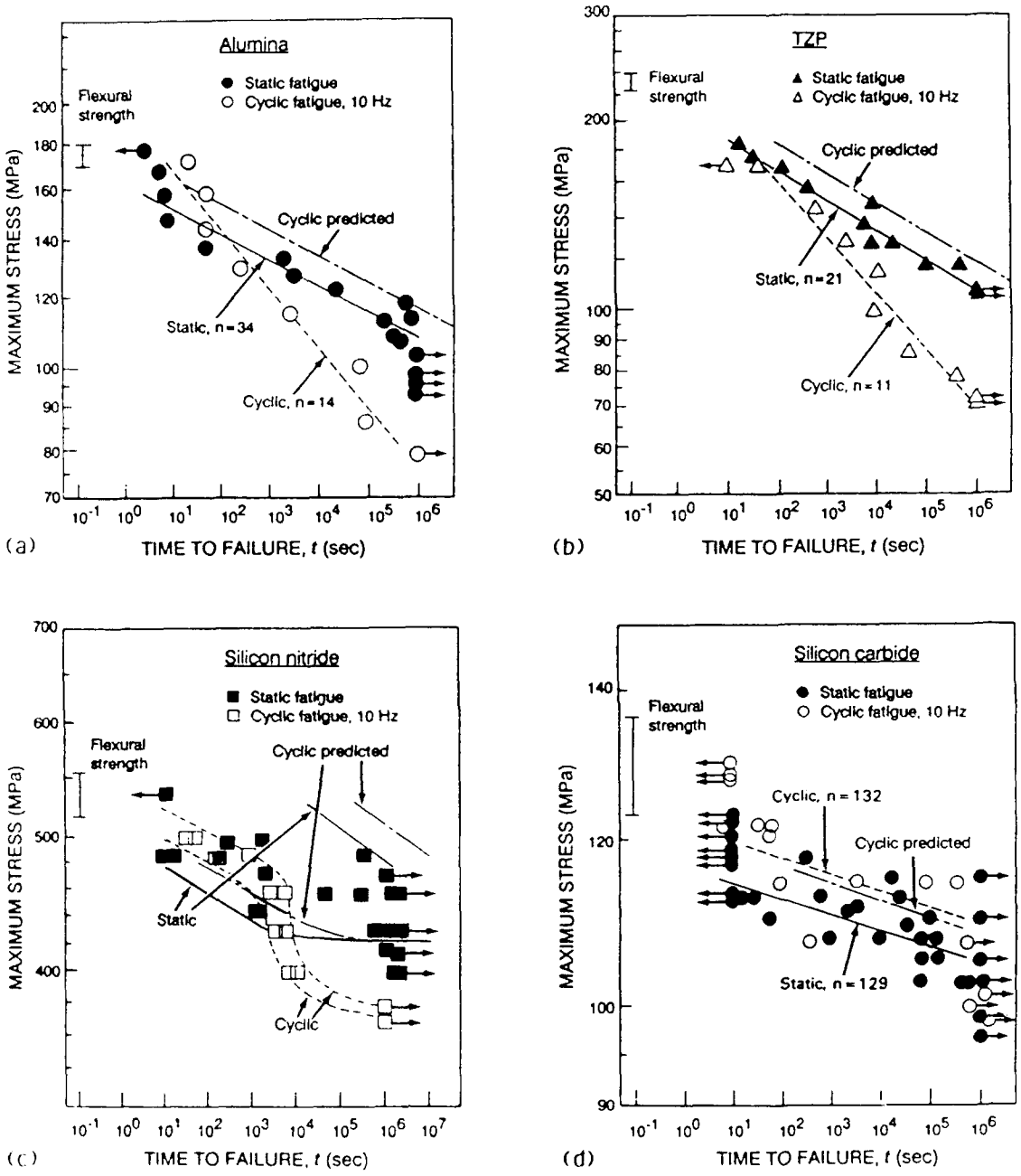

Fig. 2.2. Comparison of stress/life results for a) alumina, b) TZP, c) silicon nitride, and d) silicon carbide under cyclic and quasi-static loading at ambient temperature. Four-point bend (R = 0) data from ref. 6.

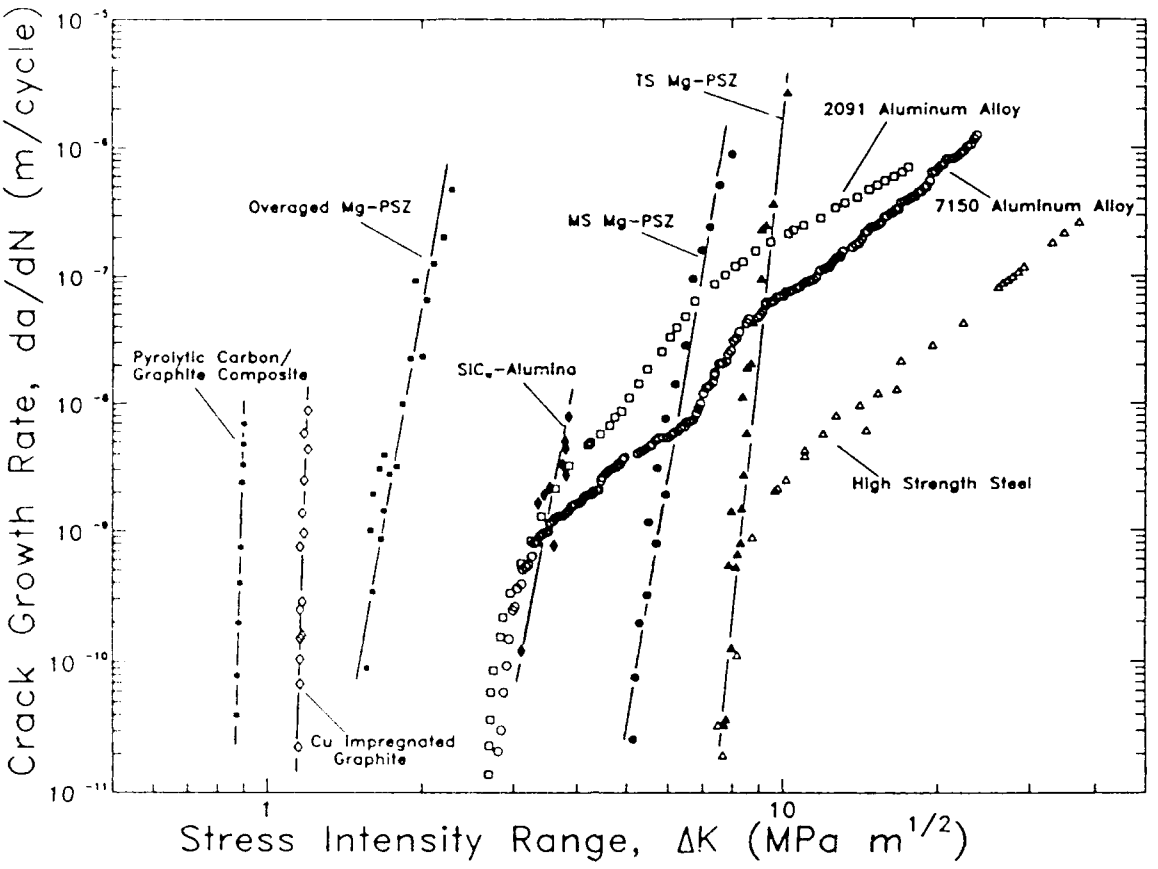

Fig. 2.3. Cyclic fatigue-crack propagation behavior for a range of ceramics, namely, Mg-PSZ [1,4], pyrolytic carbon [12], Cu-impregnated graphite, and SiC-reinforced alumina [33]; data are compared with three high-strength steel and aluminum metallic alloys [35,36]. (MS and TS Mg-PSZ are mid-toughness [$K_c \sim 11.5$ MPa$\sqrt{m}$] and peak toughness [$K_c \sim 16$ MPa$\sqrt{m}$] microstructures, achieved respectively by 3 and 7 hr sub-eutectoid aging heat-treatments at 1100°C.)

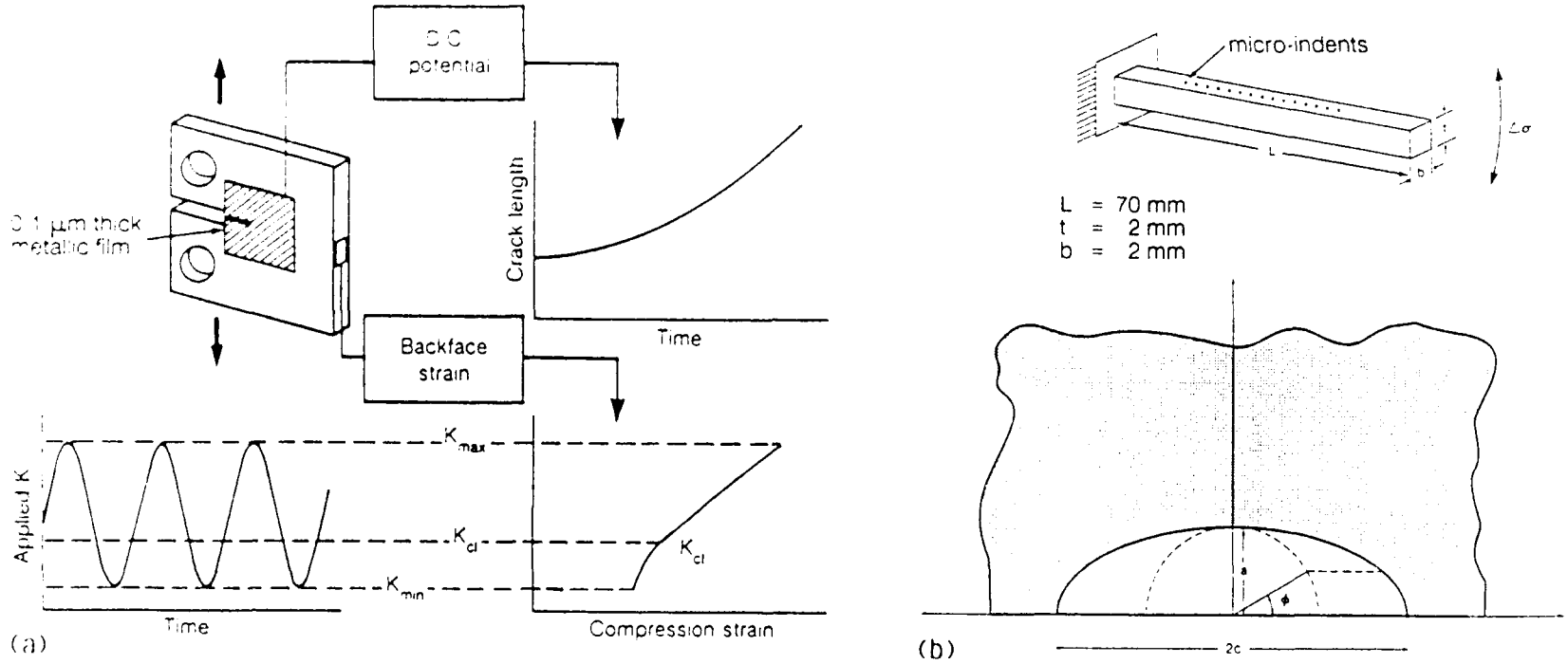

Fig. 2.4. Experimental techniques used to measure cyclic fatigue-crack growth rates, showing a) compact tension C(T) specimen and procedures used to monitor crack length and the stress intensity, K_{cl}, at crack closure for long cracks, and b) cantilever-bend specimen and semi-elliptical surface crack configuration for tests on small cracks [4,8,33].

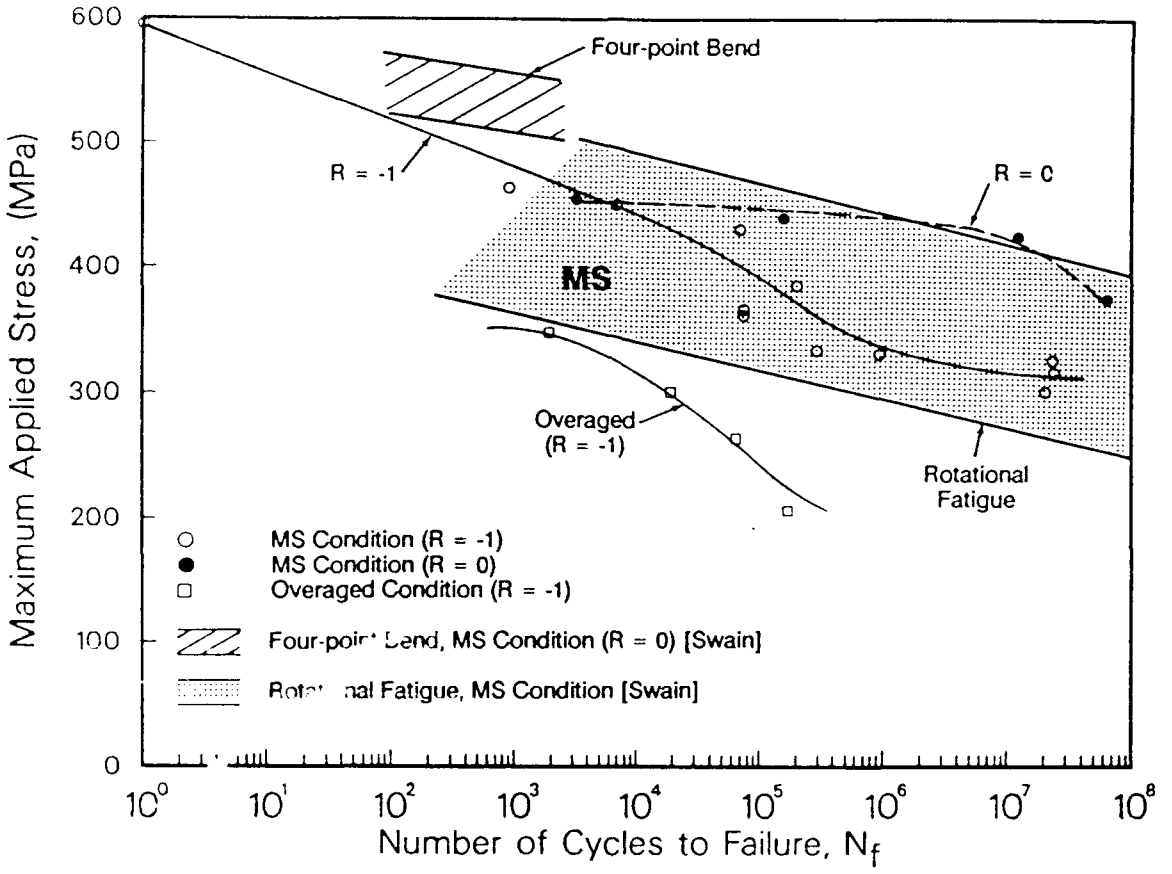

Fig. 2.5. Stress/life (S/N) curves for the overaged and MS-grade Mg-PSZ tested in cantilever bend under tension-compression (R = -1) and tension-tension (R = 0) cycling [7,8]. Data are compared with results of Swain and Zelizko [2] on a similar MS-grade Mg-PSZ material under flexural bending (R = 0) and rotating bending (R = -1).

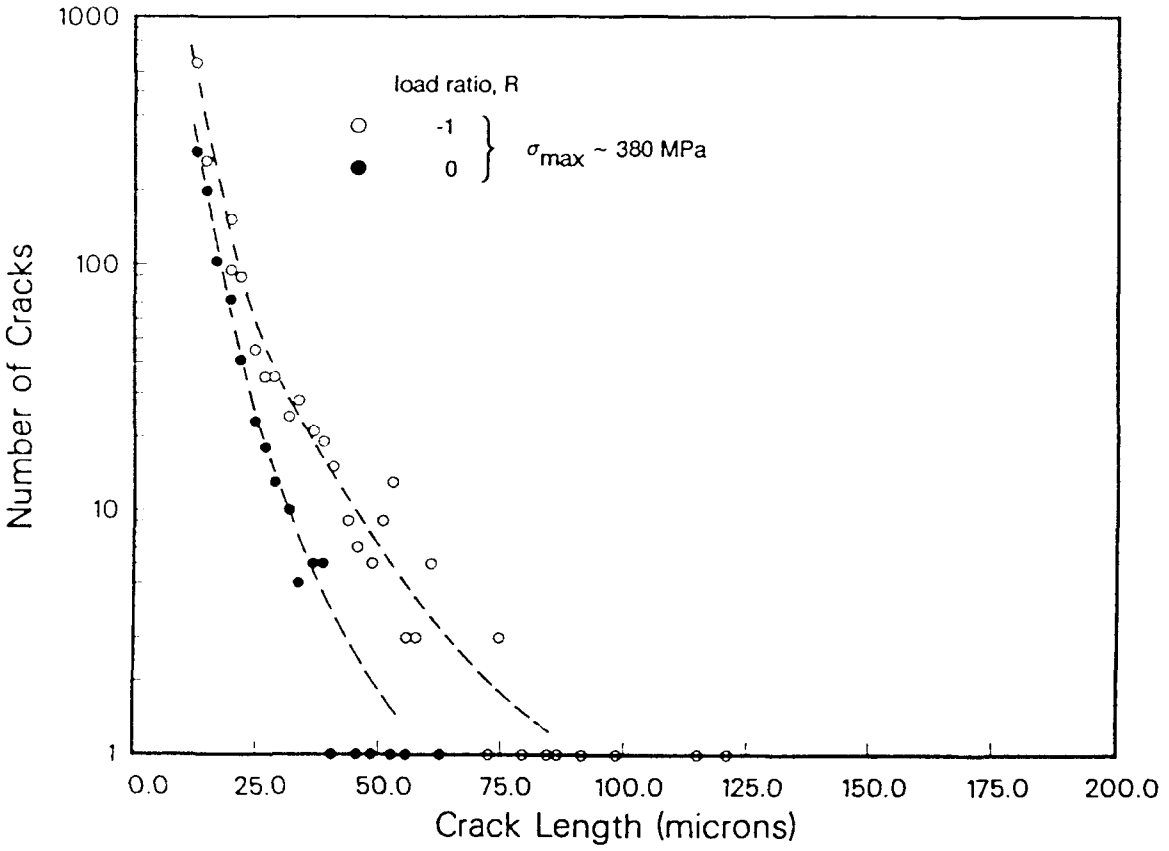

Fig. 2.6. Microcrack size distributions for MS-grade Mg-PSZ measured on the surface of unnotched cantilever-bend specimens at a maximum alternating stress of ~380 MPa for both tension-compression and tension-tension loading [8].

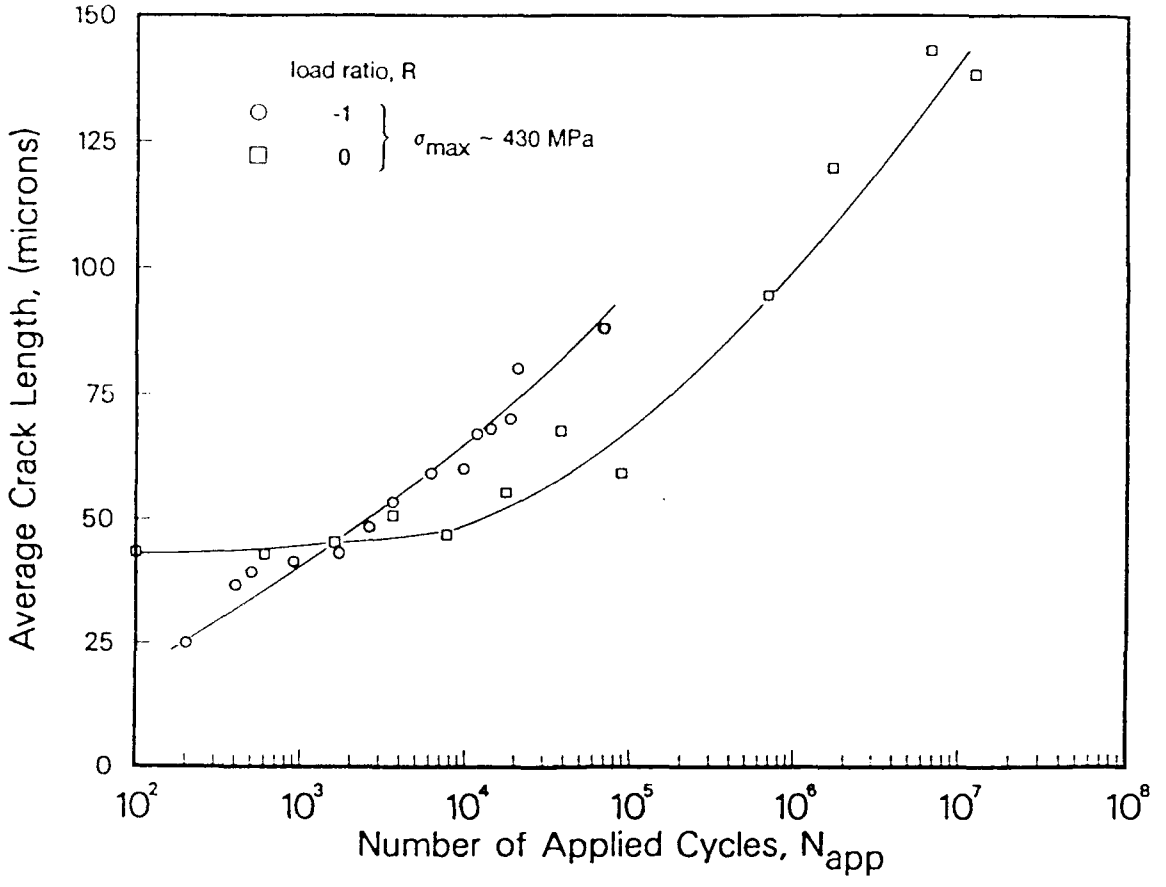

Fig. 2.7. Surface crack length vs. number of cycles for small-crack growth at similar applied stress levels in unnotched cantilever-bend specimens of MS-grade Mg-PSZ tested at R = 0 and R = -1 [8].

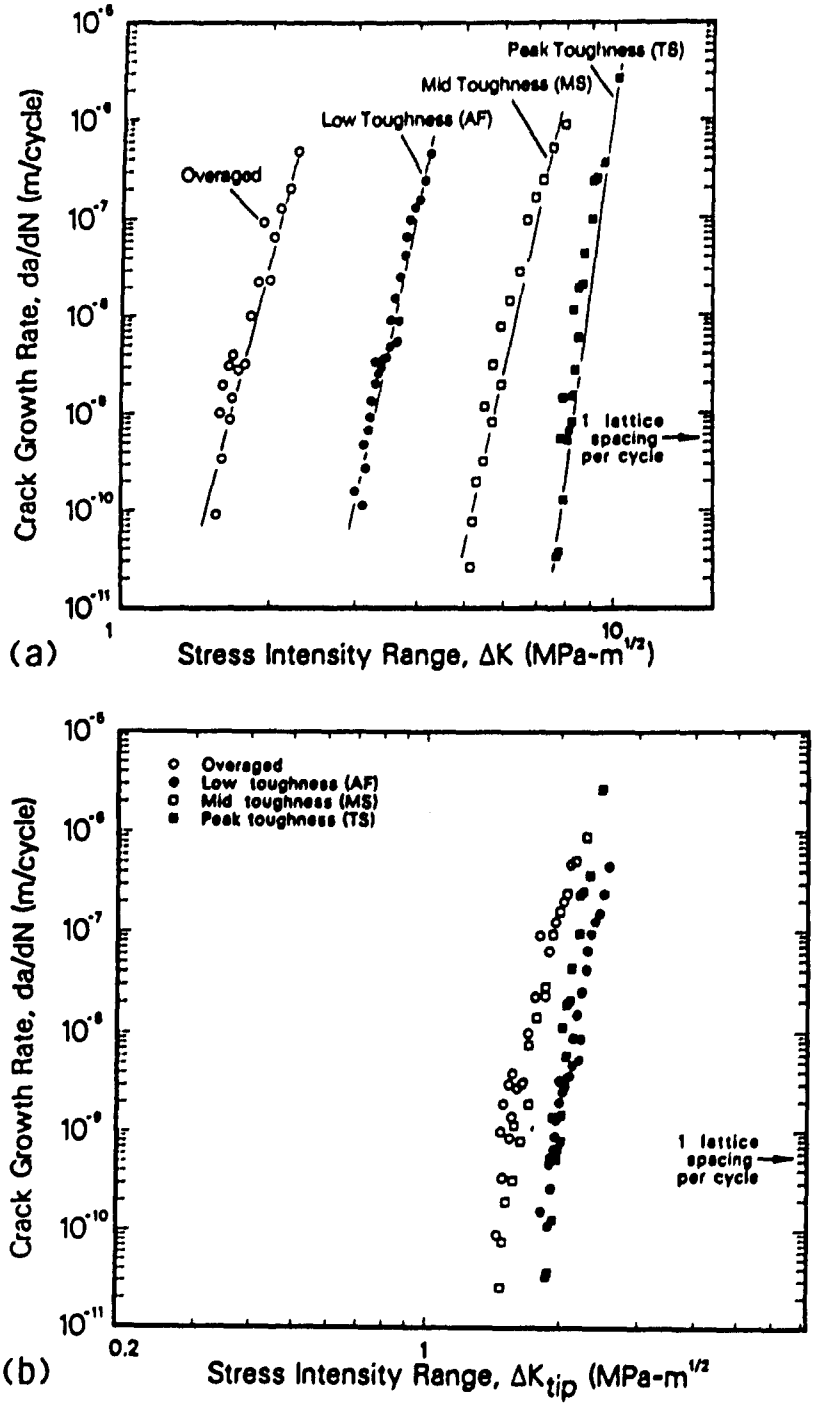

Fig. 2.8. Long-crack growth-rate data in overaged and transformation-toughened Mg-PSZ, derived from C(T) specimens, as a function of a) nominal (applied) stress-intensity range, ΔK, and b) near-tip stress-intensity range, $\Delta K_{tip} = K_{max} - K_s$, showing that cyclic crack-growth resistance is increased with the degree of transformation toughening [4]. (See Table 1 for explanation of AF, MS and TS grades of Mg-PSZ.)

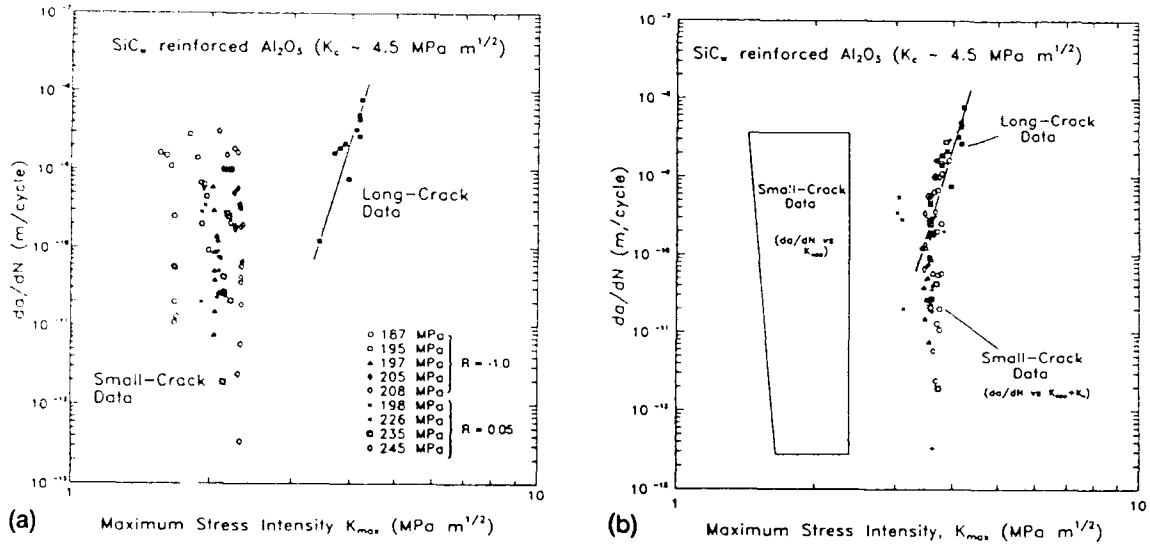

Fig. 2.9. Small-crack growth-rate data in the Al_2O_3-SiC_w from cantilever-beam specimens, a) as a function of the applied K_{max} at R = 0.05 and -1, compared to corresponding long-crack data derived from C(T) specimens, and b) as a function of the total stress intensity (K_{max} + K_r) where K_r results from the residual stress surrounding the indent. Note how small cracks propagate at applied stress-intensity (K_{app}) levels well below the long-crack threshold, ΔK_{TH}, and show an apparent negative dependency on K_{app}; however, when characterized in terms of the total stress intensity, their growth rates are in close correspondence with those of long cracks [33].

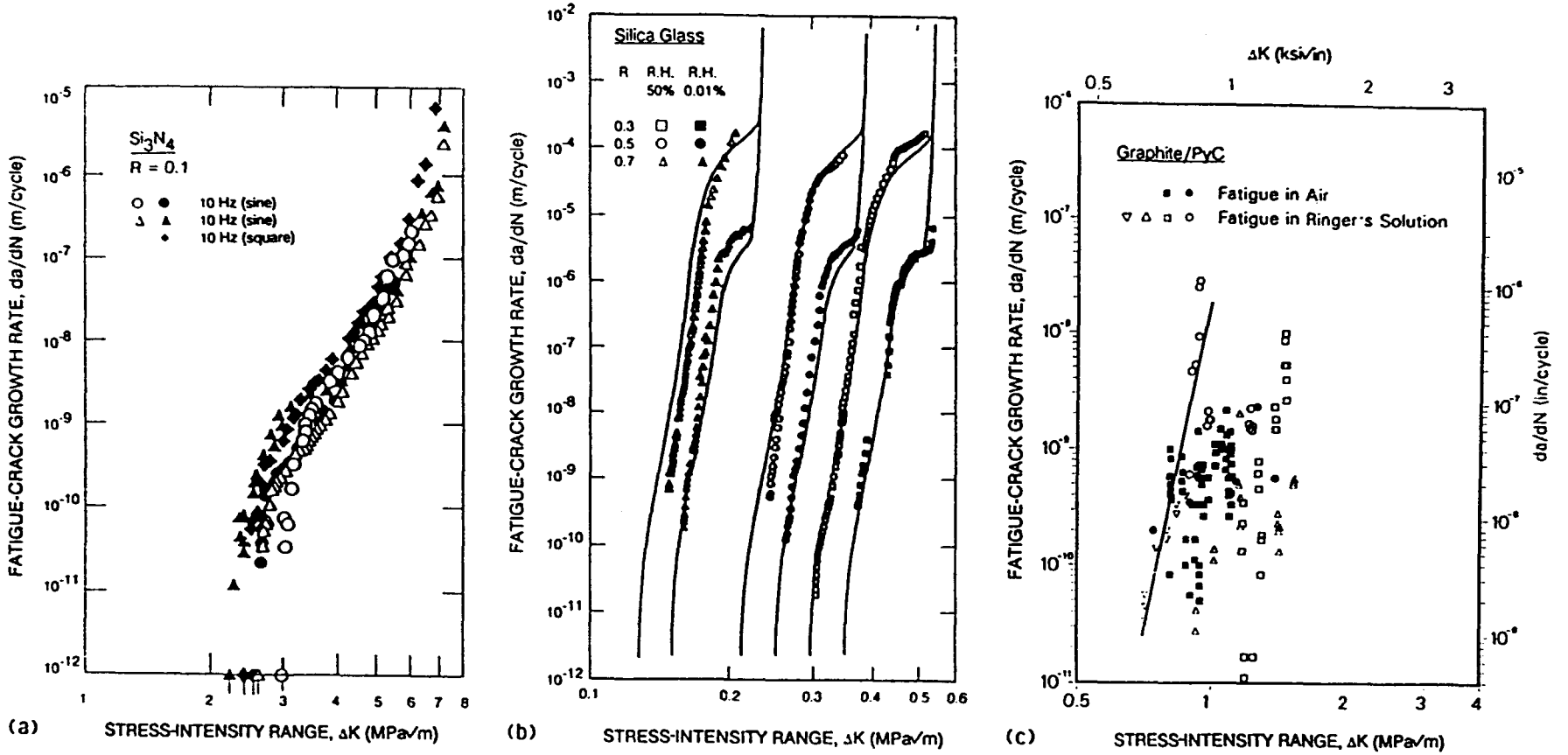

Fig. 2.10. Cyclic fatigue-crack propagation results for a) silicon nitride [29], b) silica glass [30], and a pyrolytic-carbon coated graphite laminate [12].

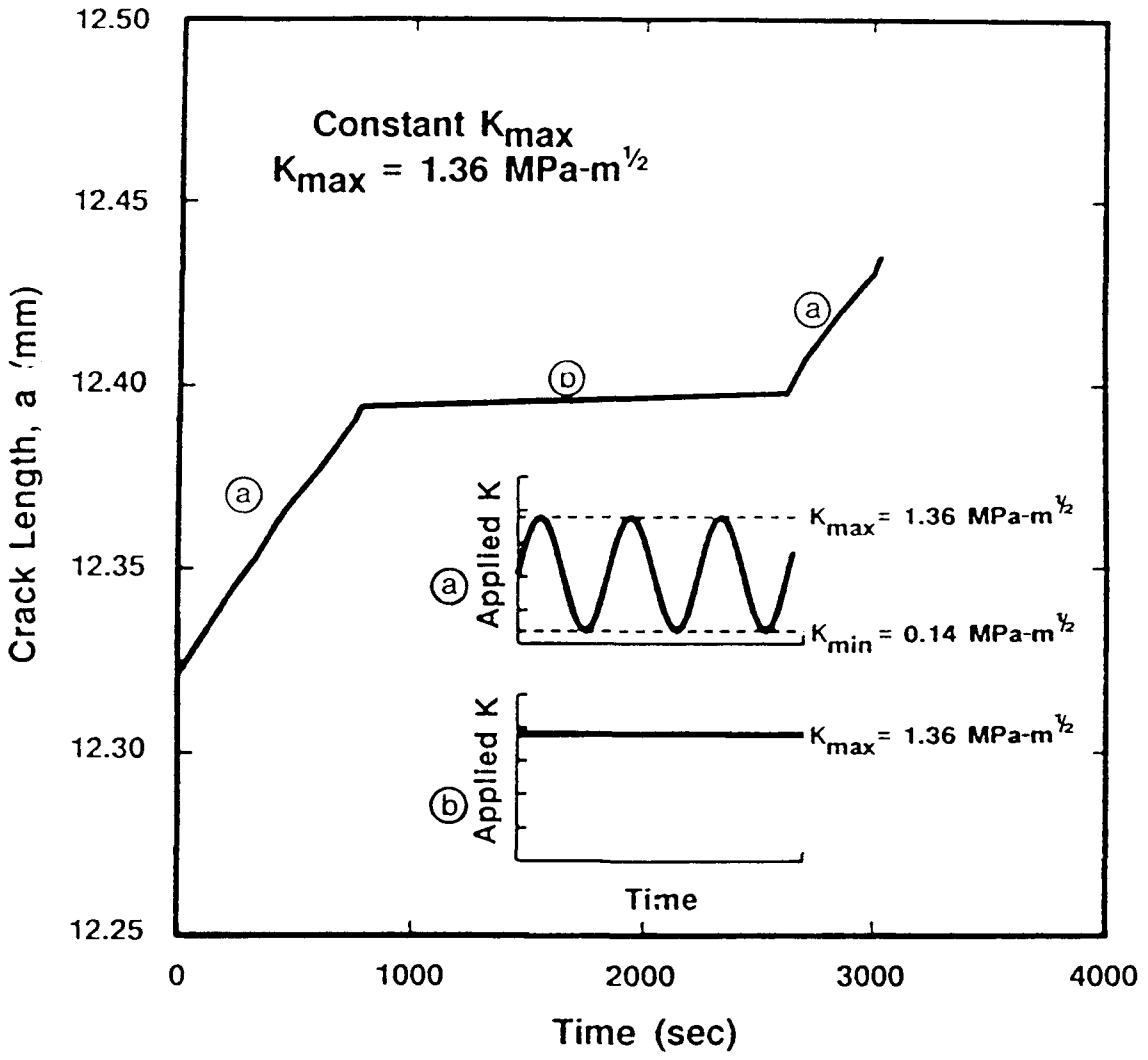

Fig. 2.11. Effect of sustained-load vs. cyclic loading conditions, at a constant K_{max}, on subcritical crack growth in pyrolytic-carbon coated graphite tested at R = 0.1 (50 Hz) in Ringer's solution at 37°C (blood analog). Note how crack-growth rates under cyclic loading (regions a) are far in excess of those measured under sustained (quasi-static) loading (region b) [12].

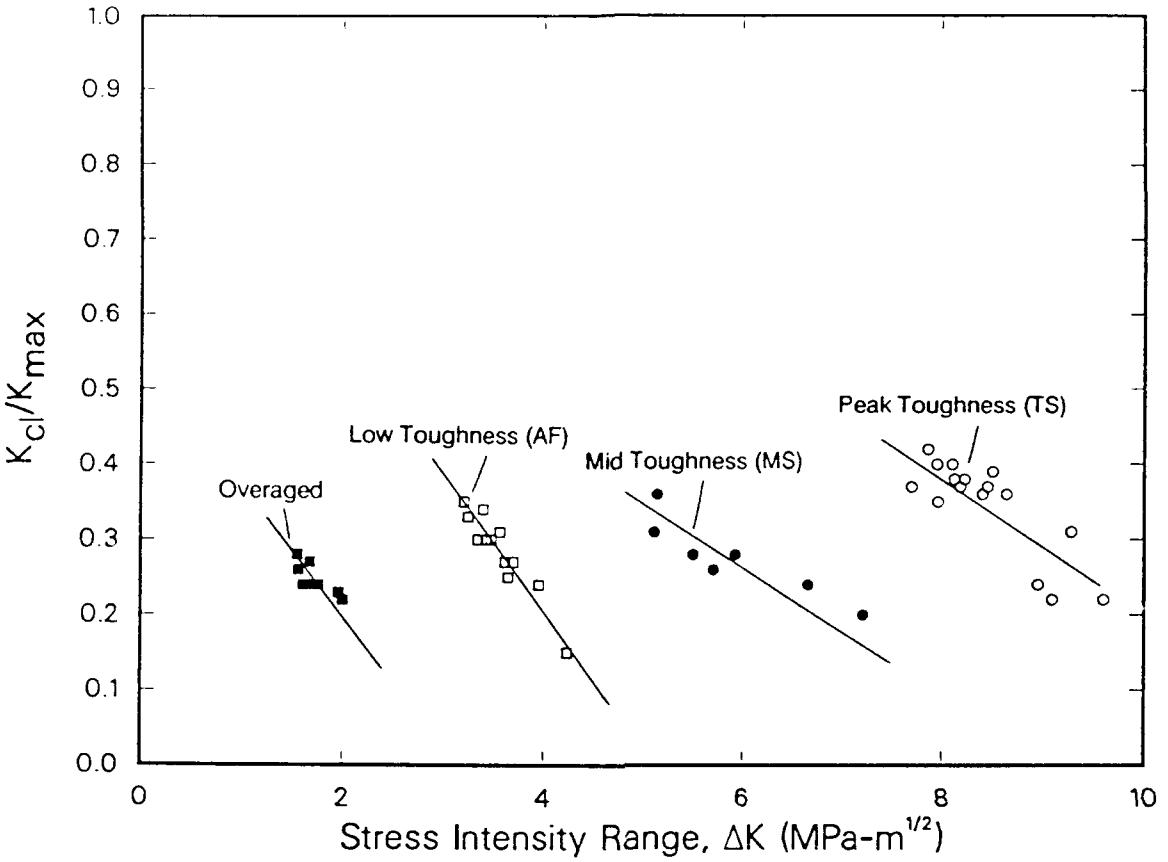

Fig. 2.12. Experimentally measured variation in fatigue crack closure corresponding to cyclic crack-growth rate data at R = 0.1 for the Mg-PSZ microstructures plotted in Fig. 8. Results are based on back-face strain compliance measurements and show the ratio of the closure to maximum stress intensities, K_{cl}/K_{max}, as a function of the applied stress-intensity range, ΔK [4]. (See Table 1 for explanation of AF, MS and TS grades of Mg-PSZ.)

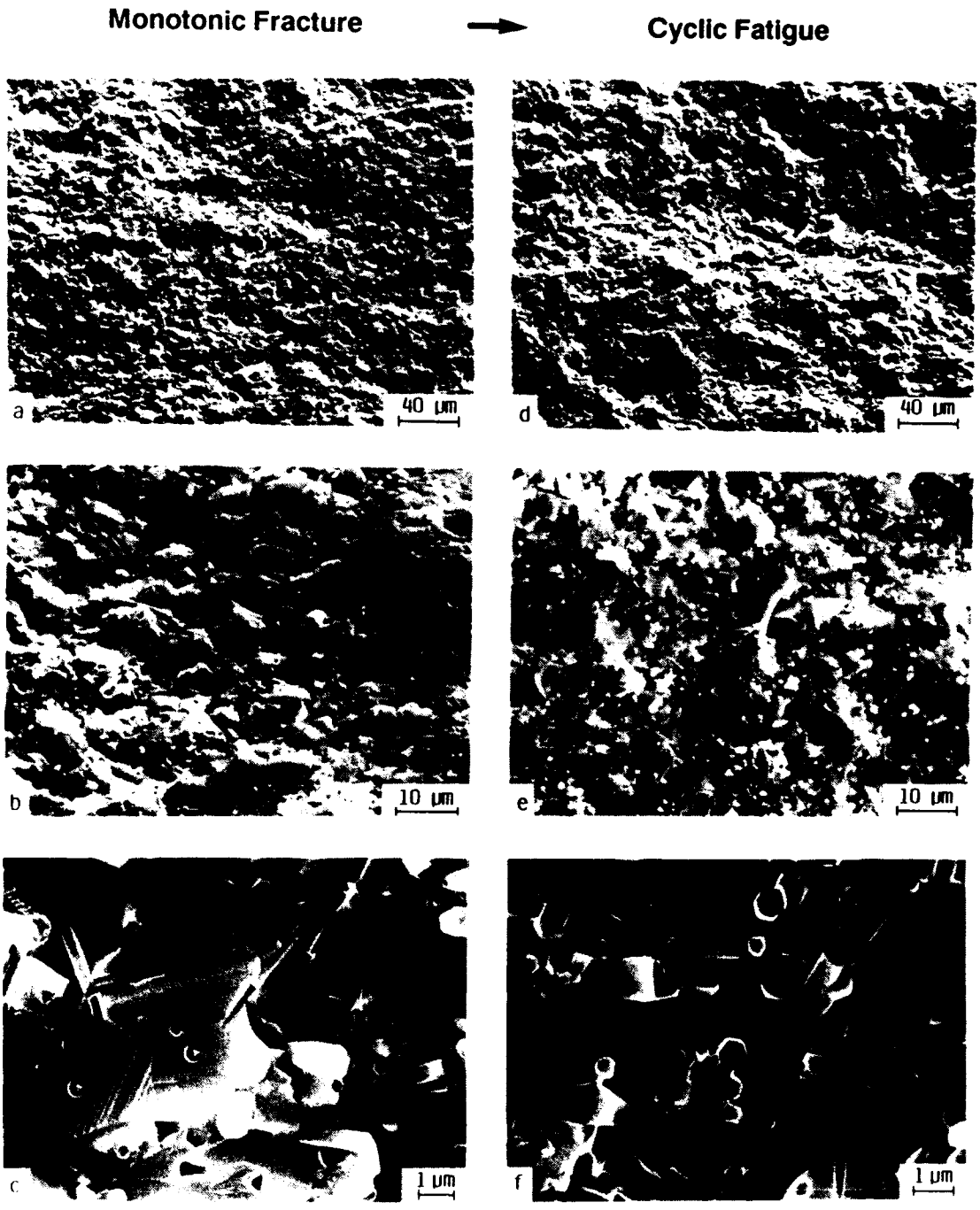

Fig. 2.13. Scanning electron micrographs at increasing magnification of a,b,c) monotonic fracture and c,d,e) cyclic fatigue fracture in a SiC-whisker-reinforced alumina composite, showing the predominantly transgranular nature of crack paths and regions of cleavage-like steps (indicated by letter C) formed under quasi-static loading, compared to the rougher more intergranular fracture surfaces induced by cyclic loading. Horizontal arrow indicates direction of crack growth [33].

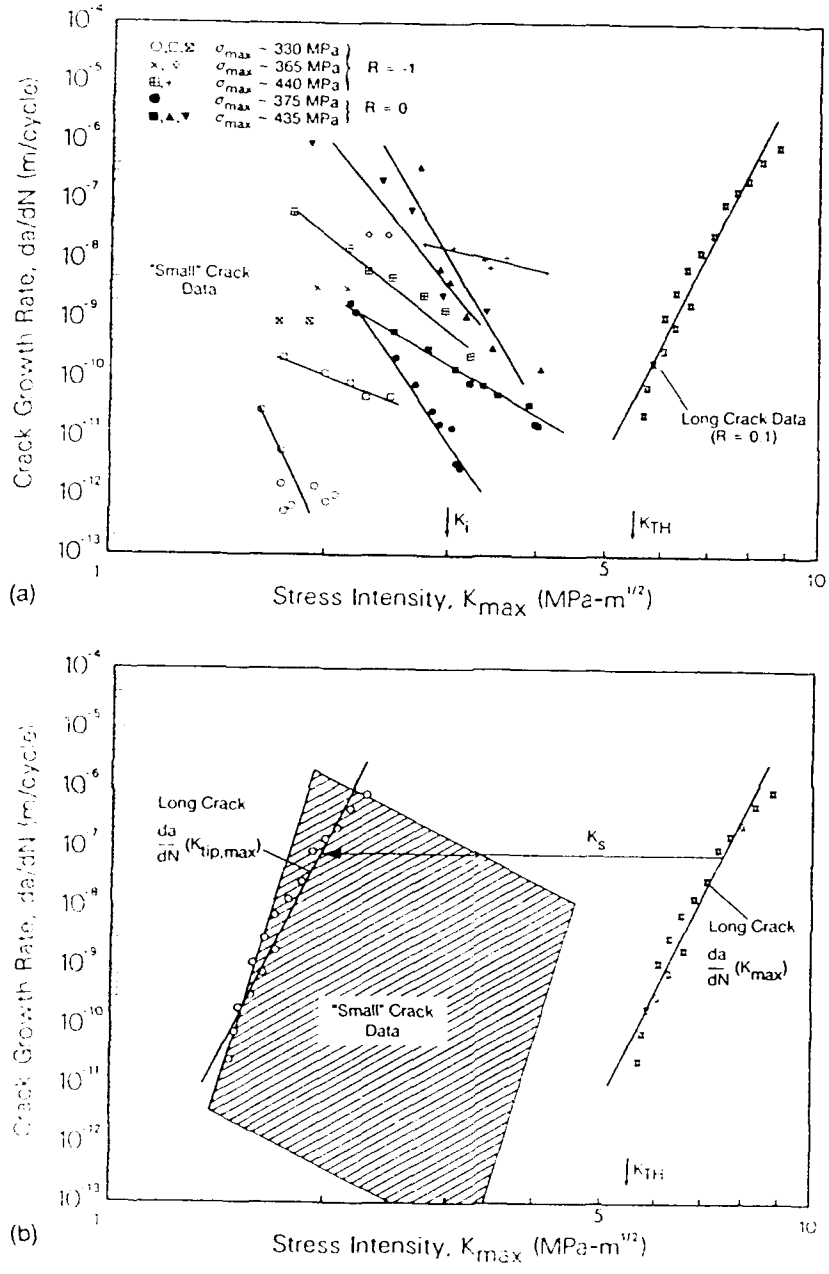

Fig. 2.14. Small-crack growth-rate data in MS-grade Mg-PSZ from cantilever-bend specimens, as a function of K_{max} at R = 0 and -1, compared to corresponding long-crack data as a function of the maximum applied stress intensity in a), and b) showing schematically small-crack data compared to the near-tip stress-intensity relationship for the long-crack data computed from Eq. 6. Note how small cracks propagate at stress-intensity levels well below the long-crack threshold, ΔK_{TH}, for cyclic crack-growth, and even below the initiation toughness, K_i, for monotonic loading in a); initial growth, however, occurs at stress intensities typical of unshielded long cracks in b) [8].

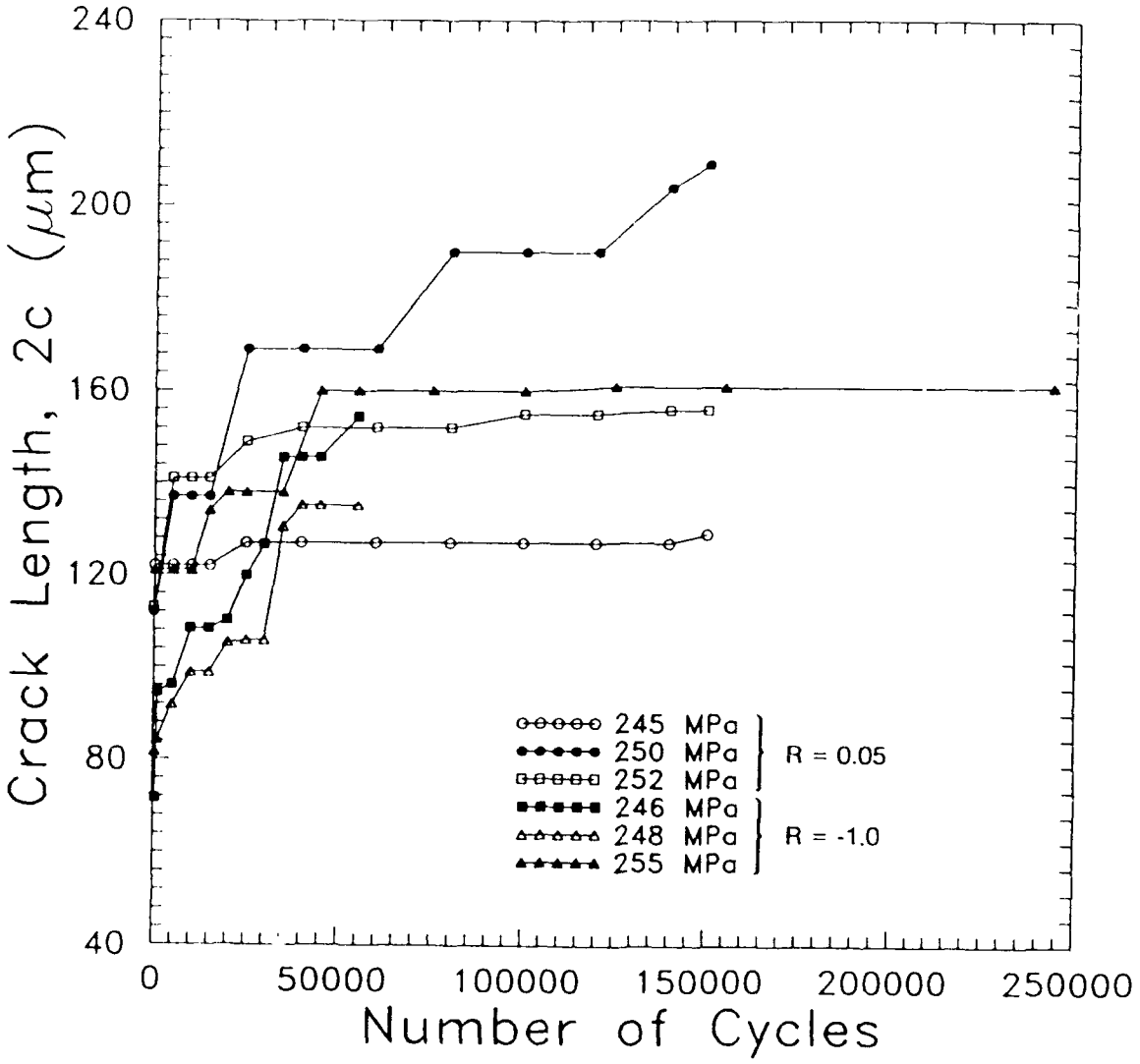

Fig. 2.15. Small-crack data from micro-indented cantilever-bend samples of a Al_2O_3-SiC_w composite, showing comparison of surface crack length 2c vs. number of cycles results for tension-tension (R = 0.05) and tension-compression (R = -1.0) cycling at similar applied stress levels [33].

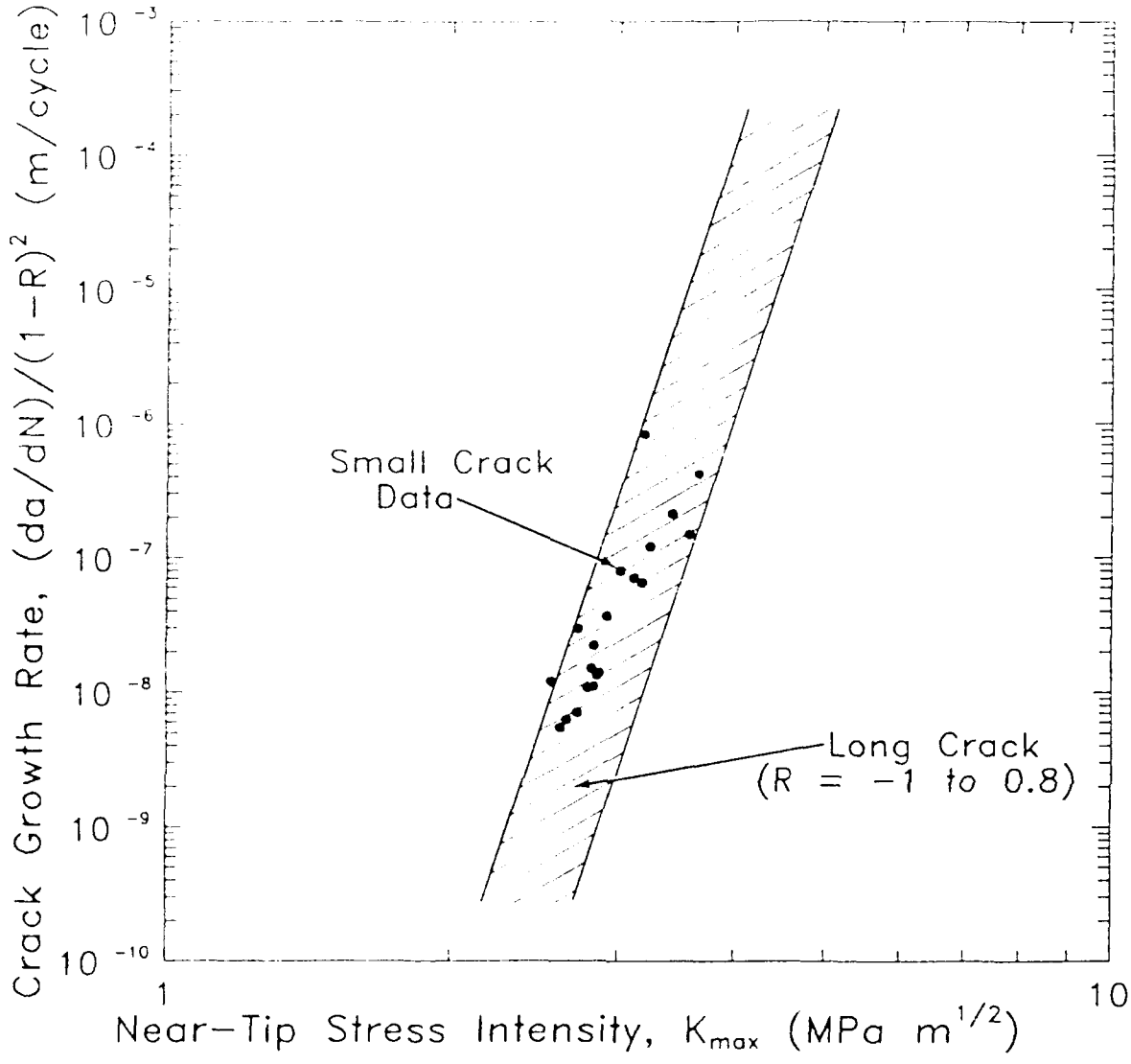

Fig. 2.16. Small-crack growth rates emanating from micro-indents in cantilever-bend samples of 3Y-TZP, plotted as a function of a) the nominal stress intensity, K_{max}, and b) the near-tip stress-intensity, $K_{tip,max}$ (= K_{max} - K_s), after correcting for shielding due to the residual stress field of the indent. Note in b) how, when characterized in terms of the near-tip stress intensity, a close correlation is obtained between long and small crack results [10].

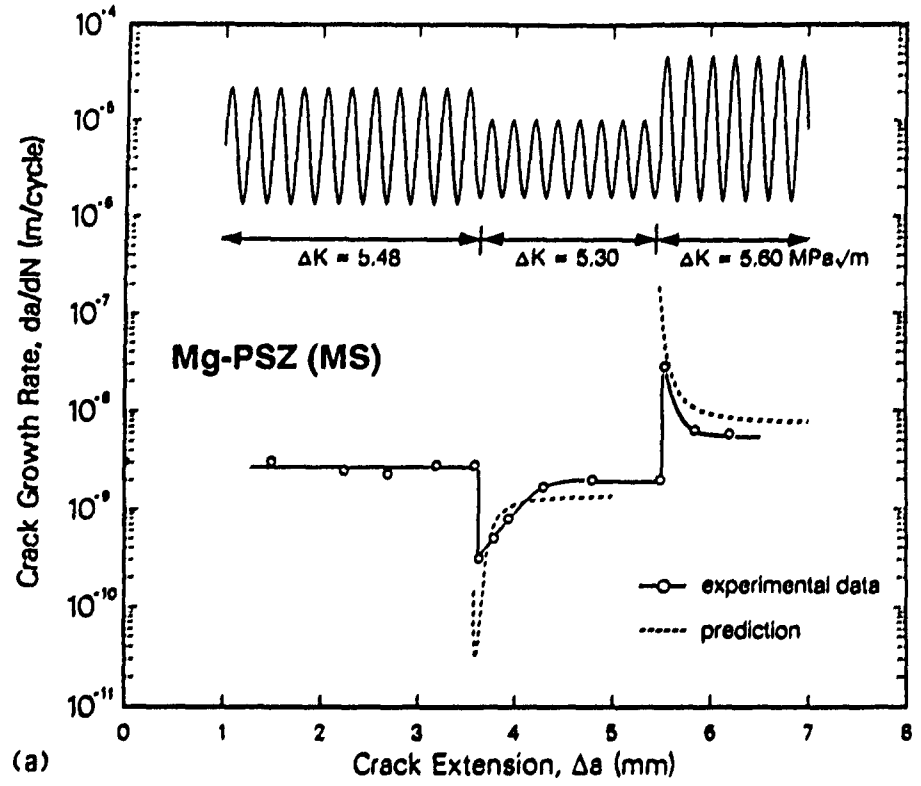

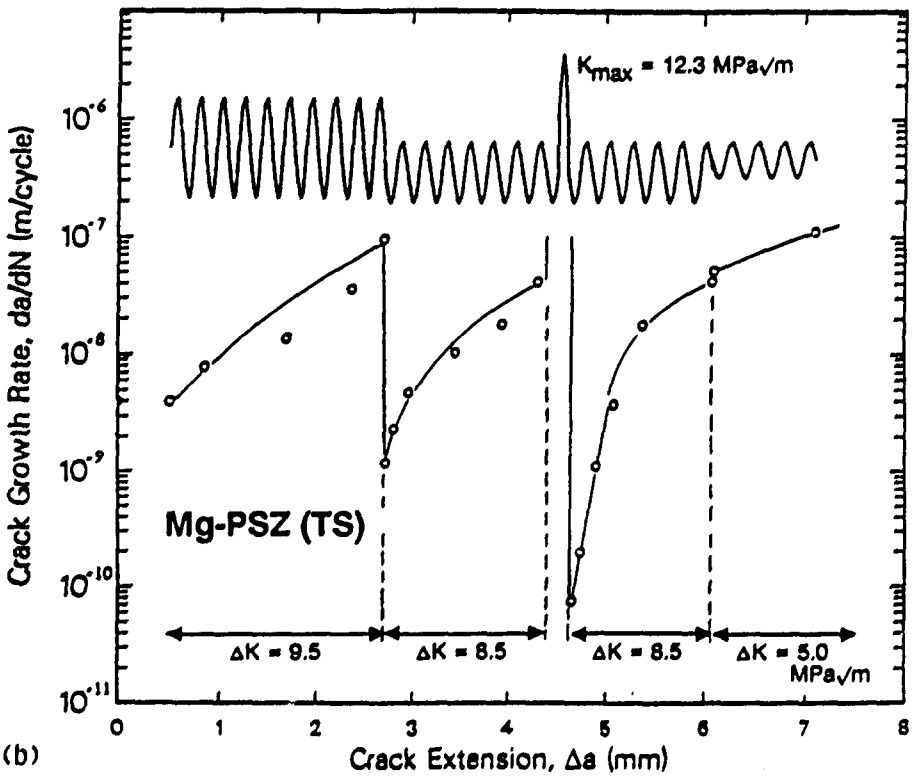

Fig. 2.17. Transient fatigue-crack growth behavior in a) MS-grade Mg-PSZ, and b) TS-grade Mg-PSZ, showing variation in crack-growth rates following high-low and low-high block overloads and single-tensile overloads. Predictions of transient crack-growth behavior in a) rely on steady-state crack-growth data (Fig. 2.8) and transformation-zone size measurements using Raman spectroscopy (Fig. 2.18) [49] to compute the crack-tip "driving force" following load changes [5].

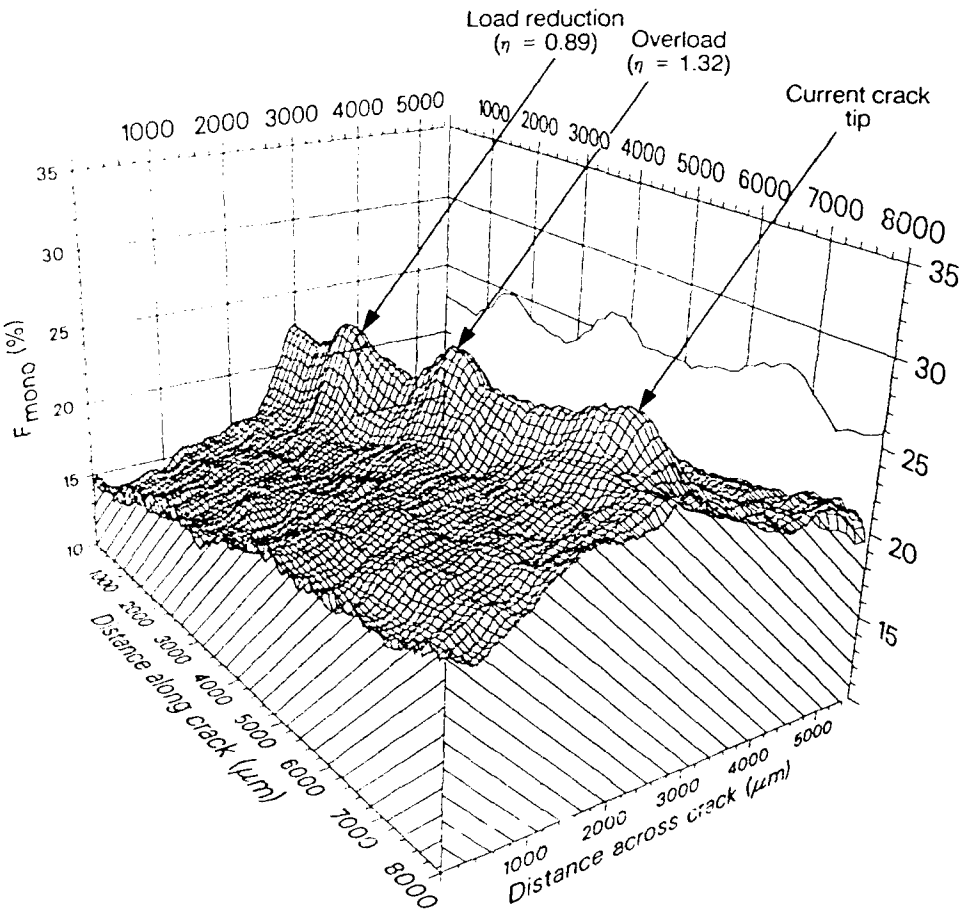

Fig. 2.18. Morphology of the transformation zone, indicated by the volume fraction of transformed phase, F_{mono}, surrounding a fatigue crack in TS-grade Mg-PSZ, following the variable-amplitude loading sequence shown in Fig. 2.17. The extent of transformation is clearly observed to respond to the applied loading conditions [5]. Results are derived from Raman spectroscopy measurements [5,49].

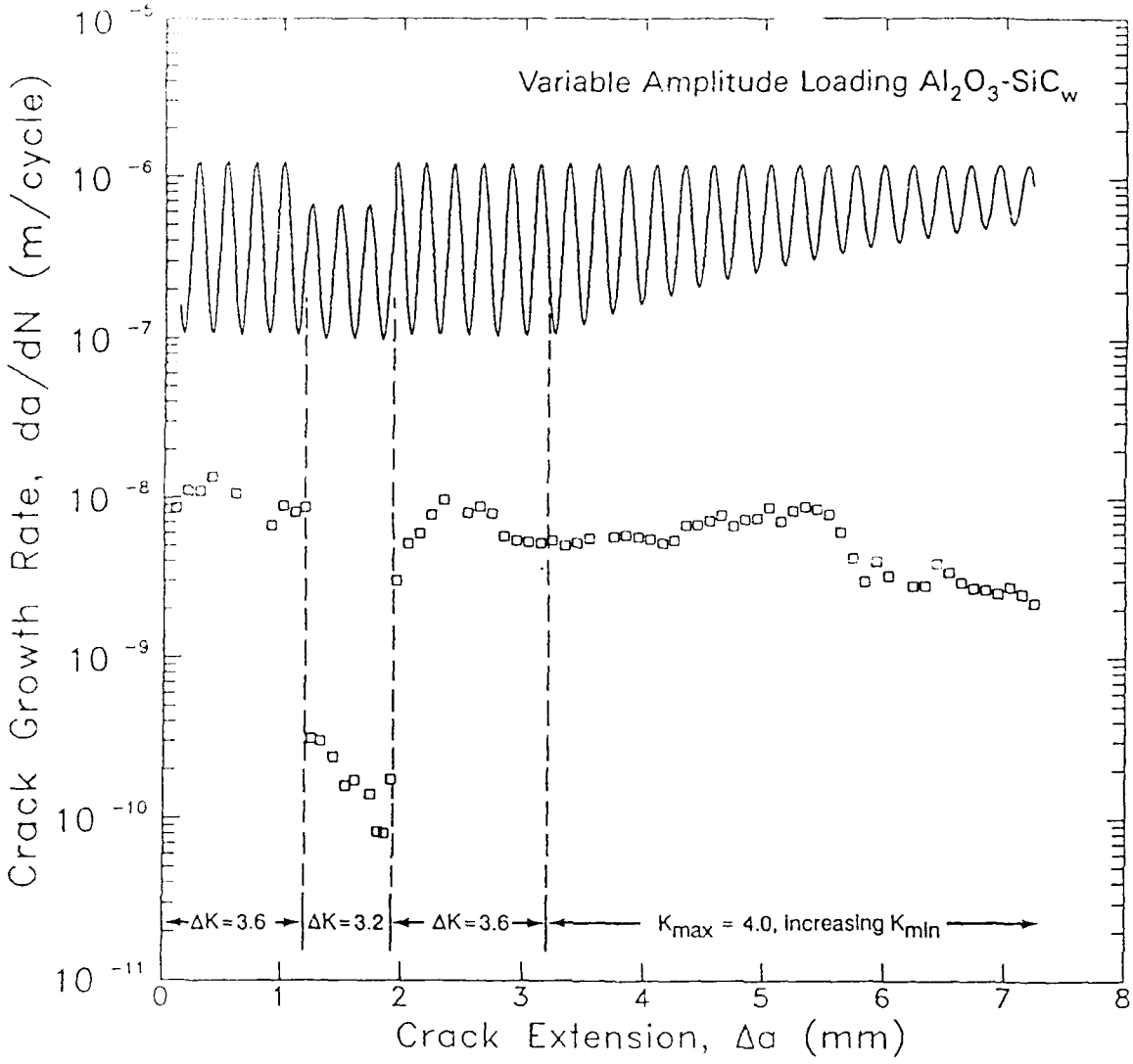

Fig. 2.19. Transient fatigue-crack growth behavior in a SiC-whisker-reinforced alumina composite, showing variation in growth-rates following high-low, low-high and constant-K_{max}/variable-R (increasing K_{min}) block-loading sequences [33].

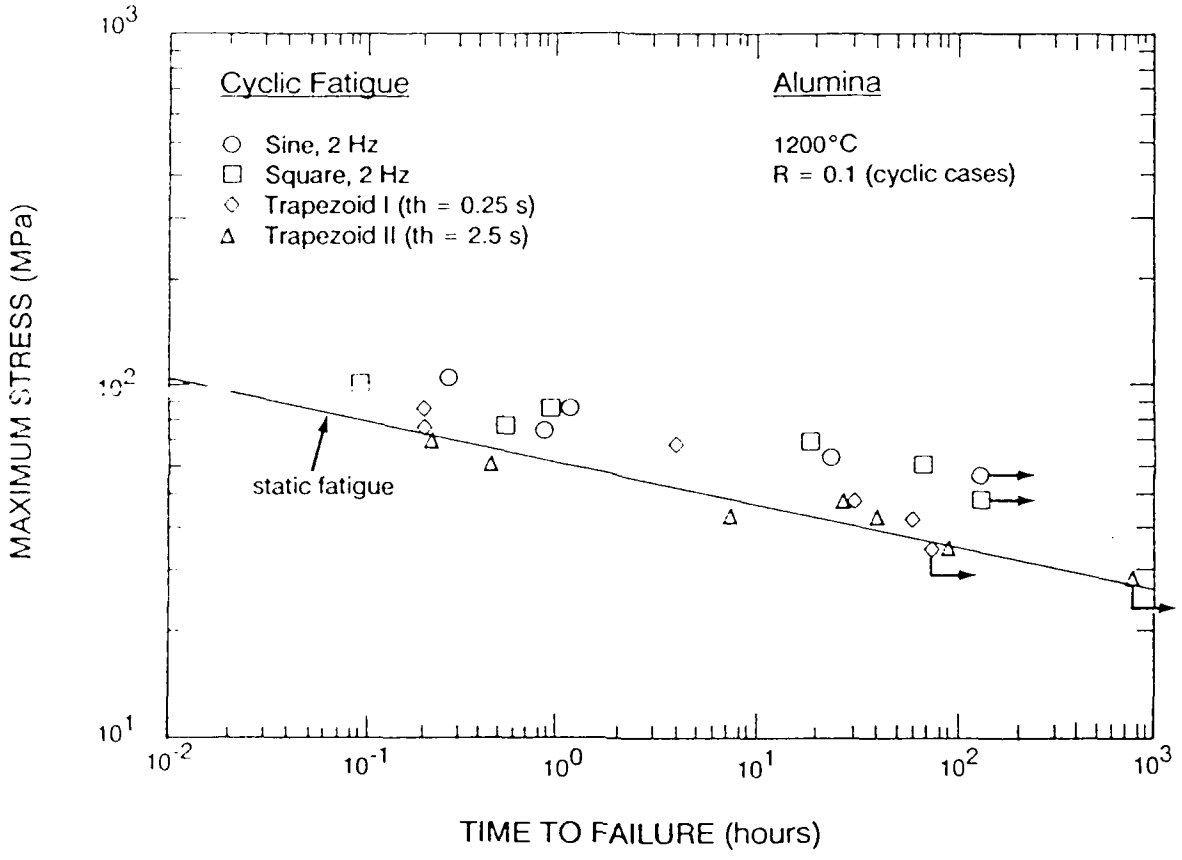

Fig. 2.20. Elevated temperature (1200°C) stress/life data for a commercial polycrystalline alumina, tested in uniaxial tension (R = -1 for cyclic tests), showing a comparison of results for cyclic and quasi-static loading. Note that in contrast to behavior at ambient temperatures (Fig. 2.2a), at a given applied stress, the cyclic fatigue samples do not necessarily yield the shortest lives [22].

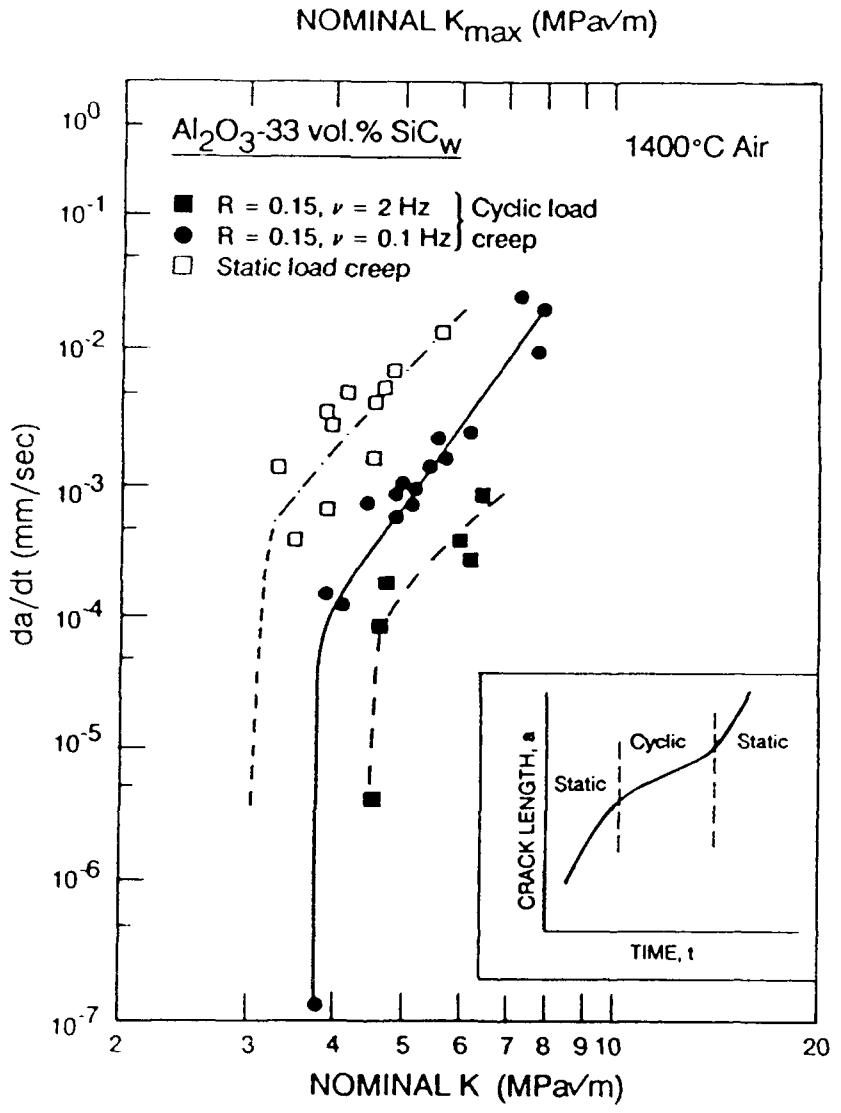

Fig. 2.21. Elevated temperature (1400°C) crack-propagation data for a SiC-whisker-reinforced alumina, tested in four-point bending (R = 0.15 for cyclic tests), showing a comparison of results for cyclic and quasi-static loading. Note that in contrast to behavior at ambient temperatures (Fig. 2.11), at a given applied stress intensity, the cyclic fatigue samples do not yield the fastest crack velocities [32].

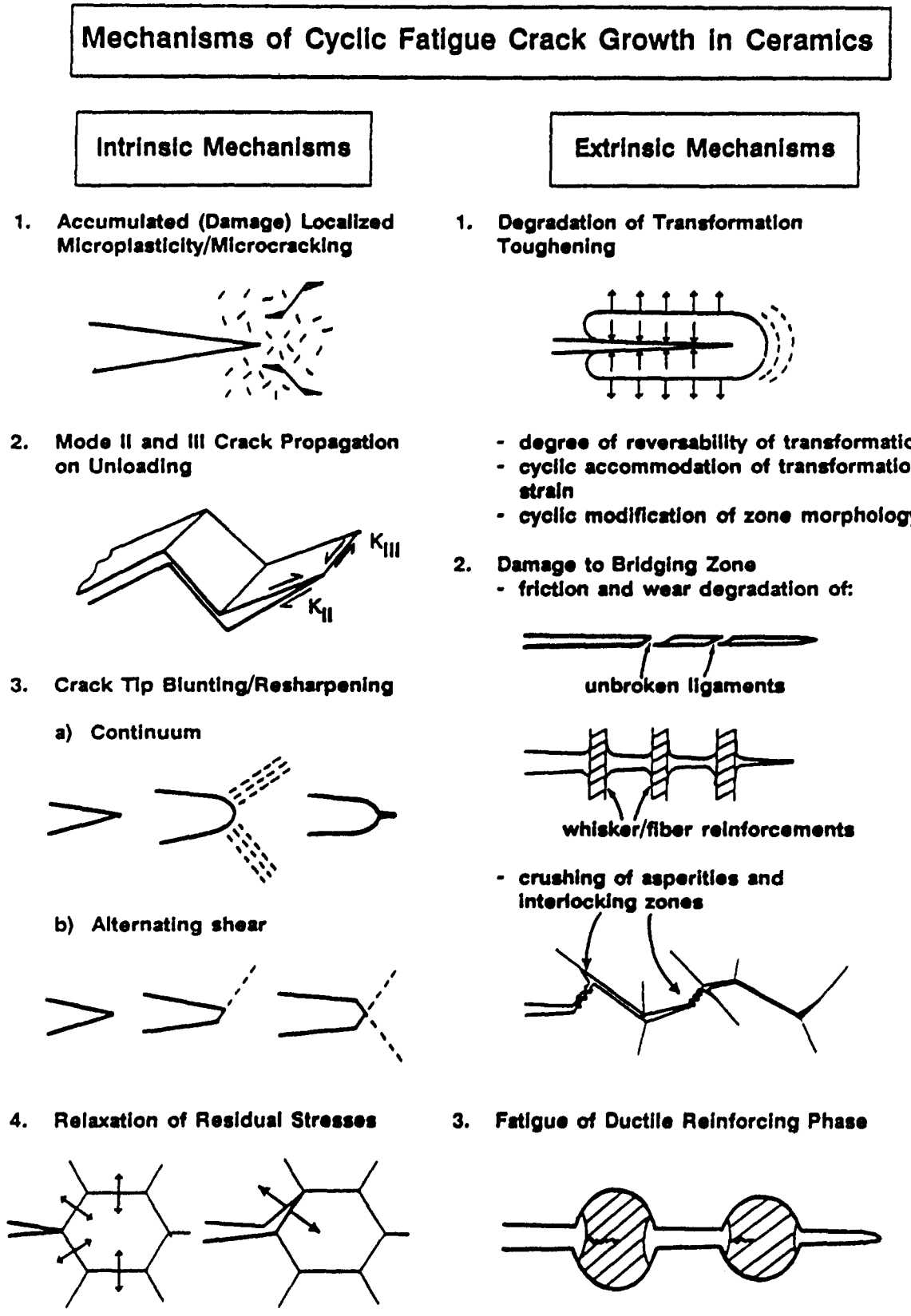

Fig. 2.22. Schematic illustration of possible crack-advance micro-mechanisms during cyclic fatigue-crack propagation in monolithic and composite ceramics [12].

3. CYCLIC FATIGUE DAMAGE IN A CONTINUOUS SiC FIBER REINFORCED Al_2O_3 COMPOSITE

(R. M. Petrany, R. H. Dauskardt and R. O. Ritchie)

3.1 Introduction

In ceramic fiber composites, substantial toughening and marked R-curve behavior can be attributed to crack bridging in the wake of the crack tip. This occurs via unbroken fibers which span the crack faces and inhibit crack opening. For such a mechanism to operate, the shear strength of the fiber-matrix interface must be sufficiently low to permit fiber pull-out with the passage of the main crack. Progressive weakening of the interface has been suggested as a possible mechanism which may lead to a cyclic fatigue response in these materials.

In recent years, there has been a growing awareness that ceramic materials can be susceptible to premature failure under alternating loads. Strength degradations have been found to occur at rates faster than predicted from tests performed under static loading. Although initially attributed to non-linearity associated with transformation toughening, other possible inelastic mechanisms at the crack tip which may give rise to a fatigue effect include microcracking and the progressive weakening of interfaces mentioned above.

Cyclic fatigue degradation has now been shown for a wide range of both monolithic and composite ceramics, including TZP, Mg-PSZ, Al_2O_3, Si_3N_4, pyrolytic-carbon-graphite, and Al_2O_3-SiC_w, in notched-bar compression-compression crack growth tests [1,2], in smooth-bar tension-tension and tension-compression low cycle fatigue tests [3-5], and in fracture-mechanics style fatigue crack growth tests under tension-tension and tension-compression loading [6-11]. Cyclic fatigue responses have also been reported in a SiC fiber-reinforced Si_3N_4 composite [12].

In the present study, cyclic fatigue crack growth is examined for a continuous SiC fiber reinforced Al_2O_3 matrix composite. Microstructural effects resulting from a variation in monotonic and cyclic loads are also shown.

3.2 Experimental Procedures

Material: This study is being conducted on a bidirectional woven silicon carbide (Nicalon) fiber reinforced alumina matrix composite developed by Alcoa. The composite consists of a 50% volume fraction of fibers ($v_f = 0.50$), 39% matrix ($v_m = 0.39$) and 11% voids ($v_v = 0.11$). Fibers run continuously through the composite with individual fiber layers positioned perpendicular to one another. Fibers are homogeneously composed of ultrafine β-SiC crystals with excess carbon and 9 to 11% oxygen supplied as silicon dioxide.

Compact tension C(T) specimens were supplied by Alcoa as shown in Figure 3.1. Specimens were polished on one side face using 6 μm diamond paste. This facilitates a better surface for the adhesion of a crack gauge used to monitor the crack length.

Test Procedures: Fatigue-crack growth tests were performed essentially according to ASTM Standard E 647-86A for measuring growth rates in metals, modified using the procedures developed for ceramics by Dauskardt and Ritchie [8]. High-resolution, computer-controlled, servo-hydraulic testing machines were utilized to measure cyclic crack-growth rates. However, prior to testing, the creation of the pre-crack was the most difficult aspect of the test and may take as long as several days. A wedge shaped starter notch was first machined into the specimen. A 50 Hz sine-wave load was then applied at a load ratio of 0.1 until crack growth can be detected. To detect crack growth, a Ni-Cr foil of ~ 0.1 μm thickness was evaporated onto the side face of the specimen. Changes in the direct-current electrical potential of the foil were then used to measure crack movement as the foil fails. This technique offers a resolution of better than ± 5 μm. Once a through-thickness crack of several millimeters was obtained, further crack growth testing could then proceed.

Unloading compliance measurements using back-face strain gauges were also used to evaluate the extent of fatigue crack closure in terms of the far-field closure stress intensity, K_{cl}, at first contact of the fracture surfaces during the unloading cycle. The K_{cl} value is calculated from the highest load where the elastic unloading compliance line deviates from linearity.

Crack-growth rates, da/dN, were determined over the range of 10^{-11} to 10^{-5} m/cycle under computer-controlled K-decreasing and K-increasing conditions. An MTS 810 servohydraulic load frame together with an MTS 458 MicroConsole controller provided the high-resolution displacement control and load stability required for testing of these brittle composite materials.

3.3 Results and Discussion

Pre-cracking: The creation of a pre-crack has presented the greatest problem in studying this material. In addition, it was often observed that the crack length recorded from the Ni-Cr foil did not represent the through-thickness crack length. This is primarily a result of large bridging zones present within the composite. Without an accurate measurement of the crack length, interpretation of cyclic fatigue-crack growth data becomes relatively uncertain.

Possible solutions that are currently under investigation include monitoring the crack length manually using optical techniques. A long-distance microscope, with a resolution of 1.1 μm, was adapted for observing crack propagation along the side face of the specimen. With the

lens positioned 150 mm from the specimen surface, a precision translation stage allows accurate positioning of the microscope to within 0.5 μm. At the present time, this microscope is being used to record and process video images, using image analysis techniques, as the crack propagates through these composite microstructures.

Compliance techniques offer a second possible solution. Fatigue-crack propagation in ceramics is accompanied by some degree of crack closure - i.e., a premature contact between the crack surfaces during the unloading cycle. Its effect is to reduce the local stress-intensity range actually experienced at the crack tip from the nominal value ($\Delta K = K_{max} - K_{min}$) to an effective value ($\Delta K_{eff} = K_{max} - K_{cl}$). Utilization of this technique will also allow the examination of the degree of bridging present behind the crack tip. Ultimately, compliance techniques combined with optical observations will lead to an accurate estimate of the through-thickness crack length.

Fractography: The basic microstructural characteristics of the composite are shown in the representative SEM micrographs shown in Figure 3.2. Detail from the side face of the specimen is shown in Figures 3.2(a),(c) while Figures 3.2(b),(d) represent the front face. One can clearly observe the orientation of the individual fiber layers relative to one another.

The crack-path morphology conveying evidence of frequent crack deflection is shown if Figure 3.3(a). The fracture surface, also shown in a montage of micrographs (Figure 3.3(b)), shows increased damage, associated with increased roughness, near the notch tip where the crack was grown under cyclic loading. Fast-fracture under monotonic loading, prior to final failure of the specimen, results in a less rough fracture surface. Better evidence is apparent at higher magnification in the set of micrographs shown if Figure 3.4. The region of the specimen that has been cyclically loading shows an increase in the degree of fiber damage and bundle pullout (Figure 3.4(a)). The less damaged fracture appearance of the fast fracture is shown is Figure 3.4(b).

Evidence of extensive crack bridging along a crack profile is shown in Figure 3.5(a). In addition, the degree of fiber pullout is shown in Figure 3.5(b). These factors, which are highly effective in promoting increased toughness and composite strength, are largely responsible for the difficulty in determining an accurate estimate of the crack length during the experiment, and thus, has made it difficult to obtain any accurate cyclic fatigue-crack growth data at this time.

3.4 Conclusions

Based on the results of the experiments on monotonic and cyclic crack growth in a bidirectional SiC-reinforced Al_2O_3 ceramic-matrix composites, the following observations can be drawn:

1. Through thickness pre-cracking of the continuous-fiber-reinforced composite has been achieved.

2. The crack was grown under both cyclic and monotonic loading conditions.

3. Cyclic tension-tension loading yields a more damaged microstructural appearance than monotonic loading.

3.6 References

1. L. Ewart and S. Suresh, *J. Mater. Sci.* **22** (1987) 1173.

2. S. Suresh, L. X. Han and J. P. Petrovic, *J. Amer. Ceram. Soc.* **71** (1988) C158.

3. T. Kawakubo K. Komeya, *J. Amer. Ceram. Soc.* **18** (1987) 400.

4. M. V. Swain and V. Zelizko, pp. 595-606 in *Advances in Ceramics, 24B Science and Technology of Zirconia III.* Edited by S. Somioya, N. Yammoto, and H. Hanagida. American Ceramic Society, Westerville, OH, 1988.

5. M. Masuda et al., *J. Ceram. Soc. Japan* **96** (1988) 275.

6. R. H. Dauskardt. W. Yu and R. O. Ritchie, *J. Amer. Ceram. Soc.* **70** (1987) C248.

7. M. J. Reece, F. Guiu and M. F. R. Sammur, *J. Amer. Ceram. Soc.* **72** (1989) 348.

8. R. H. Dauskardt and R. O. Ritchie, *Closed Loop* **17** (1989) 7.

9. L. X. Han and S. Suresh. *J. Amer. Ceram. Soc.* **72** (1989) 1233.

10. A. Grossmuller, V. Zelizko and M. V. Swain, *J. Mater. Sci.* **8** (1989) 29.

11. R. O. Ritchie, R. H. Dauskardt and F. J. Pennisi, *J. Biomed. Mat. Res.* **25** (1991) in press.

12. J. Holmes, *J. Amer. Ceram. Soc.* **74** (1991), 1639.

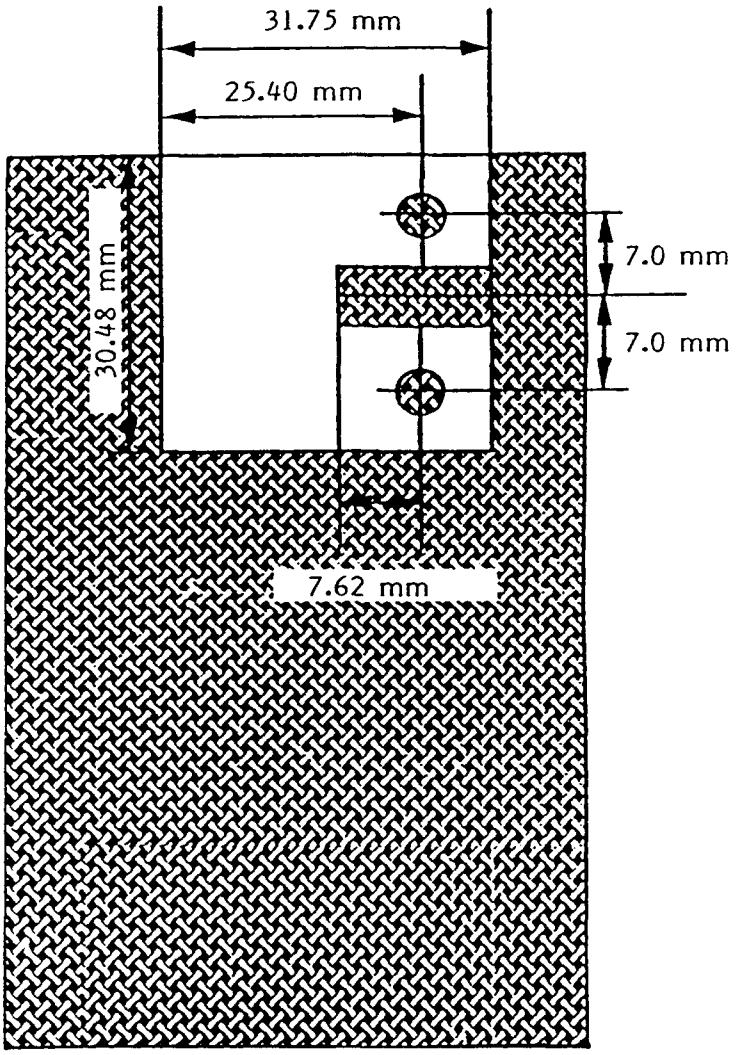

Fig. 3.1. Compact tension C(T) geometry of specimens supplied by Alcoa. Specimens were polished to a thickness of approximately 2.5 mm prior to testing.

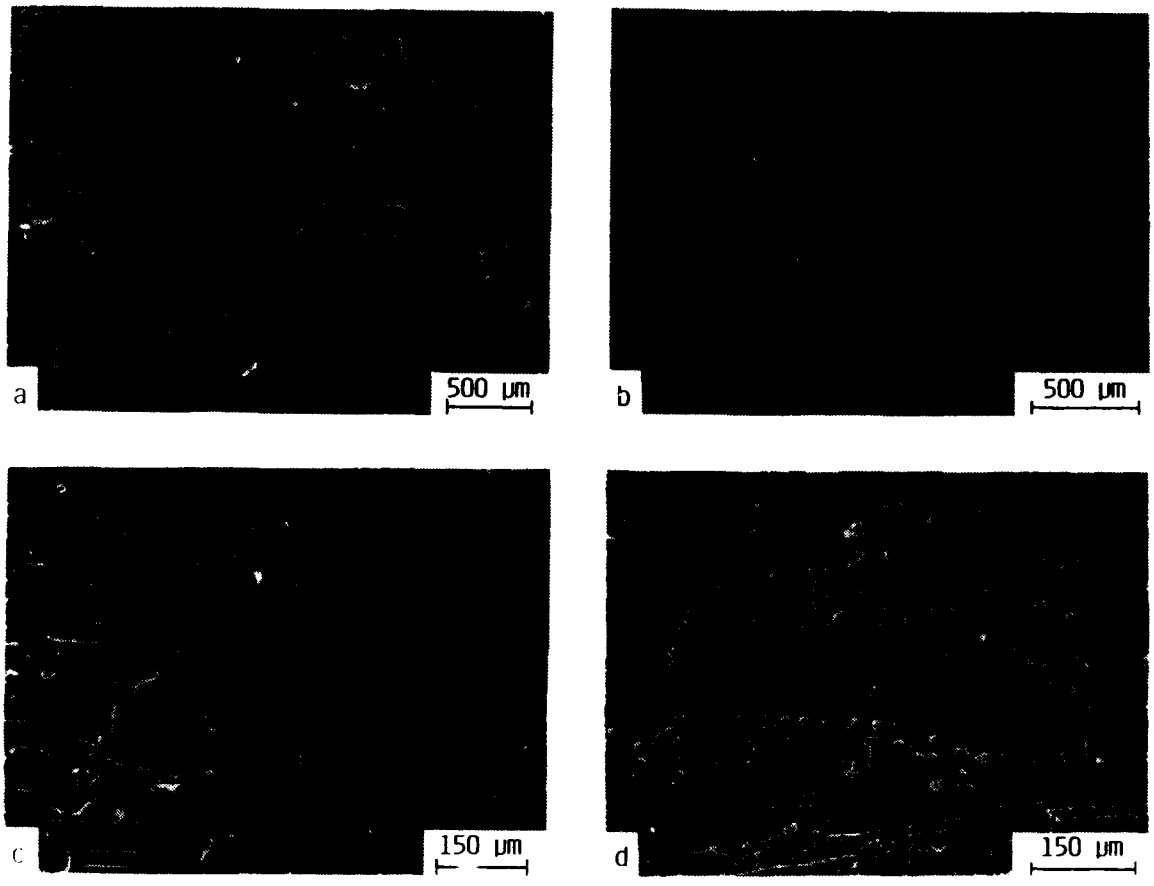

Fig. 3.2. Representative scanning electron micrographs of the Al_2O_3/SiC composite microstructure. (a) and (c) represent the side face of the specimen while (b) and (d) represent the front face. Note the relative 90 degree orientation of the individual fiber layers. Arrow indicates general direction of crack growth.

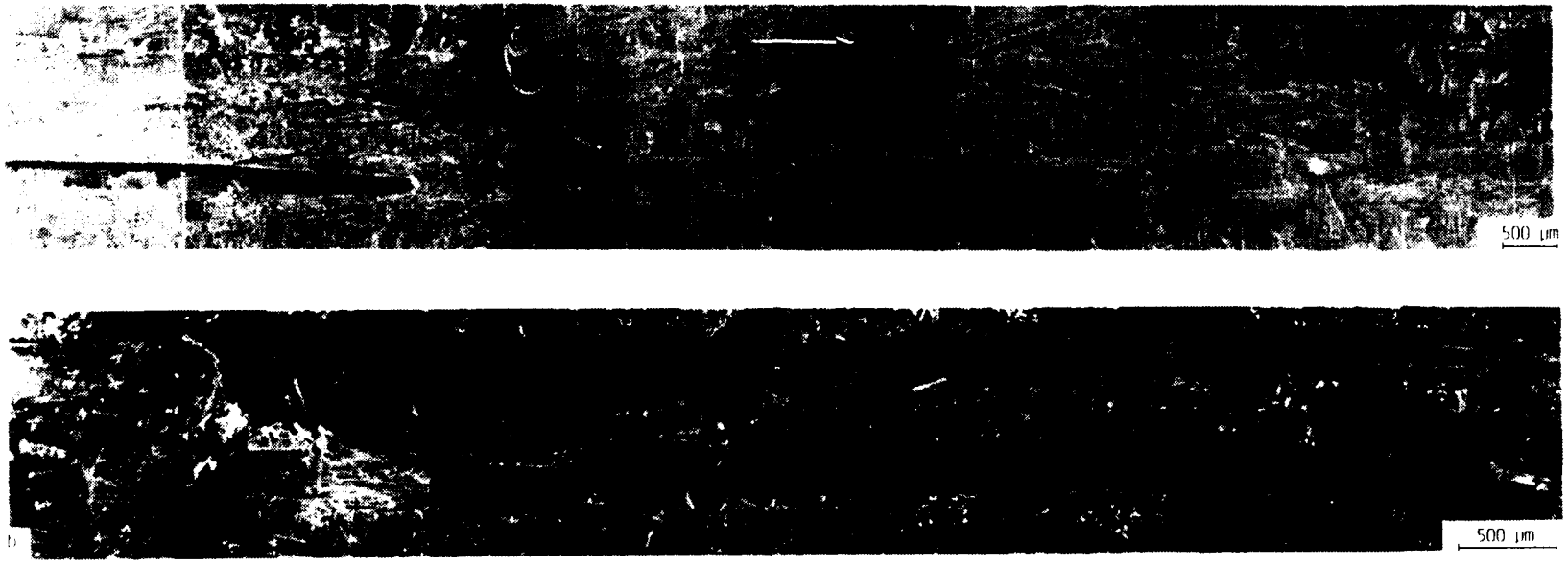

Fig. 3.3. Scanning electron micrographs showing (a) a crack path morphology conveying evidence of crack bridging and crack deflection and (b) a fracture surface showing damage caused by monotonic and cyclic loads. Note that the notch is positioned on the left side of the photograph. Arrow indicates general direction of crack growth.

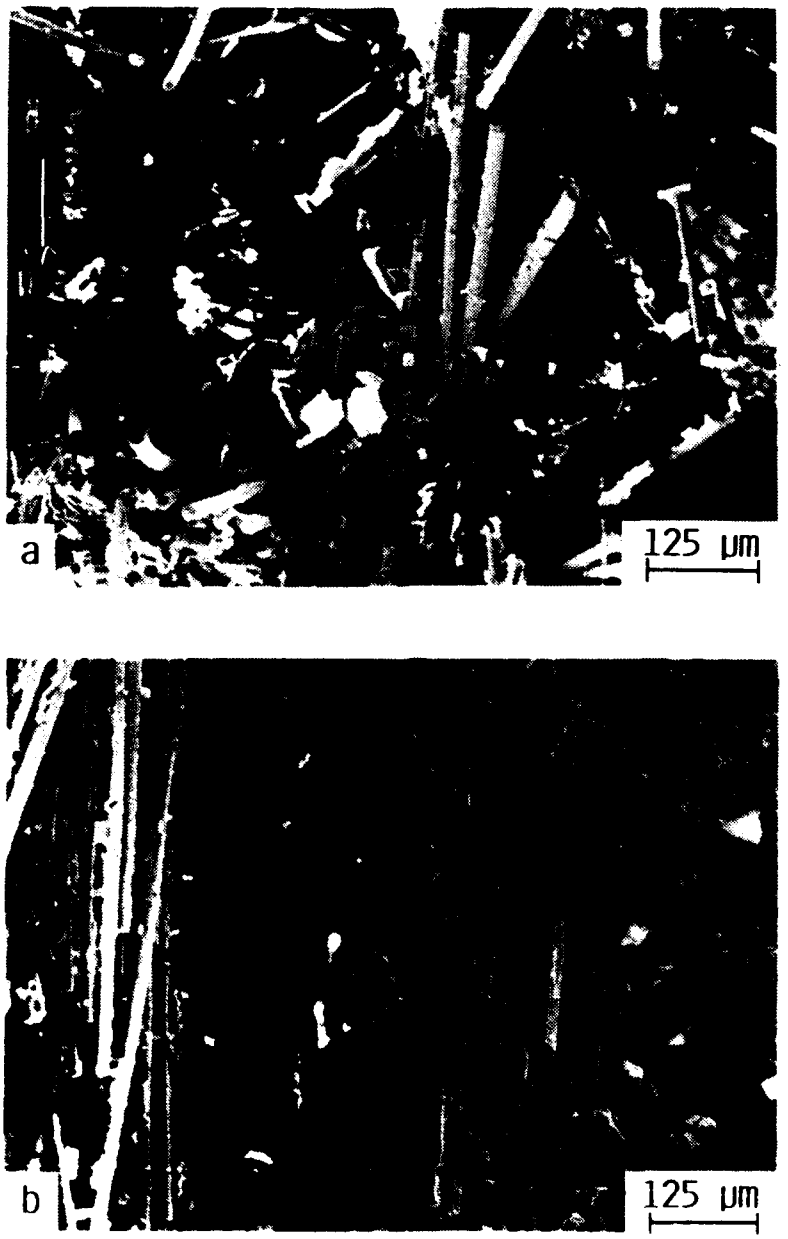

Fig. 3.4. Scanning electron micrographs of the fracture surface at higher magnifications showing the effect of (a) cyclic loading and (b) monotonic loading. Note the increase in damage caused by the application of a cyclic load. Arrow indicates general direction of crack growth.

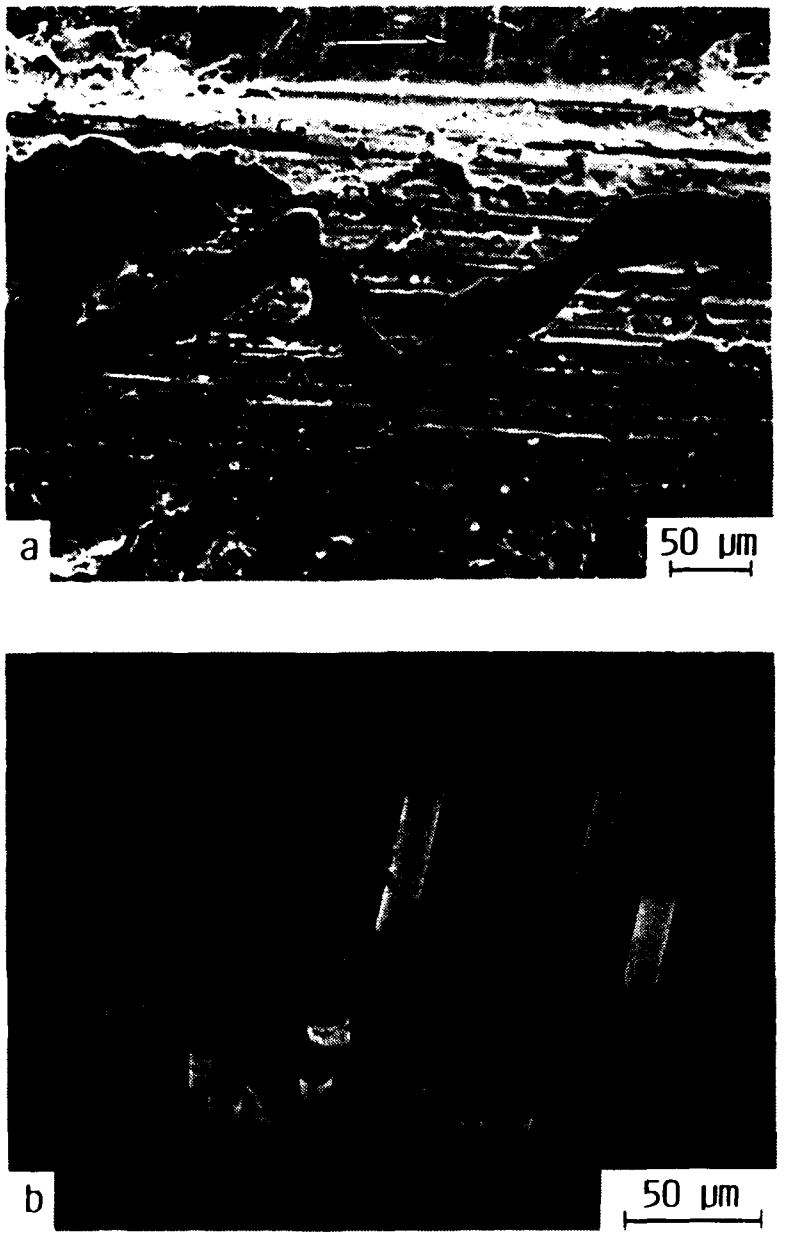

Fig. 3.5. Scanning electron micrographs showing evidence of (a) crack bridging and (b) fiber pullout. These factors have been responsible for the difficulty in accurately determining the through-thickness crack length prior to testing. Arrow indicates general direction of crack growth.

4. CYCLIC FATIGUE-CRACK GROWTH BEHAVIOR OF SHORT CRACKS IN SiC-REINFORCED LAS GLASS-CERAMIC COMPOSITE

(E. Y. Luh, R. H. Dauskardt and R. O. Ritchie)

4.1 Introduction

In recent years, there has been a growing awareness that ceramic materials can be susceptible to premature failure under alternating loads (cyclic fatigue). Essentially, strength degradations have been found to occur at rates faster than predicted from tests performed under static loading. This has now been shown for a wide range of both monolithic and composite ceramics, including Mg-PSZ, Al_2O_3, TZP, Si_3N_4, pyrolytic-carbon/graphite and Al_2O_3-SiC_w, in smooth-bar tension-tension and tension-compression low-cycle fatigue (LCF) tests [e.g., 1-3], in notched-bar compression-compression crack-growth tests [e.g., 4,5], and in fracture-mechanics style fatigue-crack growth tests under tension-tension and tension-compression loading [6-11]. In light of the very limited crack-tip plasticity apparent in ceramic materials, the mechanisms for such "ceramic fatigue" remain uncertain. However, the effect may more readily be explained in materials which show strong resistance-curve (R-curve) behavior, specifically where toughening, by such mechanisms as phase transformation, microcracking, and whisker-, fiber- and ductile-particle-reinforcement, induces significant local inelastic (non-linear) deformation behavior.

For metallic structures, the importance of cyclic fatigue in design is generally taken into account by utilizing either classical stress/life (S/N) approaches or damage-tolerant concepts which incorporate crack-growth data characterized using fracture mechanics (Fig. 2.1a,b). In the former case, smooth- or notched-bar tests are used to determine S/N or LCF curves from which the number of cycles to cause failure at a particular applied stress or strain can be estimated (with appropriate safety factors); this approach can be readily applied to ceramics. For safety-critical applications, however, more conservative damage-tolerant approaches are often used which rely on the integration of crack-velocity/stress-intensity (v/K) curves (of the form of the Paris power-law [12] - $da/dN = C\ \Delta K^m$) to estimate the time or number of cycles for a presumed initial crack to grow to critical size (e.g., defined at the fracture toughness K_{Ic}). For ceramics, such cyclic v/K data have now been generated - to date for MgPSZ, Al_2O_3, pyrolytic-carbon/graphite and Al_2O_3-SiC [6-11] - although the approach may prove difficult to utilize in practice because of the large power-law dependence of growth rates (da/dN) on the range of stress intensity (ΔK) in these materials, i.e., values of the exponent m are typically 30 and above [6-8]. This implies that the estimated life will be proportional to the reciprocal of the applied stress raised to the 30th power!

An alternative procedure is to redefine the critical crack size in terms of the cyclic fatigue threshold ΔK_{TH}, below which crack growth is presumed dormant. Based on data in Mg-PSZ and Al_2O_3 ceramics [6-8], values of ΔK_{TH} are of the order of 50% K_{Ic}. A complication with this approach, however, is the "anomalous" growth-rate behavior of small cracks. Based on extensive studies in metallic materials [e.g., 13-17], small cracks (or microcracks), of a size comparable to microstructural dimensions, the extent of local crack-tip inelasticity, or simply physically small (e.g, $\leq$ 500 μm), have been found to grow at rates well in excess of corresponding "long" cracks (or macrocracks) subjected to the same nominal stress-intensity range, and to propagate at ΔK levels below that of the (long-crack) threshold ΔK_{TH} (Fig. 2.1c).

There are currently few examples in the literature of such cyclic fatigue behavior of small cracks in ceramics [18,19]. However, observations of sub-threshold growth rates continuously decreasing with crack extension have been reported under monotonic loading (static fatigue). These involve ~100 μm long cracks growing out of the residual stress field surrounding Knoop microhardness indentations in soda-lime glass [20], and ~20-200 μm long surface cracks in dead-loaded four-point bend specimens of Mg-PSZ [21]. However, there are no small-crack results for ceramic composites under either monotonic or cyclic loading. Accordingly, the objective of the current work was to examine the cyclic fatigue behavior of short cracks (20-300 μm) emanating from notches in an advanced glass-ceramic composite.

4.2 Experimental Procedures

3-mm-thick plates of lithium-aluminosilicate glass-ceramic, continuously reinforced with 50 vol % unidirectional Nicalon fibers (LAS/SiC_f), were received from United Technologies. Microscopy indicated that the fibers, with average radius ~8 μm, consisted of fine-grained β-SiC, surrounded by both amorphous (SiO_2, Al_2O_3 and Nb_2O_5) and microcrystalline (Nb and Zr) reaction layers in a semi-crystalline LAS matrix (Table 4.1).

Table 4.1 - Mechanical Properties of LAS/SiC_f Glass-Ceramic Composite

Fiber Volume Fraction - f	Fiber Radius - r (μm)	Interfacial Shear Strength - τ (MPa)	Elastic Moduli E_f (GPa)	Elastic Moduli E_m (GPa)	Poisson's Ratio - ν
0.5	8	2	210	85	0.25

In LAS/SiC_f, substantial toughening and marked R-curve behavior has been attributed to crack bridging in the wake of the crack tip [22-25]; this occurs via unbroken fibers which span the crack faces and inhibit crack opening (Fig. 4.1). For such a mechanism to operate, the shear strength of the fiber/matrix interface must be sufficiently low to permit fiber pull-out with passage of the main crack. In LAS/SiC_f, frictional slipping has been observed at the fiber/matrix interface [23], implying a very low interfacial shear strength τ. In fact, push-through and indentation tests on individual fibers in this glass composite gave measured values of $\tau \approx 2$ MPa [23]. The low interfacial strength appears to result from the presence of the glassy reaction layer in the fiber/matrix interface, formed during prior hot pressing; although strongly bonded to the glass matrix, this amorphous layer adheres only weakly to its adjacent microcrystalline reaction layer (Fig. 4.2). With prolonged exposure to high-temperatures ($\sim$1000°C) in air, however, the composition of the glassy interfacial layer changes, resulting in increased interfacial shear resistance [25]; consequently, the reduced contribution from crack bridging results in sharply lower strength and toughness properties of the composite. In the condition tested, the composite has a fracture strength of 400 MPa and a fracture toughness K_{Ic} of >5 MPa$\sqrt{m}$ in the longitudinal orientation; in the transverse orientation, these values are $\sim$7.6 MPa and $\sim$0.2 MPa$\sqrt{m}$, respectively.

Cantilever-beam specimens (2-mm wide, 2-mm thick and 35-mm long) were cut and polished from the plates in the L-T orientation, with the fibers aligned parallel to the axis of the bar. Specimens were then notched (perpendicular to the fiber direction) with a 150-μm thick diamond wafering blade.

Specimens were cycled under tension-compression loading (load ratio $R = \sigma_{min}/\sigma_{max} = -1$) in controlled room-temperature air (22°C, 45% relative humidity) under displacement control at a frequency of 10 Hz (Fig. 4.3a). Crack initiation and growth out of the notch was monitored using periodic replication with cellulose acetate tape; tests were interrupted every $\sim$5,000 to 10,000 cycles (at a $K_{max} \sim 1.5$ MPa$\sqrt{m}$, crack initiation generally took about 2,000 cycles), and held at mean load during replication. Replicas were subsequently gold coated and examined using optical microscopy. Short crack lengths enamating from the notch between $\sim$20 and 300 μm, could be readily detected with a resolution better than $\pm$ 0.5 μm. In several tests, immediate crack bifurcation or delamination occurred on initiation of fatigue cracking from the notch (Fig. 4.4); analysis of these tests is not included in the results.

Owing to crack meandering, surface crack lengths were taken as the projected crack length normal to the direction of the tensile bending stresses. Since all cracks initiated at corners of the notch on the top surface of the specimen, stress-intensity factors, K, were computed from recently derived linear-elastic solutions for three-dimensional (quarter-

elliptical) corners cracks in bending and/or tension [26,27], in terms of the crack depth a, crack length c, ellipse parametric angle ϕ, shape factor Q, specimen width t, specimen thickness b, remote (outer fiber) bending stress σ_b (= $3/bt^2$ × applied bending moment), and applied uniform tension stress σ_t (Fig. 4.3b):

$$K = (\sigma_t + H_c\sigma_b)(\pi a/Q)^{1/2} F_c(a/c, a/t\ c/b, \phi) \quad , \tag{1}$$

where H_c is the bending mutliplier and F_c is the boundary-correction factor for a corner crack (both tabulated in ref. 26). Eq. 1 is valid for $0.2 \leq a/c \leq 1$ and for $0 \leq \phi \leq \pi/2$ at $c/b < 0.5$. Cyclic crack-growth (da/dN) data are presented in terms of the maximum stress intensity, K_{max} applied during the tensile cycle calculated at $\phi = \pi/4$.

4.3 Results and Discussion

Results showing the variation in surface fatigue-crack length emanating from the notch, as a function of number of cycles, are plotted in Fig. 4.5; an optical micrograph of the surface is shown in Fig. 4.6. Similar to the growth of short cracks from notches in metallic materials [e.g., 13-17], crack-extension rates were initially quite rapid over the first 150 to 200 μm of growth, before progressively decelerating to virtual arrest; the crack-growth rate da/dN thus decreases with increasing K_{max} (Fig. 4.7).

Mechanistically, similar observations in metallic alloys have been attributed to several factors [13-17], but principally to the restricted role of crack-tip shielding* (primarily involving crack closure) for cracks of limited wake [13,15,17]. Assuming that the stress intensity due to such shielding, K_s, reduces the applied (nominal or far-field) stress intensity, $K = K^\infty$, to an effective level actually experienced at the crack tip, K_{tip}, viz:

$$K_{tip} = K^\infty - K_s \quad , \tag{2}$$

the small crack is reasoned to experience a higher K_{tip} compared to a long crack at equivalent applied K levels. Furthermore, since the magnitude of K_s is progressively developed with the initial extension of a small crack, the initial sub-threshold growth rates of small cracks often continuously decrease with crack extension [13-19].

In LAS/SiC_f, the most potent mechanism of shielding occurs by crack bridging. To quantify the bridging effect, Marshall and co-workers [24,30] have considered the influence of crack-closure tractions on matrix cracking for a bridging zone of length a_o behind the crack tip. For the present material, the (shielding) stress intensity, K_s, due to such fiber closure tractions

was estimated from their frictional-slip model in terms of the interfacial shear strength τ, the volume fraction of fibers f, fiber radius r, Poisson's ratio of the matrix $\nu = \frac{1}{2}$, and elastic moduli of the fiber and matrix, E_f and E_m, respectively, viz:

$$K_s = (16\alpha/9\pi)^{1/2} K_{tip}^{1/2} a_o^{3/4} (2 - a_o/a)^{3/4} \quad , \tag{3a}$$

where

$$\alpha = \frac{8(1 - \nu^2)\, \tau\, f^2\, E_f\, (1 + \eta)}{[E_m(1 - f) + E_f f]\, r \sqrt{\pi}} \quad ,$$

and

$$\eta = E_f f/[E_m(1 - f)] \quad .$$

For a fully bridged crack ($a = a_o$), Eq. 3a reduces to:

$$K_s = (16\alpha/9\pi)^{1/2} K_{tip}^{1/2} a^{3/4} \quad . \tag{3b}$$

Using the mechanical properties of the LAS/SiC_f composite [23-25] listed in Table 4.1, and assuming full bridging along the *fatigue* crack length (and of course no bridging across the notch), the shielding stress intensity K_s (Eq. 3a), and effective (near-tip) value K_{tip} (Eq. 2), are plotted in Fig. 4.8a as a function of crack size for the experimental data shown in Figs. 4.5, 4.7. It is apparent that although the nominal (applied) stress intensity, K^∞, increases as expected with crack size, the stress intensity experienced *locally* at the tip, K_{tip}, is progressively decreased, consistent with the measured decrease in growth rates. The resulting plot of da/dN versus K_{tip}, shown in Fig. 4.8b, can now be seen to show a positive slope, with an exponent m of over +50.

Thus, analogous to short-crack behavior in metallic materials where crack-tip shielding results primarily from crack closure [13,15,17], shielding from fiber bridging in the glass-ceramic composite similarly leads to negative exponents in the da/dN - K relationship at short crack sizes; when plotted in terms of a *local* (near-tip) stress-intensity, however, the usual positive power-law dependency of crack-growth rates on the stress intensity is obtained.

4.4 Conclusions

Based on a study of the cyclic fatigue-crack propagation behavior of short cracks under tension-compression loading in a continuous SiC-fiber reinforced lithium-aluminosilicate glass-

ceramic composite (LAS/SiC_f), toughened by crack bridging, the following conclusions can be made:

1. Fatigue-crack growth rates, over the range 10^{-6} to 10^{-11} m/cycle, for crack sizes of between 20 and 300 μm were found to show a negative power-law dependency on the nominal (applied) maximum stress intensity, K_{max}, analogous to short-crack behavior in metals.

2. Frictional-slip models of crack bridging by unbroken fibers in the crack wake were used to estimate a shielding stress intensity in the LAS/SiC_f system; by accounting for such shielding in the computation of an effective (near-tip) stress intensity, the expected positive power-law dependency of growth rates on stress intensity was obtained, with an exponent of over 50.

3. Non-conservative estimates of the life of ceramic components are possible from da/dN vs. K damage-tolerant predictions due to the growth of short cracks below the fatigue threshold ΔK_{TH}.

4.5 References

1. T. Kawakubo and K. Komeya, *J. Am. Ceram. Soc.*, **18** (1987) 400.

2. M. V. Swain and V. Zelizko, pp. 595-608 in *Advances in Ceramics, 24B Science and Technology of Zirconia III*, eds. S. Somioya, N. Yammoto and H. Hanagida, American Ceramic Society, Westerville, OH, 1988.

3. M. Masuda, T. Soma, M. Matsui, and I. Oda, *J. Ceram. Soc, Japan Int. Ed.*, **96** (1988) 275.

4. L. Ewart and S. Suresh, *J. Mater. Sci.*, **22** (1987) 1173.

5. S. Suresh, L. X. Han, and J. P. Petrovic, *J. Am. Ceram. Soc.*, **71** (1988) C158.

6. R. H. Dauskardt, W. Yu, and R. O. Ritchie, *J. Am. Ceram. Soc.*, **70** (1987) C248.

7. M. J. Reece, F. Guiu, and M. F. R. Sammur, *J. Am. Ceram. Soc.*, **72** (1989) 348.

8. R. H. Dauskardt and R. O. Ritchie, *Closed Loop*, **17** (1989) 1233.

9. L. X. Han and S. Suresh, *J. Am. Ceram. Soc.*, **72** (1989) 1233.

10. A. Grossmüller, V. Zelizko, and M. V. Swain, *J. Mater. Sci.*, **8** (1989) 29.

11. R. O. Ritchie, R. H. Dauskardt, W. Yu, and A. M. Brendzel, *J. Biomed. Mat. Res.*, **24** (1990) 189.

12. P. C. Paris and F. Erdogan, *J. Basic Eng.*, Trans. ASME, **85** (1963) 528.

13. S. Suresh and R. O. Ritchie, *Int. Met. Rev.*, **29** (1984) 445.

14. M. M. Hammouda and K. J. Miller, *ASTM STP 668* (1979) 703.

15. K. Tanaka and Y. Nakai, *Fat. Eng. Mat. Struct.*, **6** (1983) 315.

16. J. Lankford and D. L. Davidson, p. 51 in *Small Fatigue Cracks*, eds. R. O. Ritchie and J. Lankford, TMS-AIME, Warrendale, PA, 1986.

17. R. O. Ritchie and W. Yu, *ibid.*, p. 167.

18. T. Hoshide, T. Ohara, and T. Yamada, *Int. J. Fract.*, **37** (1988) 47.

19. D. C. Cardona and C. J. Beevers, *Scripta Met.*, **23** (1989) 945.

20. M. Yoda, *Int. J. Fract.*, **39** (1989) R23.

21. D. Jensen, V. Zekizko, and M. V. Swain, *J. Mater. Sci.*, **8** (1989) 1154-57.

22. J. J. Brennan and K. M. Prewo, *J. Mater. Sci.*, **17** (1982) 2371.

23. D. B. Marshall and A. G. Evans, *J. Am. Ceram. Soc.*, **68** (1985) 225.

24. D. B. Marshall and A. G. Evans, p. 1 in *Fracture Ceramics of Ceramics*, ed. R. C. Bradt *et al.*, Plenum Press, New York, NY, vol. 7, 1986.

25. E. Y. Luh, *M.S. Thesis*, University of California, Berkeley, 1985.

26. J. C. Newman and I. S. Raju, p. 311 in *Computational Methods in the Mechanics of Fracture*, ed S. N. Atluri, North-Holland, vol. 2, 1986.

27. I. S. Raju, S. N. Atluri, and J. C. Newman, "Stress-Intensity Factors for Small Surface and Corner Cracks," NASA Tech. Memo 100599, Langley Research Center, Hampton, VA, April 1988.

28. R. O. Ritchie, *Mater. Sci. Eng. A*, **103** (1988) 15.

29. A. G. Evans, pp 267-91 in *Fracture Mechanics: Perspectives and Directions (Twentieth Symp.)*, ASTM STP 1020, eds. R. P. Wei and R. P. Gangloff, American Society for Testing and Materials, Philadelphia, PA, 1989.

30. D. B. Marshall and B. N. Cox, *Acta Met.*, **35** (1987) 2607.

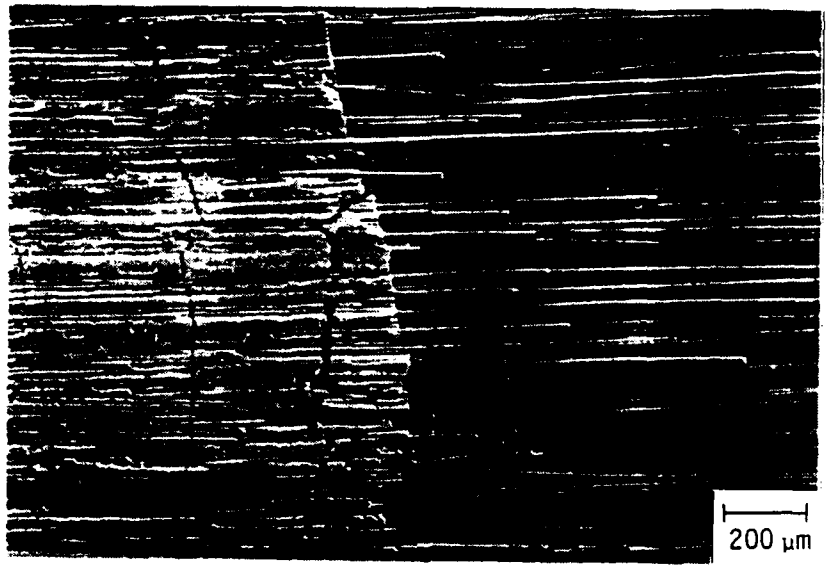

Fig. 4.1. Scanning electron micrograph of a flexure specimen (tensile surface) of LAS/SiC_f composite, showing crack bridging via unbroken fibers across the crack [25].

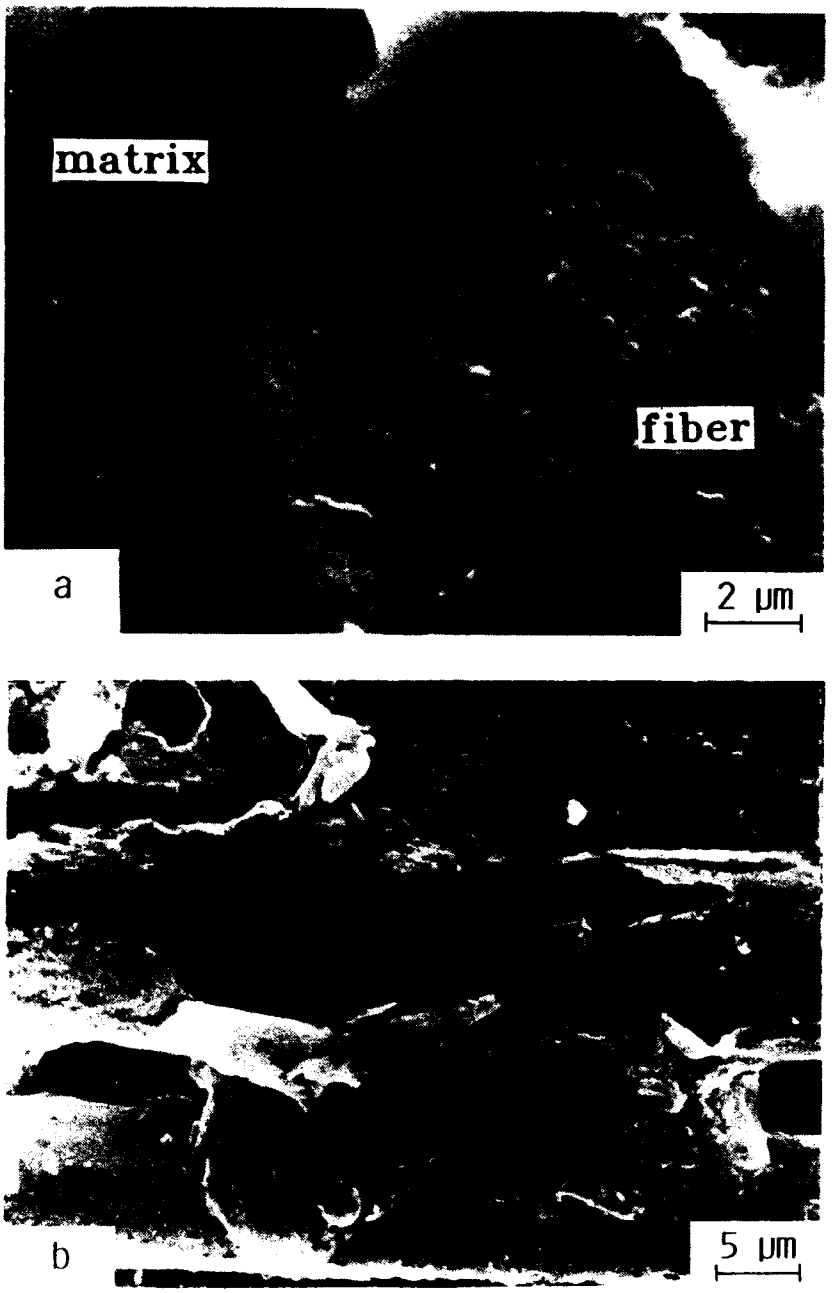

Fig. 4.2. Scanning electron micrographs of the glassy reaction layer between the LAS matrix and SiC fiber (a); the weakness of this layer can be seen on cooling following heat treatment in air, where the layer separates from the matrix and "peels" away from the fiber (b).

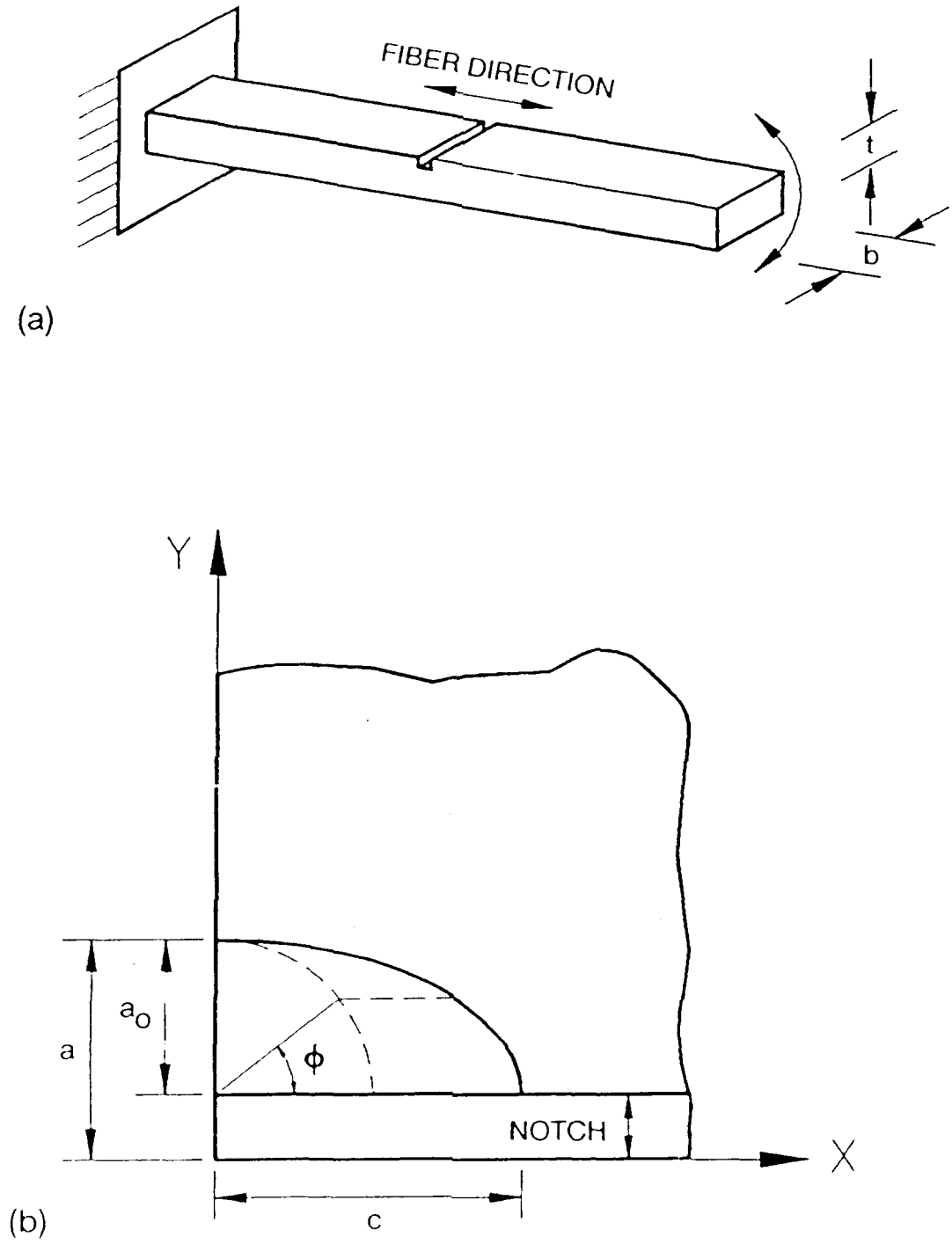

Fig. 4.3. Schematic illustration of a) the cantilever beam specimen arrangement with notch cut perpendicular to the fiber direction, and b) the quarter-elliptical corner crack configuration emanating from the notch.

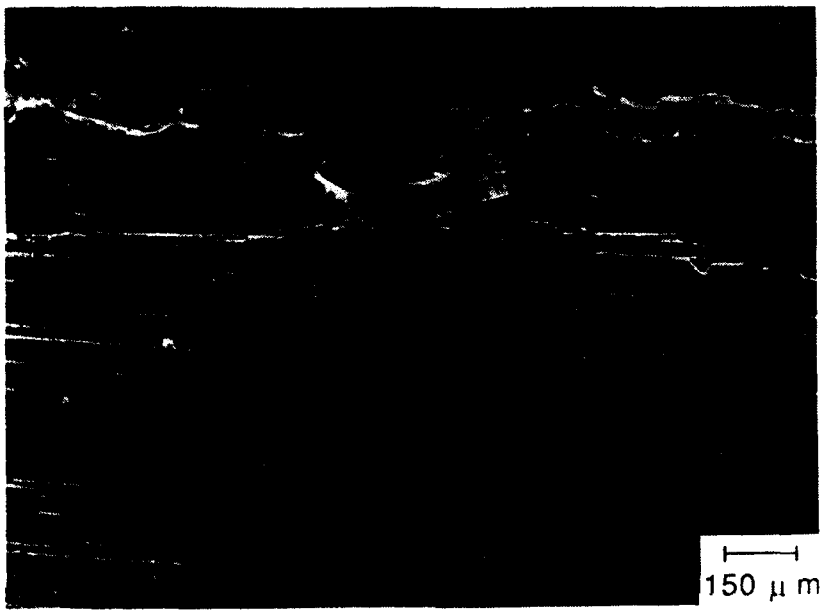

Fig. 4.4. Scanning electron micrograph (replication) of crack initiation at the specimen notch showing immediate crack deflection by delamination along the fiber direction in the LAS/SiC_f composite.

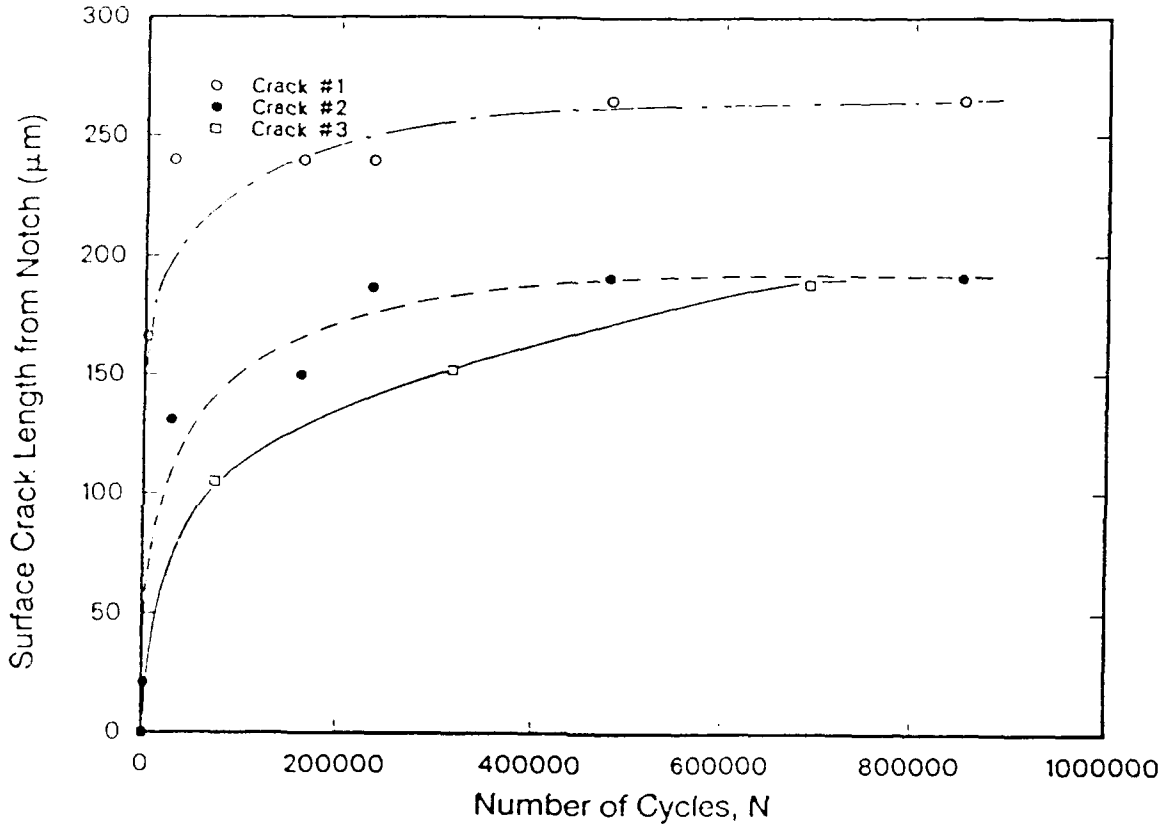

Fig. 4.5. Experimentally measured variation in length of surface fatigue cracks, emanating from the notch, as a function of number of cycles N, in the LAS/SiC_f composite.

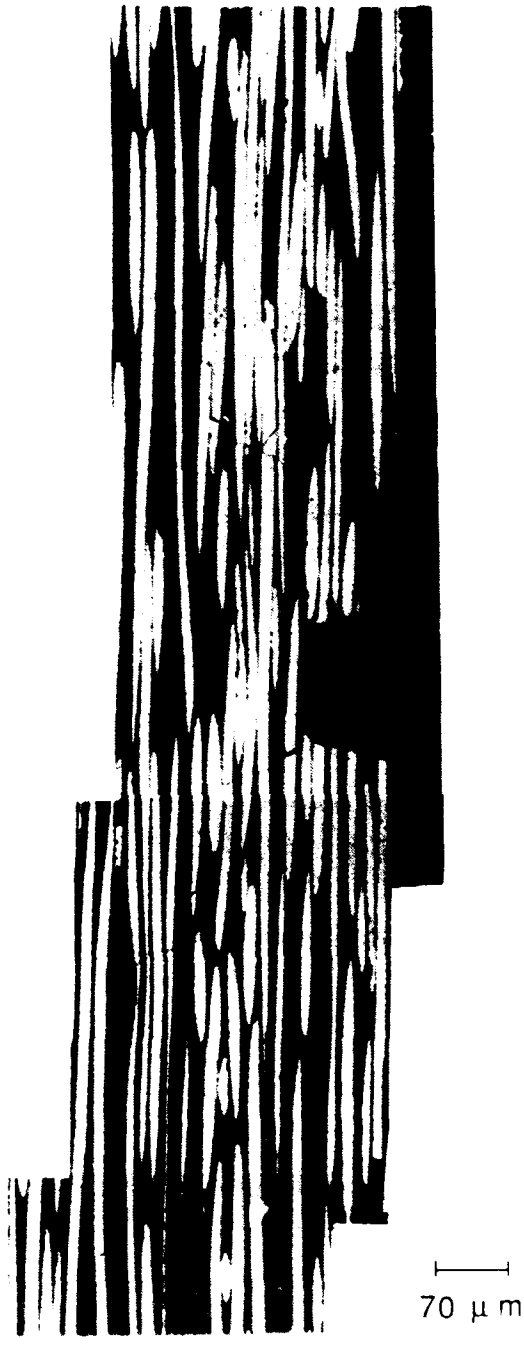

Fig. 4.6. Scanning electron micrograph showing short-crack initiation and growth from the specimen notch in LAS/SiC_f. In the figure, the crack has been grown well past the short-crack regime.

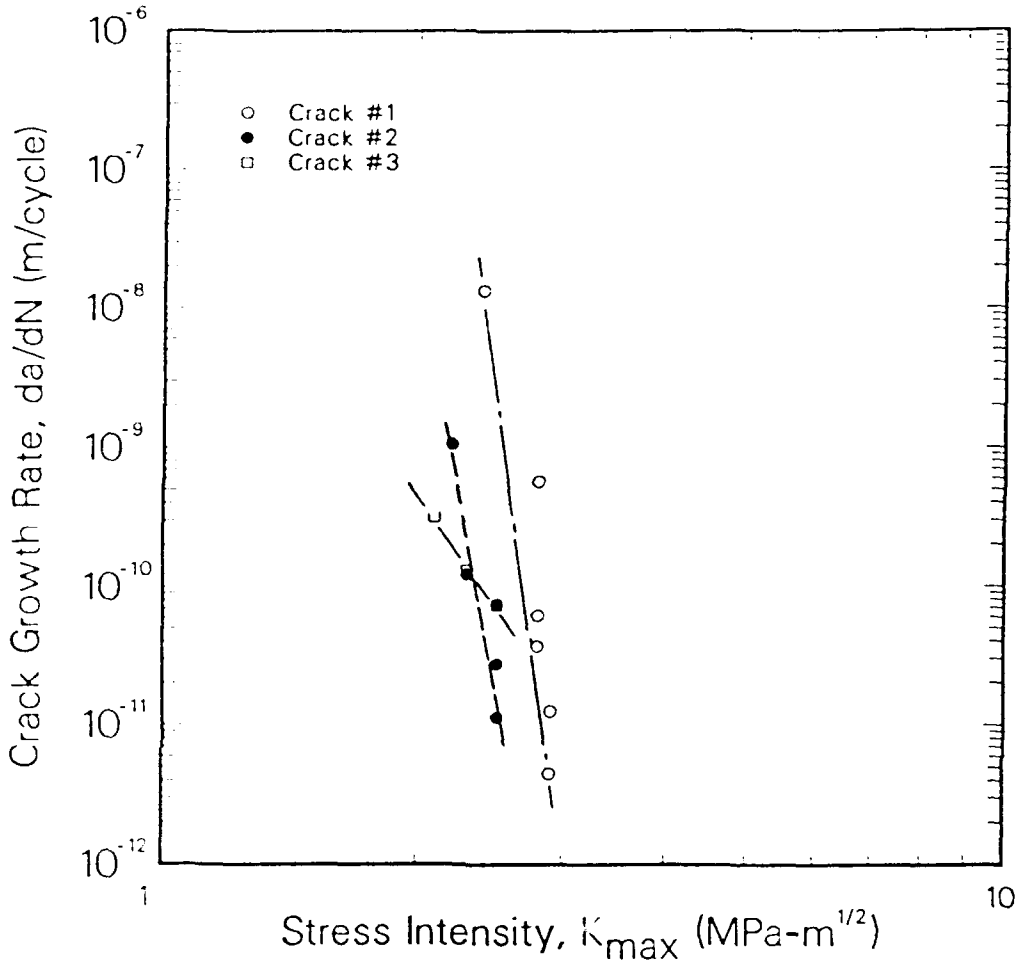

Fig. 4.7. Variation in cyclic fatigue-crack growth rates, da/dN, as a function of the nominal (applied) maximum stress intensity, $K_{max} = |\Delta K|$, for short cracks in LAS/SiC_f. Note the negative power-law dependency of growth rates on stress intensity.

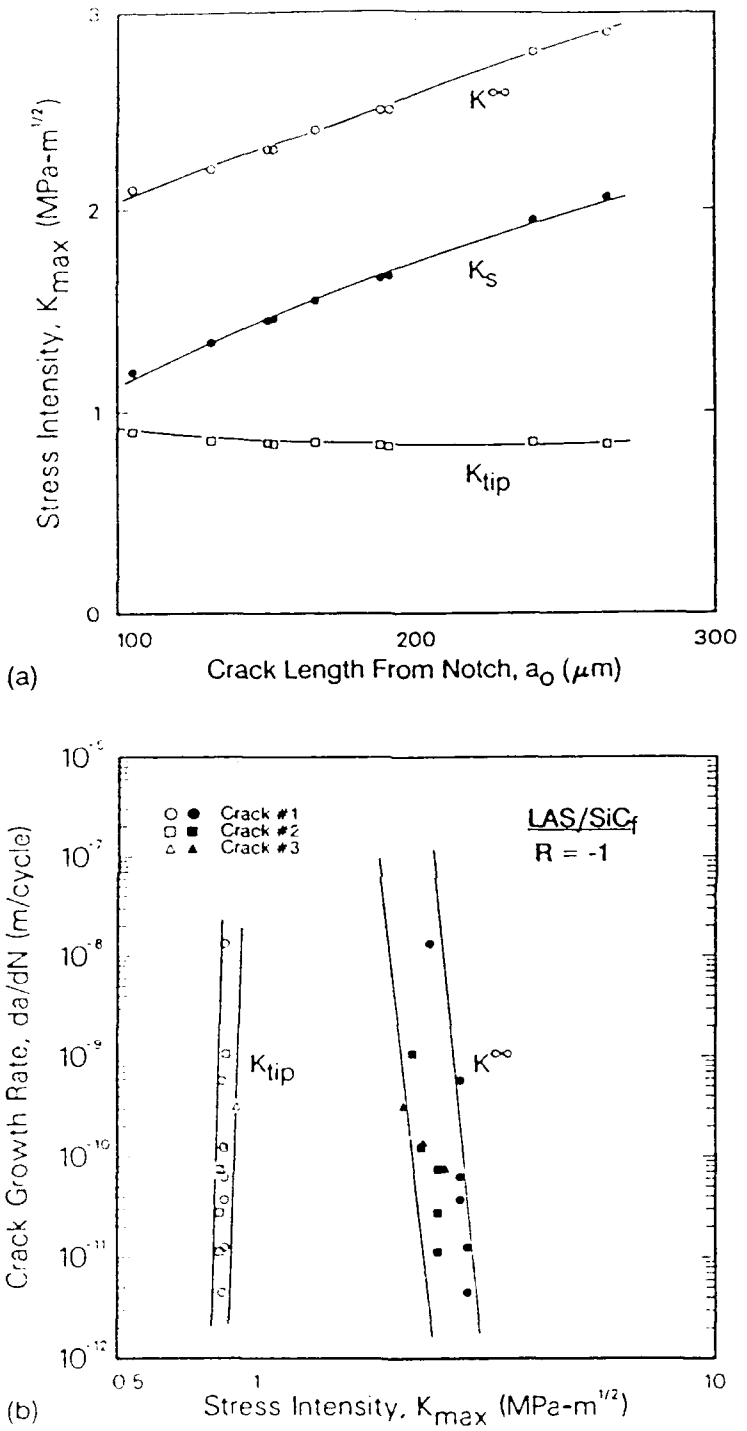

Fig. 4.8. (a) Predicted variation in shielding stress intensity, K_s, due to crack bridging (Eq. 3a), and effective (near-tip) stress intensity, K_{tip}, with measured crack size from notch, over the range of nominal stress intensities, K^{∞}, utilized in the experiments. (b) Corresponding plot of the short-crack growth rate data for LAS/SiC$_f$ from Fig. 4.7 with K_{tip}, showing the expected positive power-law dependency of growth rates on stress intensity.

5. CYCLIC FATIGUE-CRACK PROPAGATION IN A SILICON CARBIDE WHISKER-REINFORCED ALUMINA CERAMIC COMPOSITE: LONG AND SMALL-CRACK BEHAVIOR

(R. H. Dauskardt, M. R. James,† J. R. Porter,† and R. O. Ritchie)

5.1 Introduction

Recent studies have provided convincing evidence of the susceptibility of a wide range of ceramic and ceramic-matrix composite materials to mechanical degradation under cyclic loading. Data now exist indicating reduced lifetimes during cyclic fatigue stress/life (S/N) testing and significant cyclic-crack propagation at loads less than those required for environmentally-enhanced (static fatigue) crack growth during fracture mechanics testing in zirconia [1-11], graphite [12], alumina [6,13-24], silicon nitride [16,25-29] and silica glass [30] ceramics and LAS/SiC_f [31], Al_2O_3-SiC [32,33] and laminated graphite/pyrolytic carbon [12] composites at ambient, and to a far less numerous extent, elevated temperatures. While the precise micro-mechanisms underlying such behavior are still unclear, the characteristics of fatigue degradation are in many cases qualitatively similar to those of metallic materials. For example, cyclic fatigue-crack propagation rates of long (typically in excess of ~3 mm) cracks in ceramic materials have been shown to be power-law dependent on the applied stress intensity. In the simplest form, the growth increment per cycle (da/dN) has been related to the applied stress-intensity range (ΔK) via a Paris power-law expression* [34]:

$$da/dN = C(\Delta K)^m \quad , \tag{1}$$

where C and m are experimentally measured scaling constants; however, unlike metals, the value of m can be far higher (i.e., in the range ~15 to 50) than the exponents of ~2 to 4 typically observed in metals [35].

*Depending upon the desired level of detail, more complex expressions involving the maximum stress intensity (K_{max}), the load ratio (R = ratio of minimum-to-maximum load) and material properties such as the fracture toughness (K_c) or the fatigue threshold (ΔK_{TH}) etc., can be utilized.

In view of this susceptibility to fatigue, the projected use of ceramics and ceramic-matrix composites for safety-critical structural applications subject to cyclic loading will

†Rockwell International Science Center, Thousand Oaks, CA 91360

increasingly require reliable in-service fatigue-lifetime prediction. Traditionally, damage-tolerant approaches are used in safety-critical applications involving metallic structures where failure results from the extension of a single dominant crack; these rely on the integration of crack velocity-stress intensity curves to estimate the time or number of cycles for a presumed initial defect to grow to faildure. Although cyclic data are now available, the approach may prove difficult to utilize in practice for many ceramics and ceramic-matrix composites because of the large power-law dependence of growth rates (da/dN) on stress intensity, which implies that the estimated life will be proportional to the reciprocal of the applied stress raised to a large power [35].

For example, the change in predicted lifetime, ΔN_f, for a cracked structure subjected to an applied alternating stress, $\Delta\sigma$, resulting from a factor of two change in the applied loads is listed for typical metals, intermetallics and ceramics in Table 5.1. For a metallic structure where the exponent m ideally is of the order of 2 to 4, a factor of two increase in the applied stress $\Delta\sigma$ depletes the projected life by roughly an order of magnitude; in ceramic structures, conversely, where m values can be as high as ~50 and above, this same factor of two increase in stress reduces the projected life by some six to fifteen orders of magnitude!

Table 5.1 - Change in Predicted Fatigue Lifetime for a Factor of Two Change in Applied Stress

Fatigue exponent, m	ΔN_f	Material
~2-4	~10	metals
~10	~10^3	intermetallics
~20	~10^6	ceramics
~50	~10^{15}	ceramics

An alternative procedure is to redefine the critical crack size in terms of the fatigue threshold ΔK_{TH}, below which the growth of long cracks is presumed dormant; this in essence is a crack-initiation criterion where ΔK_{TH} is taken as the effective toughness, rather than the fracture toughness K_c. However, recent evidence [7-10,16,26,29] has shown that, akin to metals [e.g., 36,37], where cracks are physically small (typically of a length less than ~500 μm) or approach the dimensions of microstructure or local crack-tip inelasticity [37], crack-propagation rates can exceed those of long cracks at equivalent applied stress intensities, and more importantly occur at ΔK levels *less than* ΔK_{TH}.

In the present study, an in-depth examination of the cyclic fatigue-crack growth of both long and microstructurally-small cracks in a SiC_w-reinforced Al_2O_3 ceramic composite is reported. Detailed fractography of the resulting fatigue fracture surfaces are compared with those of monotonically loaded cracks in order to provide some elucidation of the mechanisms of cyclic fatigue. In addition, the effect of variable-amplitude cyclic loading sequences to determine post-overload crack-growth behavior is investigated. Implications of the observed crack-growth behavior on possible mechanisms of cyclic fatigue in ceramics are discussed.

5.2 Experimental Procedures

5.2.1 Material

Cyclic crack-growth experiments were conducted on a SiC-whisker reinforced alumina (Al_2O_3-SiC_w) composite, fabricated by dispersion processing, pressure filtration and hot pressing of high purity alumina powder# with 15 vol% SiC whiskers@. The resulting microstructure consisted of < 5 μm alumina grains, with a uniform dispersion of < 1 μm diameter SiC whiskers, with an aspect ratio of up to 100, and predominantly of the α form (hexagonal structure). Whiskers tended to be oriented perpendicularly to the hot pressing direction. The fabrication process has been shown to eliminate flaw populations and promote uniform microstructures; further details of processing techniques and microstructure are reported elsewhere [38,39]. Mechanical properties are listed in Table 5.2.

#A-HPS 40 grade, Sumitomo Chemical America, New York, NY.
@Silar SC-9 grade, Arco Chemical Co., Greer, SC.

Table 5.2 - Mechanical Properties of Al_2O_3-SiC_w Composite

Volume Fraction SiC (%)	Green Density (%)	Final Density (%)	Young's Modulus, E (GPa)	Tensile Strength (MPa)	Fracture Toughness K_c (MPa$\sqrt{m}$)
15	65	99.5	400	652 $\pm$100	4.5

5.2.2 Test Methods

Cyclic Fatigue: Long Cracks: Cyclic fatigue-crack propagation was measured using compact C(T) specimens, containing long (> 3 mm) through-thickness cracks (Fig. 2.4a), in general

accordance with the ASTM Standard E 647-86a for measurement of fatigue-crack growth rates in metallic materials [40], modified for ceramics using the procedures outlined by Dauskardt and Ritchie [41]. Test pieces were 3 mm in thickness, with all other dimensions scaled appropriately to the ASTM Standard specimen geometry with a width (W) of 24.5 mm. Specimens were cyclically loaded at a load ratio of 0.1 and a frequency of 50 Hz (sine wave) in high-resolution, computer-controlled electro-servo-hydraulic testing machines, operating under closed-loop displacement, load or stress-intensity control. Testing was performed in controlled room air (22°C, 45% relative humidity) environments.

Electrical-potential measurements across ~0.1 μm NiCr foils, evaporated onto the specimen surface, were used to monitor crack lengths *in situ* to a resolution better than ± 2 μm [41,42]. Since the SiC whiskers are slightly conducting, a thin (< 0.1 μm) layer of alumina was first sputtered onto the specimen surface to insulate the metal film from the specimen. Unloading compliance measurements using back-face gauges were also used to assess the extent of fatigue crack closure in terms of the far-field closure stress intensity, K_{cl}, defined at first contact of the fracture surfaces during the unloading cycle [43]. The K_{cl} value is calculated from the highest load where the elastic unloading compliance line deviates from linearity (Fig. 2.4a). It should be noted that the back-face strain technique provides a global (far-field) measure of the closure stress intensity and is typically not sensitive to near-tip closure effects. Test techniques are described in detail elsewhere [1,4,41].

Crack-growth rates, da/dN, were determined over the range ~10^{-11} to 10^{-5} m/cycle under computer-controlled K-decreasing and K-increasing conditions. Data are presented in terms of the applied stress-intensity range ($\Delta K = K_{max} - K_{min}$, where K_{max} and K_{min} are the maximum and minimum stress intensities in the fatigue cycle). By considering the effect of crack closure, an effective (near-tip) stress-intensity range can also be estimated as $\Delta K_{eff} = K_{max} - K_{cl}$ [44,45].

The fatigue threshold, ΔK_{TH}, was operationally defined as the maximum value of ΔK at which growth rates did not exceed 10^{-10} m/cycle, consistent with ASTM E 647 procedures [40]. Thresholds were approached by varying the applied loads so that the instantaneous values of crack length (a) and ΔK changed according to the equation [46]:

$$\Delta K = \Delta K_o \exp [C^* (a - a_o)] \ , \qquad (2)$$

where a_o and ΔK_o are the initial values of a and ΔK, and C^* is the normalized K-gradient ($1/K \cdot dK/da$) which was set to ± 0.08 mm^{-1}. For the C(T) geometry, stress intensities were computed from handbook solutions, in terms of the applied load P, crack length a, test-piece thickness B, and width W, as [47,48]:

$$K = (P/BW^{1/2}) \cdot g(a/W) \ ,$$

where for $0.3 < a/W < 1$,

$$g(a/W) = \frac{[2+(a/W)][0.886+4.64(a/W)-13.32(a/W)^2+14.72(a/W)^3-5.6(a/W)^4]}{[1-(a/W)]^{3/2}} \quad .(3)$$

Owing to the brittleness of the material, the initiation of the pre-crack was one of the most critical procedures in the test. In the current work, as previously [e.g., 1], this was achieved by machining a wedge-shaped starter notch and carefully growing the crack roughly 2 mm out of this region by fatigue under displacement control.

Cyclic Fatigue: Small Cracks: Fatigue-crack propagation data for small (<300 μm) surface cracks were determined by monitoring the top surface of cantilever-bend specimens (2 mm square and 70 mm long), with surfaces polished to a micron finish. A series of micro-indentations (made using a 2 kg load pyramidal indenter) were placed along the longitudinal axes of the surface to initiate multiple small cracks along the specimen length (Fig. 2.4b). Specimens were cycled for up to 10^6 cycles under tension-compression ($R = -1$) and tension-tension ($R = 0.05$) loading in controlled room-temperature air (22°C, 45% relative humidity) at a nominal sinusoidal frequency of 30 Hz in a variable-speed constant-displacement testing machine.

Tests were periodically interrupted, by removing the specimen from the test fixture for optical examination, after the first cycle to determine crack extension during initial loading and after subsequent 10^2 to 10^4 cycle intervals until failure. Initial rapid growth in the first few loading cycles was ignored where it involved crack extension in the residual stress field immediately surrounding the indent [16,49]. Small-crack lengths could be readily quantified with a resolution better than $\pm$ 2 μm. The contrast of the crack was significantly enhanced by adjustment of the incident light to illuminate only a small region of the object field (specimen) immediately behind the crack tip, similar to techniques of indirect illumination using light scattered from a small restricted region reported elsewhere [50]. Following final fracture of test specimens, the crack depth-to-surface-length ratio (a/2c) was readily determined from fractographic examination of the cyclically grown semi-eliptical surface cracks to derive a calibration relating a/2c values to a (Fig. 5.1).

Stress-intensity factors were computed from linear-elastic solutions [51,52] for three-dimensional semi-elliptical surface cracks in bending (and/or tension) in terms of crack depth, a, crack length, 2c, elliptical parametric angle, ϕ, shape factor, Q, specimen width, t,

specimen thickness, b, and remote (outer surface) bending stress, σ_b:

$$K_{app} = H_c \sigma_b (\pi a/Q)^{1/2} F(a/c, a/t, c/b, \phi) , \quad (4)$$

where H_c is the bending multiplier and F is a boundary correction factor (Fig. 2.4b). Eq. 4 is valid for $0.2 \leq a/c \leq 1$, $0 \leq \phi \leq \leq 90°$ at $c/b \leq 0.5$. Owing to crack meandering, surface crack lengths were taken as the projected crack length normal to the direction of the bending stress. Crack-growth rates were determined over the range 10^{-12} to 10^{-6} m/cycle from crack length/number of cycles (a vs. N) curves. Cyclic crack-growth rates are presented in terms of the maximum stress intensity, from the tensile portion of the fatigue cycle, calculated with $\phi = 0°$ and a/2c taken from the calibration curve shown in Fig. 5.1.

To account for the effect of the residual stress field of the indent, the additional stress-intensity factor K_r from the residual crack-opening stress was computed in terms of the peak indentation load P, and the half crack length c, by [53]:

$$K_r = \chi_r P_r c^{-3/2} , \quad (5)$$

where χ_r is a material constant dependent upon the ratio of Young's modulus to hardness. The total stress intensity is thus given by:

$$K = K_{app} + K_r . \quad (6)$$

Note that with increasing crack length, K_{app} increases while the residual K_r decreases.

Cyclic Fatigue: Transient Crack Growth: To examine the influence of non steady-state crack growth, crack-propagation tests were performed on long cracks subject to variable-amplitude cyclic-loading conditions. Block-loading sequences, comprising selected constant stress-intensity ranges, were applied during steady-state fatigue-crack growth. Transient crack-growth response following the load change was observed as a function of crack extension until steady-state growth was re-established. In addition, constant K_{max}/variable-R tests were conducted by holding K_{max} constant and increasing K_{min} (with an appropriate value of C^* such that ΔK satisfied Eq. 2).

Fracture Toughness: Following completion of the fatigue-crack growth tests, the fracture toughness was determined by under monotonically increasing loads (displacement control) to generate a resistance curve, $K_R(\Delta a)$. Procedures essentially conform to ASTM Standard E 399-

87 for the measurement of the toughness at crack initiation [40]. Since these tests all involve sharp cracks, measured toughness values may be smaller than values obtained from other methods that rely on a machined notch as the initial crack. In addition, the maximum toughness, K_c, was calculated subsequent to failure of the cantilever-beam specimens from estimates of the maximum load and crack length immediately prior to failure.

Fractography: Fracture surfaces were examined using optical and scanning electron microscopy, and in profile using sections cut perpendicular to the crack path in the plane of loading. The roughness of these surfaces was evaluated in terms of the lineal toughness parameter (R_L), defined as the ratio of the total length L of the profile to the projected length L′ on the plane of maximum tensile stress. By evaluating R_L as a function of measuring step size η, a fractal dimension D was computed from the expression [54,55]:

$$R_L = L/L' = R_o \eta^{(1-D)} . \tag{7}$$

where R_o is a constant. Details of this technique are discussed elsewhere [54].

5.3 Results and Discussion

5.3.1 Long Cracks

Growth-Rate Behavior: Cyclic fatigue-crack propagation data are plotted in Fig. 5.2a as a function of the applied ΔK, for a controlled room-air environment. The composite displays extensive cyclic fatigue-crack propagation, with a power-law dependence on the stress-intensity range. Similar to metallic materials and in agreement with data from a range of other ceramic materials, growth rates can be fitted to a conventional Paris law relationship [34] of the form shown in Eq. 1, with an exponent m of 15. This value is considerably larger than typically reported for metals (2 to 4), but is in the range commonly observed for brittle materials [e.g., 1-12]. The value of the fatigue threshold, measured at a maximum growth rate of 10^{-10} m/cycle, was found to be approximately 60% of K_c. Values of C, m and ΔK_{TH} for the present Al_2O_3-SiC_w composite are compared with other ceramic materials in Table 5.3. It would appear that in general resistance to cyclic fatigue-crack growth in ceramic materials, as indicated by the value of ΔK_{TH}, is enhanced with increasing fracture toughness.

Table 5.3 - Values of C and m (in Eq. 1) and the Threshold ΔK_{TH} for some Ceramic Materials

	K_c (MPa$\sqrt{m}$)	C (m/cycle (MPa$\sqrt{m}$)$^{-m}$)	m	ΔK_{TH} (MPa$\sqrt{m}$)*	Ref.
Al_2O_3-SiC_w	4.5	1.12×10^{-17}	15	2.7	-
alumina	~4.0	-	27-33	2.5-2.7	18,20
Mg-PSZ (TS-grade)	16.0	1.70×10^{-48}	42	7.7	4
(MS-grade)	11.5	5.70×10^{-28}	24	5.2	4
(AF-grade)	5.5	4.89×10^{-22}	24	3.0	1,4
(overaged)	2.9	2.00×10^{-14}	21	1.6	4
silicon nitride	6.0	1.01×10^{-21}	12-18	2.0-4 3	21
3Y-TZP	5.3	4.06×10^{-18}	21	2.4	10
graphite/pyrolytic C	~1.6	1.86×10^{-18}	19	~0.7	12

As in previous studies [e.g., 1,4,12], crack growth was shown to be a true cyclic fatigue phenomenon, with crack advance dependent on both the loading and unloading cycle, rather than environmentally enhanced (static fatigue) cracking at maximum load. This was verified by monitoring crack-growth rates at constant K_{max}, and with the load cycled between K_{max} and K_{min} (R = 0.1) for which crack growth was observed; with the loads held constant at K_{max}, no appreciable crack extension was apparent.

Fatigue Crack Closure: Similar to behavior in Mg-PSZ [4], fatigue-crack growth in the Al_2O_3-SiC_w composite showed evidence of crack closure, as has been reported widely in metals [e.g., 44,45). Far-field crack closure levels, corresponding to the growth-rate data in Fig. 5.2a, are presented as a ratio of K_{cl}/K_{max} in Fig. 5.2b. The phenomenon involves premature contact between the crack surfaces during the unloading cycle, which raises the effective K_{min} ($\equiv K_{cl}$), thereby lowering the effective ΔK [44].

An increasing K_{cl}/K_{max} ratio seen in Fig. 5.2b as the threshold is approached, is characteristic of (contact) crack-tip shielding* by crack wedging, which is promoted by the smaller crack-opening displacements at low stress-intensity levels. The deflected nature of the crack paths, protruding grain-sized asperities, together with fractured SiC whiskers standing proud of the fracture surface, may well provide the fracture-surface asperities required for such wedging action.

*Crack tip shielding mechanisms act to impede crack advance by lowering the local stress intensity actually experienced at the crack tip [56,57]. Such mechanisms, which act principally in the crack wake, include transformation and microcrack toughening in ceramics, crack bridging in composites, and crack closure during fatigue-crack growth.

Fractography: Little distinction is apparent between cyclic and monotonic fracture surfaces in low magnification fractographs, although the fatigue surfaces appear more textured indicating increased roughness. At higher magnification, however, crack paths formed under monotonic loading are predominantly *transgranular*, with a high incidence of cleavage steps (indicated by the label C on the micrograph), whereas the increased roughness of the cyclically loaded surfaces appears to be associated with an increasing degree of *intergranular* fracture (Fig. 2.13). Limited regions of abrasion and a larger number of "pulled out" SiC whiskers were also apparent on the cyclic fracture surfaces, suggesting that the effect of cyclic loading may be a progressive weakening of the whisker/matrix interfaces, resulting in the larger pull-out lengths observed. Such distinction between the cyclic and monotonic fractography is not always observed in ceramic materials where identical fracture-surface morphologies are most often reported [1,4,12].

5.3.2 Small Cracks

Fatigue Life: Stress versus life (S/N) data, derived from results on the micro-indented cantilever-bend specimens, are listed in Table 5.4 for both tension-compression (R= -1) and tension-tension (R = 0.05) loading. Unlike reported data for *smooth* specimens of PSZ [2,7,8] and Si_3N_4 [25,27] ceramics, cycling in tension-compression does not appear to be more damaging (i.e., to give reduced lifetimes) than in cyclic tension. In the present case with pre-existing defects in the form of micro-indents, comparable lifetimes are found for tension-tension and tension-compression loading as the defects grow at comparable crack-growth rates. However, with smooth specimens where the development of a macro-sized crack accounts for a significant proportion of the life, reduced lifetimes result under tension-compression loading

TABLE 5.4 - Comparison of Fatigue Lifetimes at R = 0.05 and -1

Material	Test Specimen	Load Ratio ($\sigma_{min}/\sigma_{max}$)	σ_{max}* (MPa)	Life, N_f (cycles)
SiC_w-Al_2O_3	Indented Cantilever Beam	0.05	245	60×10^3
"	"	"	247	140×10^3
"	"	"	252	150×10^3
"	"	-1.0	248	60×10^3
"	"	"	255	240×10^3

* σ_{max} and σ_{min} are the remote (outer surface) bending stresses at maximum and minimum load, respectively.

because of the more damaging nature of fully reversed loads in *initiating* microcrack fatigue damage. For example, in PSZ, the more damaging nature of tension-compression cycling is clearly apparent from the higher density of microcracks observed after cycling at R = -1 compared to R = 0 [8].

Small-Crack Growth: Crack lengths of selected microcracks, derived from monitoring the top surface of the cantilever-beam specimens at various maximum applied stress levels and plotted as a function of the number of stress cycles, are shown in Fig. 5.3a,b at load ratios R of 0.05 and -1, respectively. The small cracks can in general be seen to grow at progressively decreasing growth rates with increase in size. Significant variations in growth rate are apparent for cracks at different locations along the specimen, occasionally resulting in final fracture not being associated with the indent at the highest stress region of the cantilever specimen. Such behavior is typical of small-crack growth which is highly sensitive to local stresses and microstructural inhomogeneities.

Using Eqs. 4-6 to compute stress intensities, such data are used to derive plots of crack-propagation rates as a function of the applied K_{max}, as shown in Fig. 5.4a, and as a function of the total stress intensity ($K_{max} + K_r$) in Fig. 5.4b. Similar to small-crack data reported for Al_2O_3, Si_3N_4 zirconia and LAS/SiC_f ceramics [7-10,16,31] and for metals [36,37,47], small-crack growth rates appear to display a negative dependency on the applied K_{max}; moreover, they are not a unique function of K_{max} and appear to be sensitive to the level of applied stress. Small-crack effects are generally rationalized in terms of the mutual competition between the applied *crack driving* force, normally associated with estimations of the far-field stress-intensity factor, and mechanisms of crack-tip shielding, typically attributed to local microstructural or mechanical mechanisms, which act to diminish the applied driving force [e.g., refs. 10,31,43]. Depending on the relative contributions from these competing effects, both the negative slope of growth rates with applied stress intensity and V-shaped crack-growth behavior may be understood. In the present study, when the residual stress intensity K_r associated with the indent is included (Fig. 5.4b), small crack-growth data are found to be similar to that of the long-crack data. This indicates that near steady-state shielding is probably achieved during the brief rapid growth of cracks in the first few loading cycles.

Closer examination of individual small-crack growth rate data, however, often revealed interesting fine scale features; representative examples are given in Fig. 5.4c. Small-crack growth rates frequently exhibited a number of local minima resulting in V-shaped growth-rate behavior, similar to behavior reported for both cyclic and static fatigue in other ceramics [16,49,58]. The crack extension between successive minima in the growth-rate data increased with increasing average stress, from ~7 μm at 190 MPa to ~33 μm at 250 μm.

The occurrence of multiple crack-growth minima over crack extensions of hundreds of microns from the indent is unlikely to be associated with the indent-induced K_r which decreases smoothly with crack length (Eq. 5). Instead, these minima are probably associated with local microstructural barriers to small-crack extension, such as the interaction of whiskers with the crack (Fig. 5.5), from mechanisms such as crack wedging by fracture-surface asperities (roughness-induced crack closure [45]) and crack bridging from intact whiskers spanning the crack or from uncracked ligaments, e.g., interlocking grains due to the intergranular nature of the fracture surface. Both the matrix grain size and the mean whisker spacing are similar in dimension (~5 μm) to the crack-extension distance (~7 μm) at which the first growth-rate minima occurs at the lowest applied stress levels, i.e., they are characteristic of dimensions at which bridging from a single whisker or roughness-induced crack closure might be expected to occur. At higher applied stress levels, longer crack extensions were observed between growth-rate minima consistent with the notion that increased degrees of shielding must be achieved before a significant effect is observed on the growth rate.

Fractography: Microstructural evidence for such shielding effects can be found from scanning electron microscopy (SEM) of the polished test samples. The morphology of a single microcrack after tension-compression cycling (maximum stress, σ_{max} = 450 MPa) is shown in the sequence in Fig. 5.5. Crack growth is predominantly intergranular. Evidence of crack bridging by both uncracked matrix ligaments (Fig. 5.5b) and SiC whiskers (Fig. 5.5c,d) in the wake of the crack tip is clearly apparent.

5.3.3 Variable-Amplitude Loading

Growth-Rate Behavior: The long-crack fatigue results described above pertain to constant-amplitude cyclic loading; to examine the influence of variable-amplitude loading, block overload and constant-K_{max}/increasing-K_{min} sequences were applied during steady-state fatigue-crack growth. Results for high-low and low-high block overloads are shown in Fig. 5.6a. Over the first ~1.2 mm of crack advance, the crack-growth rate remains approximately constant for a constant baseline ΔK of 3.6 MPa$\sqrt{m}$. On reducing the cyclic loads so that ΔK = 3.2 MPa$\sqrt{m}$ (high-low block overload), crack-growth rates decrease by approximately one and one half orders of magnitude, with no transient retardation. Similarly, by increasing the cyclic loads back to a ΔK of 3.6 MPa$\sqrt{m}$ (low-high block overload), growth rates increase almost instantaneously to roughly their previous baseline levels. With a subsequent increase in K_{min} (from 0.4 to 2.6 MPa$\sqrt{m}$) at constant K_{max} (=4 MPa$\sqrt{m}$), growth rates show a gradual

decline following a small initial retardation, but in general do not vary by more than half an order of magnitude.

The significant variations in growth rates with small changes in ΔK and/or K_{max} are consistent with the characteristic steep slope of da/dN vs. K relationships in ceramics [35]. However, the growth-rate behavior described above is quite different to that seen in ceramics such as transformation-toughened zirconia [5] and metallic materials [e.g., refs. 59-61] following excursions in load. The latter materials show marked transient crack-growth behavior, i.e., crack-growth retardation after high-low block loading sequences or acceleration after low-high sequences, followed by a gradual change in growth rates until the (new) steady-state velocity is achieved. By comparison, such transient crack-growth effects in Al_2O_3-SiC_w are minimal. In metals, the transient behavior results primarily from residual stresses in the larger (or smaller) plastic zones generated ahead of the crack following the change in loads (this in turn influences the development of such mechanisms as crack closure in the wake of the crack tip and in certain materials crack deflection [44,59-61]); somewhat similarly in phase-transforming ceramics, the larger (or smaller) transformation zones result in more (or less) transformation shielding and hence to locally retarded (or accelerated) growth rates [5]. Unfortunately, the degree of scatter in the present experiments does not permit a precise determination of the nature of the transient variations in growth rates in this material; however, some insight into the salient micromechanisms can be gained from examination of the crack closure and fracture-surface roughness data, as described below.

Measured far-field crack-closure levels for this sequence of loads are plotted as a function of crack extension in Fig. 5.6b. In general, the closure stress intensity did not vary appreciably with the above changes in ΔK; however, K_{cl} levels did show a marked increase during the constant-K_{max}/increasing-K_{min} sequence. This increase in closure is consistent with the small decrease in growth rates during the latter sequence, because in terms of a near-tip "driving force", $\Delta K_{eff} = K_{max} - K_{cl}$, the local stress-intensity range changes far less than the applied ΔK, i.e., the increase in K_{min} is below the value of K_{cl} and hence does not significantly affect growth rates.

Fractography: The closure-corrected ΔK_{eff} approach does suffer from several limitations in that wedging in the *immediate* vicinity of the crack tip, which is difficult to detect, often controls the post-overload behavior [61], it assumes that the only shielding is derived from crack-face contact by wedging, which is clearly not the case with a bridging material, and in general the precise nature of the crack-closure phenomena in ceramics is as yet undocumented. However, the fractography of the fatigue crack during the block-loading sequence does provide some clue as to the nature of the closure mechanism.

A low magnification SEM micrograph of both sides of the fracture is shown in Fig. 5.7. Regions of cyclic crack growth, which are predominantly intergranular, are clearly discernible from the transgranular monotonic fracture region. Closer scrutiny also reveals bands showing different texture associated with the various block-loading sequences applied during the test. Of particular note is the increased roughness of the fracture surface during the constant-K_{max}/increasing-K_{min} portion of the test. The variation in lineal roughness, as a function of measuring step size, for the various loading excursions is shown in Fig. 5.8; fractal dimensions representing these fracture-surface roughnesses are listed in Table 5.5. It is apparent that the overload (monotonic) fracture region displays the lowest roughness, whereas under cyclic loading the roughness steadily increases with each sequence. Since there is a concomitant increase in far-field closure measured over these cyclic loading sequences, it would appear that the primary source of closure is from premature contact of fracture-surface asperities during the fatigue cycle, i.e., from roughness-induced closure.

TABLE 5.5 - Fracture-Surface Roughness and Crack Closure During Variable-Amplitude Fatigue

Region	Loading Conditions ΔK, K_{max}, K_{min} ($MPa\sqrt{m}$)	Crack Closure Stress Intensity, K_{cl} ($MPa\sqrt{m}$)	Lineal Roughness Fractal Dimension, D
a	$\Delta K = 3.6$, $K_{max} = 4.0$, $K_{min} = 0.4$	0.9	1.02
b	$= 3.2$, $= 3.5$, $= 0.3$	1.1	1.04
c	$= 3.6$, $= 4.0$, $= 0.3$	1.1	1.06
d	$= 3.6$, $= 4.0$, $= 0.4$	1.2	-
	$= 2.5$, $= 4.0$, $= 1.5$	1.6	-
	$= 1.6$, $= 4.0$, $= 2.4$	2.4	1.07
e	overload fracture	-	1.03

5.3.4 Mechanisms of Fatigue Crack Growth

A number of mechanisms have been postulated to explain the susceptibility to fatigue-crack growth in ceramic materials [e.g. ref. 35]; due to a paucity of mechanistic data, however, precise mechanisms remain elusive. In ceramic-matrix composites reinforced with a brittle second phase, careful control of the reinforcement/matrix interface strength during processing is required to provide debonding and controlled pullout of the reinforcement fibers or whiskers in the wake of a crack. The resulting bridging zone exerts closing tractions on the crack surfaces and hence shields the crack tip from the applied (far-field) stresses. These materials may be expected to be susceptible to cyclic-fatigue effects where progressive degradation of the bridging zone can occur. Similar effects may be expected if bridging by frictional/geometrical

interlocking of microstructurally rough fracture surfaces contributes significantly to the toughness.

In the current study, the close similarity of fracture surfaces resulting from cyclic and monotonic loading suggests that fracture modes similar to those under monotonic loading (static modes) may be operating. In this case, crack-growth rates during cyclic loading may be expected to display a marked sensitivity to the maximum stress intensity factor, K_{max}, or the load ratio, R, in addition to ΔK. In fact, this sensitivity has been reported for cyclic fatigue in a yttria-stabilized zirconia ceramic [10]; it is also very similar to fatigue in metals at high growth rates where K_{max} approaches the fracture toughness, K_{Ic} [62]. A number of models have been reported to describe R ratio effects in a variety of metallic alloys [e.g. 44, 63, 64]. In the present study, the relative effects of K_{max} and ΔK were determined by explicitly including K_{max} in the growth-rate relationship*, thus:

$$da/dN = C' (K_{max})^n (\Delta K)^p \quad , \tag{8}$$

*This is equivalent to the empirical model of Walker [64] commonly used to predict R ratio effects in metal fatigue where an effective stress intensity factor, K_{eff}, is defined such that $K_{eff} = K_{max} (1 - R)^{n'}$, where n' is a material property. By comparison to Eq. 8, $n' = p/(p + n)$.

where C', n and p are constants. The similarity of the above relationship with that of Eq. 1 is apparent by noting that $K_{max} = \Delta K/(1 - R)$, and hence rewriting Eq. 8 as:

$$da/dN = C'/(1 - R)^n (\Delta K)^{(n + p)} \quad , \tag{9}$$

where for constant R, the values of C and m from Eq. 1 are:

$$C = C'/(1 - R)^n \quad , \tag{10a}$$

and

$$m = (n + p) \quad . \tag{10b}$$

The known values for C and m (from Table 5.3) for the long-crack growth behavior at R = 0.1 are insufficient to solve for the three unknowns in Eq. 10. The effect of ΔK was therefore experimentally determined by conducting a constant-K_{max}/decreasing-ΔK test. Resulting crack-growth rates are shown in Fig. 5.9a as a function of crack length. The power-law dependence of growth rates on the applied ΔK expected from Eq. 8, where $(C' (K_{max})^n)$ is a constant, is apparent in Fig. 5.9b where the value of the slope, p, from Eq. 8 is 4.8. Using Eq. 10, the

crack-growth relationship may finally be written as:

$$da/dN = 6.79 \times 10^{-18} (K_{max})^{10.2} (\Delta K)^{4.8} \quad , \qquad (11)$$

in which the sensitivity of crack growth rates to K_{max} is immediately apparent.

The sensitivity of growth rates to K_{min}, which may be indicative of a wedging mechanism for crack-growth where asperity contact behind the crack tip on the unloading cycle produces localized shear and tensile forces, was subsequently assessed by abruptly reducing the load ratio following the K_{max}-constant portion of the test. Following a recently proposed wedging model for fatigue-crack growth in silicon nitride [65], the wedging force and hence growth rates are assumed proportional to $(K_{cl} - K_{min})$. Prior to reducing R, K_{cl} is less than K_{min} and could not be measured. Following the load-ratio reduction, K_{cl}/K_{max} ratios as high as 0.7 were measured, indicating that increased wedging forces should be present. However, no measurable crack growth was noted until K_{max} was again increased to a value close to that where prior crack growth was recorded. It is therefore concluded that based on the present evidence, a wedging model similar to that proposed for Si_3N_4 is not likely for Al_2O_3-SiC_w. Rather, a mechanism similar to the static fracture mode which occurs on monotonic loading is likely. Crack advance thus is expected at or near the maximum stress intensity during the load cycle;* the critical role of the unloading cycle, however, in promoting progressive degradation of the bridging zone behind the crack tip or accumulated microcrack damage ahead of the crack tip, remains unclear.

*Preliminary indications from fatigue cracks grown at very low frequencies (~0.1 Hz) are that crack extension each cycle does in fact occur just prior to the maximum load during the rising tensile portion of the fatigue cycle.

5.3.5 Fracture Toughness

Monotonic loading of long cracks in the C(T) specimens following the fatigue tests did not produce any detectable resistance-curve (R-curve) behavior. Unstable fracture of the specimen occurred at $K_c \sim 4.5$ MPa$\sqrt{m}$, which is similar to toughness values measured using indentation techniques [38,39]. Note that since R-curve measurements were attempted directly after fatigue testing, the first measurement was taken at the K_{max} of the previous fatigue loading cycle; this may preclude determination of the full R-curve since the existing long crack is already fully bridged. The maximum measured toughness was, however, significantly greater than for the unreinforced Al_2O_3 matrix material, which had a toughness of 2.2 MPa$\sqrt{m}$.

Toughness estimates derived from indentations in the cantilever-beam specimens which failed during cyclic loading revealed significantly reduced K_c values approaching that of the

unreinforced matrix toughness. Toughness values are compared with the monotonically loaded and unreinforced values in Table 5.6. The effect of cyclic fatigue appears to decrease the fracture toughness by almost 50% with fully reversed loading being more damaging than tension-tension loading; this implies that cyclic loading results in intrinsic damage to the microstructure, although whether this occurs as true intrinsic microstructural damage ahead of the crack tip or as a degradation of the shielding zone behind the crack tip is as yet uncertain.

TABLE 5.6 - Indentation Fracture Toughness of Al_2O_3-SiC_w Following Monotonic and Cyclic Loads

Material	Conditions	Measured K_c (MPa$\sqrt{m}$)
Al_2O_3	monotonic	2.2
Al_2O_3-SiC_w	monotonic	4.6
Al_2O_3-SiC_w	cyclic (R = -1)	2.4
Al_2O_3-SiC_w	cyclic (R = 0.05)	3.2

5.4 Conclusions

Based on a study of the growth of both long (> 3mm) and microstructurally-small (< 300 μm) fatigue cracks in a SiC-whisker-reinforced alumina ceramic under tension-tension (R = 0.05) and tension-compression (R = -1.0) cyclic loads, the following conclusions can be drawn:

1. Fatigue-crack growth in Al_2O_3-SiC_w ceramic is shown to be a mechanically-induced cyclic process. Growth rates (da/dN) can be described in terms of a power-law function of the applied stress-intensity range (ΔK), with an exponent m of the order of 15.

2. An apparent threshold for fatigue-crack growth (ΔK_{TH}), below which (long) cracks are presumed dormant, was found to be approximately 60% of the fracture toughness K_c, similar to behavior in other ceramic materials.

3. Cyclic crack growth shows evidence of crack closure in addition to other crack-tip shielding mechanisms (crack deflection, uncracked ligament and whisker bridging). However, when subjected to variable-amplitude cyclic loading, fatigue cracks in Al_2O_3-SiC_w ceramics do not exhibit marked transient crack-growth retardations immediately following high-low block overloads and transient acceleration immediately following low-high block overloads, as have been reported for phase-transforming ceramics and metallic alloys.

4. Cyclic fatigue-crack growth rates for small surface cracks are found to occur at applied stress-intensity levels significantly smaller than the nominal long-crack threshold ΔK_{TH};

however, when the residual stress intensity K_r associated with the indent is included in the analysis, growth rates are found to be similar to the long-crack data.

5. Long crack-growth rates display a marked sensitivity to K_{max}, suggesting that crack advance occurs during the loading cycle at or near K_{max}, similar to the static fracture mode which occurs on monotonic loading. The critical role of the unloading cycle, in degrading the bridging zone or damaging material ahead of the crack tip, remains unclear.

5.5 References

1. R. H. Dauskardt, W. Yu and R. O. Ritchie, *J. Am. Ceram. Soc.*, **70** (1987) 248-52.

2. M. V. Swain and V. Zelizko, pp. 595-606 in *Advances in Ceramics, 24B Science and Technology of Zirconia III*, S. Somioya, N. Yammoto and H. Hanagida, eds., American Ceramic Society, Westerville, OH, 1988.

3. L. A. Sylva and S. Suresh, *J. Mater. Sci.*, **24** (1989) 1729-38.

4. R. H. Dauskardt, D. B. Marshall and R. O. Ritchie, *J. Am. Ceram. Soc.*, **73** (1990) 893-903.

5. R. H. Dauskardt, W. C. Carter, D. K. Veirs and R. O. Ritchie, *Acta Metall. Mater.*, **38** (1990) 2327-36.

6. T. Kawakubo, N. Okabe and T. Mori, pp. 717-32 in *Fatigue '90* (Proc. 4th Intl. Conf. on Fatigue and Fatigue Thresholds), Vol. 2, H. Kitagawa and T. Tanaka, eds., Mat. Comp. Eng. Publ., Ltd., Edgbaston, U.K. (1990).

7. A. A. Steffen, R. H. Dauskardt and R. O. Ritchie, pp. 745-52 in *Fatigue '90* (Proc. 4th Intl. Conf. on Fatigue and Fatigue Thresholds), Vol. 2, H. Kitagawa and T. Tanaka, eds., Mat. Comp. Eng. Publ., Ltd., Edgbaston, U.K. (1990).

8. A. A. Steffen, R. H. Dauskardt and R. O Ritchie, *J. Am. Ceram. Soc.*, **74** (1991) 1259-68.

9. D. C. Cardona and C. J. Beevers, pp. 1023-29 in *Fatigue '90* (Proc. 4th Intl. Conf. on Fatigue and Fatigue Thresholds), Vol. 2, H. Kitagawa and T. Tanaka, eds., Mat. Comp. Eng. Publ., Ltd., Edgbaston, U.K. (1990).

10. S.-Y. Liu and I.-W. Chen, *J. Am. Ceram. Soc.*, **74** (1991) 1197-216.

11. D. L. Davidson, J. B. Campbell and J. Lankford, J., *Acta Metall. Mater.*, **39** (1991) 1319-30.

12. R. O. Ritchie, R. H. Dauskardt, W. Yu and A. M. Brendzel, *J. Biomed. Mater. Res.*, **24** (1990) 189-206.

13. F. Guiu, *J. Mater. Sci. Lett.*, **13** (1978) 1357-61.

14. H. N. Ko, *J. Mater. Sci. Lett.*, **5** (1986) 464-66.

15. L. Ewart and S. Suresh, *J. Mater. Sci. Lett.*, **5** (1986) 774-78.

16. T. Hoshide, T. Ohara and T. Yamada, *Int. J. Fracture*, **37** (1988) 47-59.

17. G. Grathwohl and T. Liu, *J. Am. Ceram. Soc.*, **72** (1989) 1988-90.

18. H. N. Ko. *J. Mater. Sci. Lett.*, **8** (1989) 1438-41.

19. S. Lathabai, Y.-W. Mai and B. R. Lawn, *J. Am. Ceram. Soc.*, **72** (1989) 1760-63.

20. M. J. Reece, F. Guiu and M. F. R. Sammur, *J. Am. Ceram. Soc.*, **72** (1989) 348-52.

21. I. Bar-On and J. T. Beals, pp. 793-98 in *Fatigue '90* (Proc. 4th Intl. Conf. on Fatigue and Fatigue Thresholds), Vol. 2, H. Kitagawa and T. Tanaka, eds., Mat. Comp. Eng. Publ., Ltd., Edgbaston, U.K. (1990).

22. C.-K. J. Lin and D. F. Socie, *J. Am. Ceram. Soc.*, **74** (1991) 1511-18.

23. T. Fett, G. Martin, D. Munz and G. Thun, *J. Mater. Sci.* (1991) 3320-28.

24. T. Fett and D. Munz, Proc. 7th World Ceramics Congress (CIMTEC), Montecatini Therme, Italy (1990), in press.

25. T. Kawakubo and K. Komeya, *J. Am. Ceram. Soc.*, **70** (1987) 400-05.

26. S. Horibe, *J. Mater. Sci. Lett.*, **7** (1988) 725-27.

27. M. Masuda, T. Soma, M. Matsui and I. Oda, *J. Ceram. Soc. Japan Inter. Ed.*, **96** (1988) 275-80.

28. A. Ueno, H. Kishimoto, H. Kawamoto and M. Asakwa, pp. 733-38 in *Fatigue '90* (Proc. 4th Intl. Conf. on Fatigue and Fatigue Thresholds), Vol. 2, H. Kitagawa and T. Tanaka, eds., Mat. Comp. Eng. Publ., Ltd., Edgbaston, U.K. (1990).

29. Y. Mutoh, M. Takahashi, T. Oikawa and H. Okamoto, pp. 211-25 in *Fatigue of Advanced Materials*, R. O. Ritchie, R. H. Dauskardt and B. N. Cox, eds., Mat. Comp. Eng. Publ., Ltd., Edgbaston, U.K. (1991).

30. S. Lauf, V. Gerold and R. F. Pabst, pp. 775-80 in *Fatigue '90* (Proc. 4th Intl. Conf. on Fatigue and Fatigue Thresholds), Vol. 2, H. Kitagawa and T. Tanaka, eds., Mat. Comp. Eng. Publ., Ltd., Edgbaston, U.K. (1990).

31. E. H. Luh, R. H. Dauskardt and R. O. Ritchie, *J. Mater. Sci. Lett.*, **9** (1990) 719-25.

32. L. X. Han and S. Suresh, *J. Am. Ceram. Soc.*, **72** (1989) 1233-38.

33. J. W. Holmes, *J. Am. Ceram. Soc.*, **74** (1991) 1639-45.

34. P. C. Paris and F. Erdogan, *J. Bas. Eng.*, Trans. ASME, **85** (1963) 528-34.

35. R. O. Ritchie and R. H. Dauskardt, *J. Ceram. Soc. Japan*, **99** (1991) 1047-62.

36. S. Suresh and R. O. Ritchie, *Intl. Metals Rev.*, **29** (1984) 445-76.

37. R. O. Ritchie and J. Lankford, *Mater. Sci. Eng.*, **84** (1986) 11-16.

38. J. R. Porter, F. F. Lange and A. H. Chokshi, *Ceramic Bulletin*, **66** (1987) 343.

39. J. R. Porter, in *Proc. of Interfacial Effects on Mechanical Behavior of Metal-Matrix and Ceramic-Matrix Composites*. Brown University, Providence, RI (1988).

40. Anon, *Annual Book of ASTM Standards*, Vol. 3.01, Section 3. American Society for Testing and Materials, Philadelphia, PA (1987).

41. R. H. Dauskardt and R. O. Ritchie, *Closed Loop*, **17** (1989) 7.

42. P. K. Liaw, H. R. Hartmann and W. A. Lodgson, *J. Test. Eval.*, **44** (1983) 222-207.

43. R. O. Ritchie and W. Yu, pp. 167-89 in *Small Fatigue Cracks*, R. O. Ritchie and J. Lankford, eds., The Metallurgical Society of the American Institute of Mining, Metallurgical, and Petroleum Engineers, Warrendale, PA (1986).

44. W. Elber, pp. 230-42 in *Damage Tolerance in Aircraft Structures*, ASTM STP 486, American Society for Testing and Materials, Philadelphia, PA (1971).

45. S. Suresh and R. O. Ritchie, pp. 227-61 in *Fatigue Crack Growth Threshold Concepts*, D. L. Davidson and S. Suresh, eds., The Metallurgical Society of the American Institute of Mining, Metallurgical, and Petroleum Engineers, Warrendale, PA (1984).

46. A. Saxena, S. J. Hudak, Jr., J. K. Donald and D. W. Schmidt, *J. Test. Eval.*, **6** (1978) 167-75.

47. J. C. Newman, Jr., pp. 105-21 in *Fracture Analysis* (8th Conference), ASTM STP 560, American Society for Testing and Materials, Philadelphia, PA (1974).

48. J. E. Srawley, *Int. J. Fract.*, **12** (1976) 475-76.

49. M. Yoda, *Int. J. Fract.*, **39** (1989) R23-28.

50. D. Johnson-Walls, M. D. Drory, A. G. Evans, D. B. Marshall and K. T. Faber, *J. Am. Ceram. Soc.*, **70** (1985) 363-67.

51. J. C. Newman, Jr. and I. S. Raju, pp. 312-34 in *Computational Methods in the Mechanics of Fracture*, Chapter 9, Vol. 2, S. N. Atluri, ed., North Holland, Amsterdam (1986).

52. I. S. Raju, S. N. Atluri and J. C. Newman, Jr., pp. 297-316 in *Fracture Mechanics: Perspectives and Directions (Twentieth Symp.)*, ASTM STP 1020, R. P. Wei and R. P. Gangloff, eds., American Society for Testing and Materials, Philadelphia, PA (1989).

53. P. Chantikul, G. R. Anstis, B. R. Lawn and D. B. Marshall, *J. Am. Ceram. Soc.*, **64** (1981) 539-543.

54. B. B. Mandelbrot, *The Fractal Geometry of Nature*, Freeman, New York, NY (1983).

55. R. H. Dauskardt, F. Haubensak and R. O. Ritchie, *Acta Metall. Mater.*, **38** (1990) 143-159.

56. R. O. Ritchie, *Mater. Sci. Eng.*, **A103** (1988) 15-28.

57. A. G. Evans, pp. 267-01 in *Fracture Mechanics: Perspectives and Directions (Twentieth Symp.)*, ASTM STP 1020, R. P. Wei and R. P. Gangloff, eds., American Society for Testing and Materials, Philadelphia, PA (1989).

58. D. Jensen, V. Zelizko and M. V. Swain, *J. Mater. Sci. Lett.*, **8** (1989) 1154-57.

59. R. W. Hertzberg, *Deformation and Fracture Mechanics of Engineering Materials*, 3rd ed., Wiley, New York, NY (1989).

60. S. Suresh, *Eng. Fract. Mech.*, **18** (1983) 577-593.

61. C. M. Ward-Close, A. F. Blom and R. O. Ritchie, *Eng. Fract. Mech.*, **32** (1989) 613-638.

62. C. J. Beevers, R. J. Cooke, J. F. Knott and R. O. Ritchie, *Met. Sci.*, **9** (1975) 119-126.

63. R. G. Forman, V. E. Kearney and R. M. Engle, *J. Basic Eng., Trans. ASME Ser. D*, **89** (1967) 459.

64. K. Walker, p. 1 in ASTM STP 462, American Society for Testing and Materials, Philadelphia, PA (1970).

65. M. Okazaki, A. J. McEvily and T. Tanaka, *Metall. Trans. A*, **22A** (1991) 1425-1434.

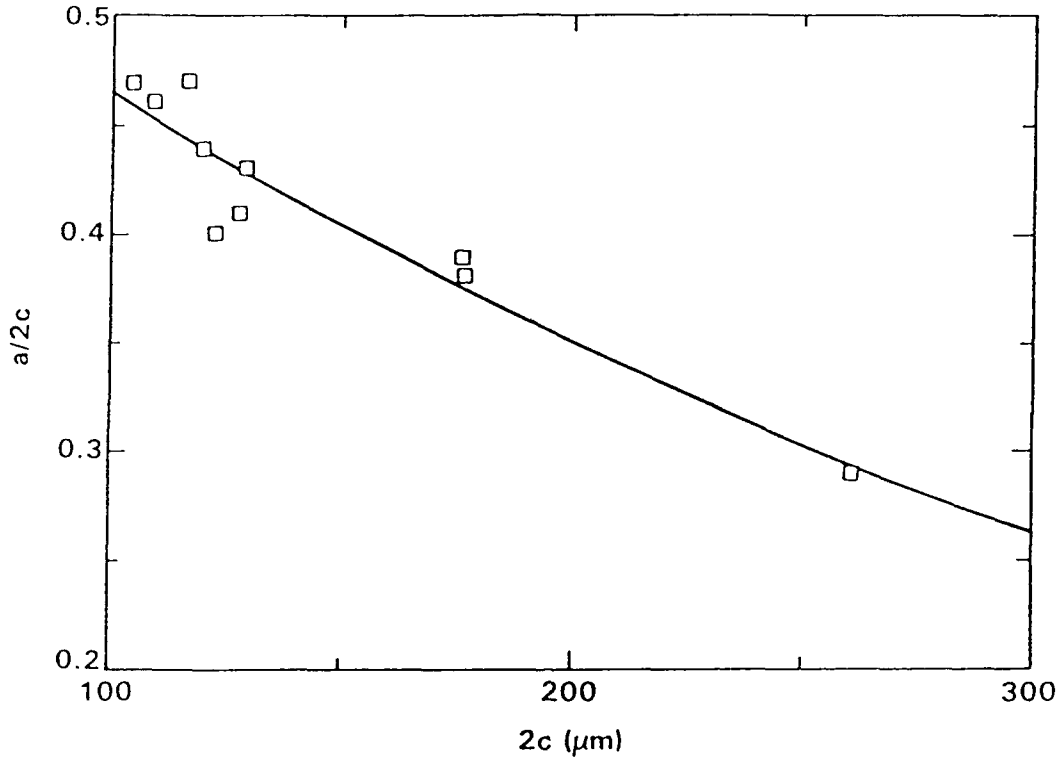

Fig. 5.1. Variation in the aspect ratio, a/2c, of small cracks in Al_2O_3-SiC_w with surface crack length, 2c.

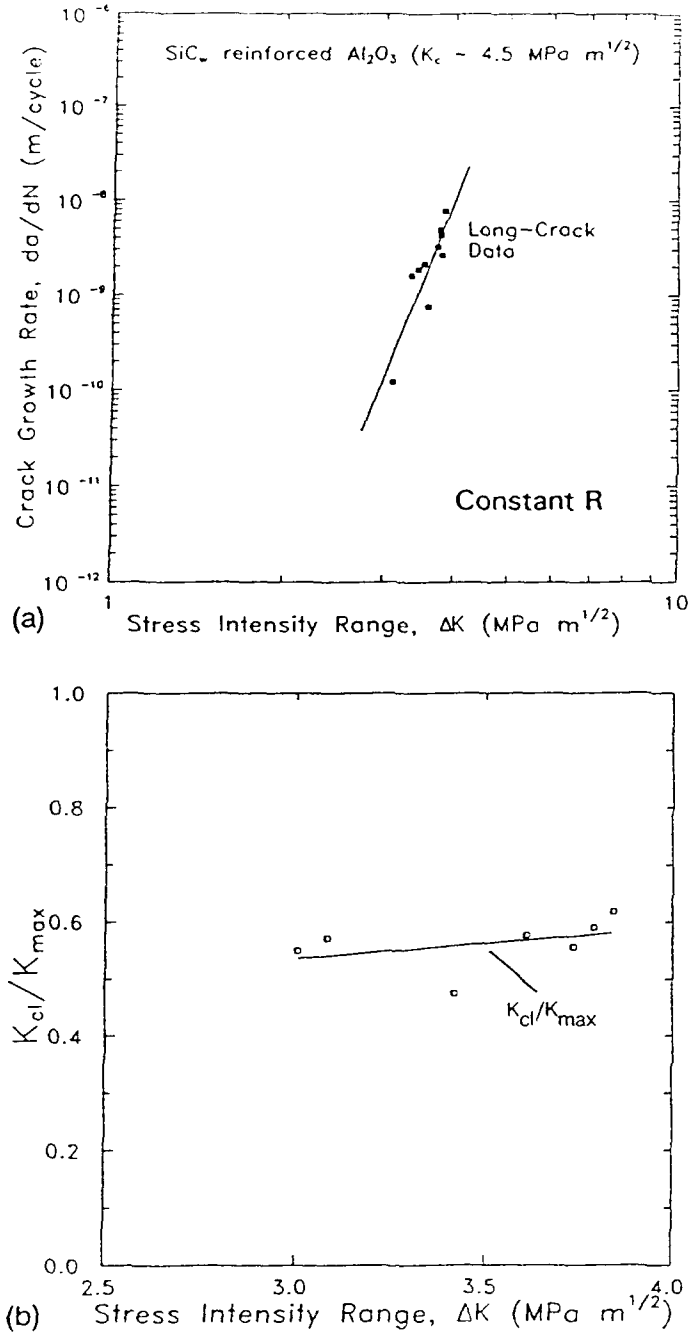

Fig. 5.2. a) Cyclic fatigue-crack propagation rates, da/dN, and b) corresponding crack-closure data, K_{cl}/K_{max}, as a function of the applied stress-intensity range ΔK for SiC_w reinforced alumina. Data obtained for long cracks on C(T) samples in a room-air environment at 50 Hz with a constant load ratio ($R = K_{min}/K_{max}$) of 0.1.

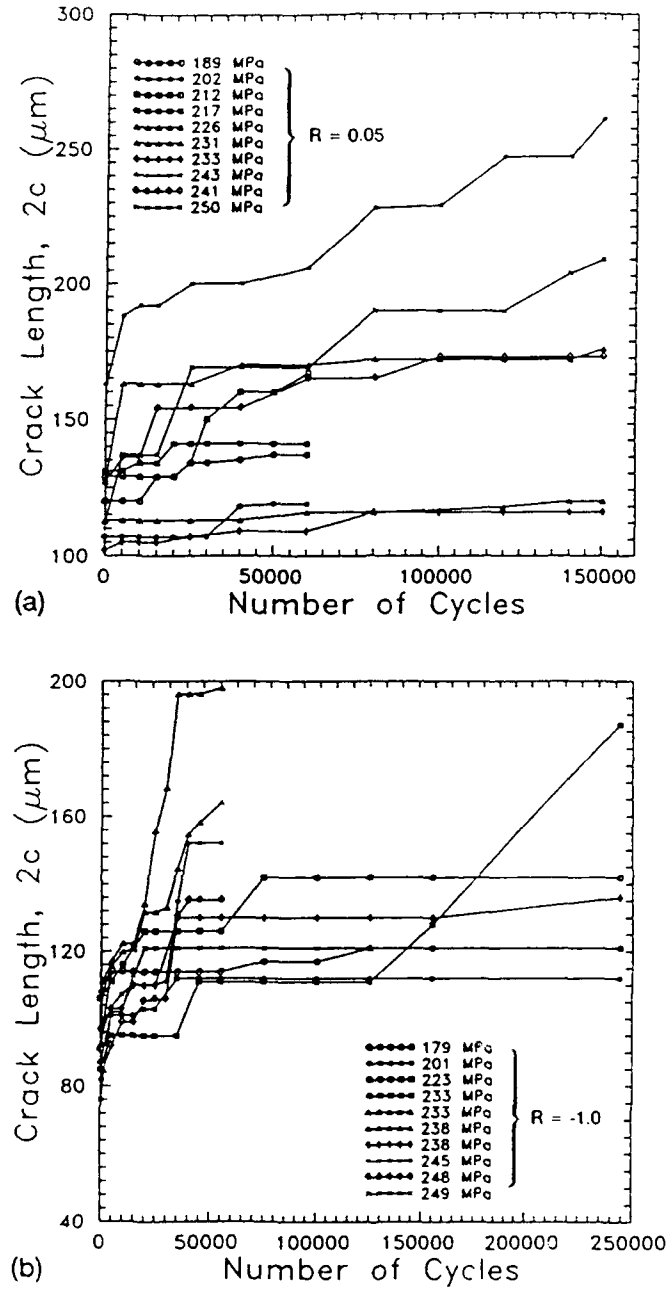

Fig. 5.3. Small-crack data in Al_2O_3-SiC_w showing variation in surface crack length (2c) with number of cycles at a) R = 0.05 and b) R = -1.0.

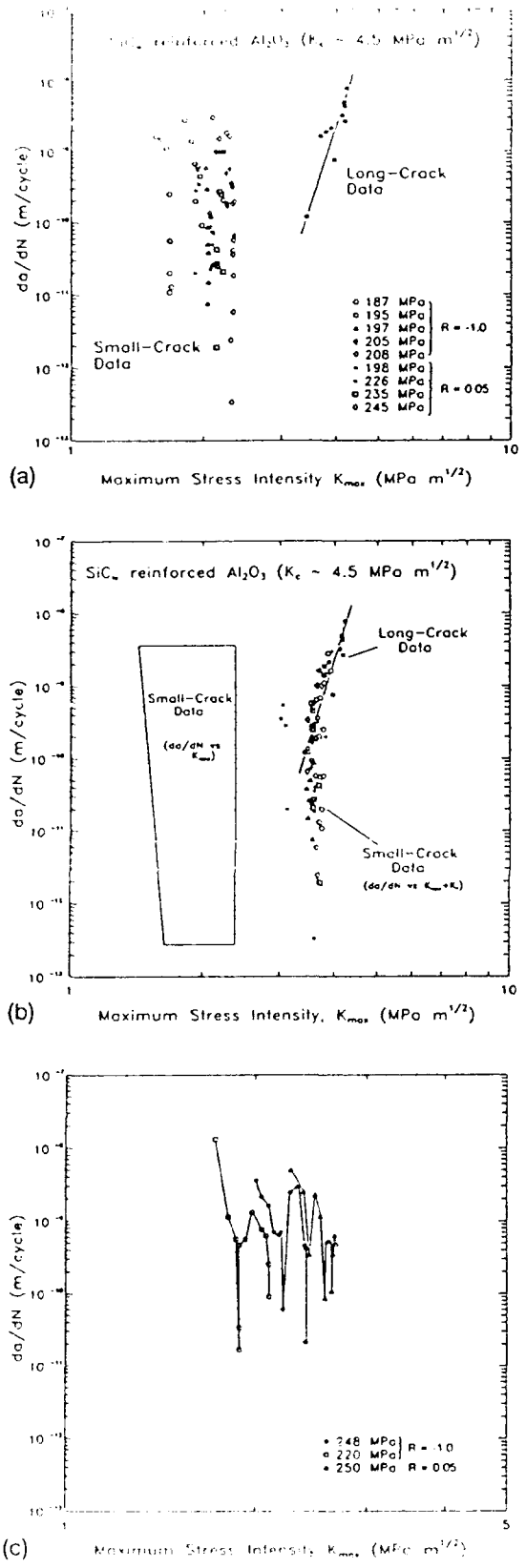

Fig. 5.4. Small-crack growth-rate data in Al_2O_3-SiC_w from cantilever-beam specimens, a) as a function of the applied K_{max} at R = 0.05 and -1, compared to corresponding long-crack data derived from C(T) specimens, bas a function of the total stress intensity (K_{max} + K_r) where K_r results from the residual stress surrounding the indent, and c) showing individual V-shaped crack-growth curves for a limited number of specimens. Note how small cracks propagate at applied stress-intensity (K_{app}) levels well below the long-crack threshold, ΔK_{TH}, and show an apparent negative dependency on K_{app}; however, when characterized in terms of the total stress intensity, their growth rates are in close correspondence with those of long cracks.

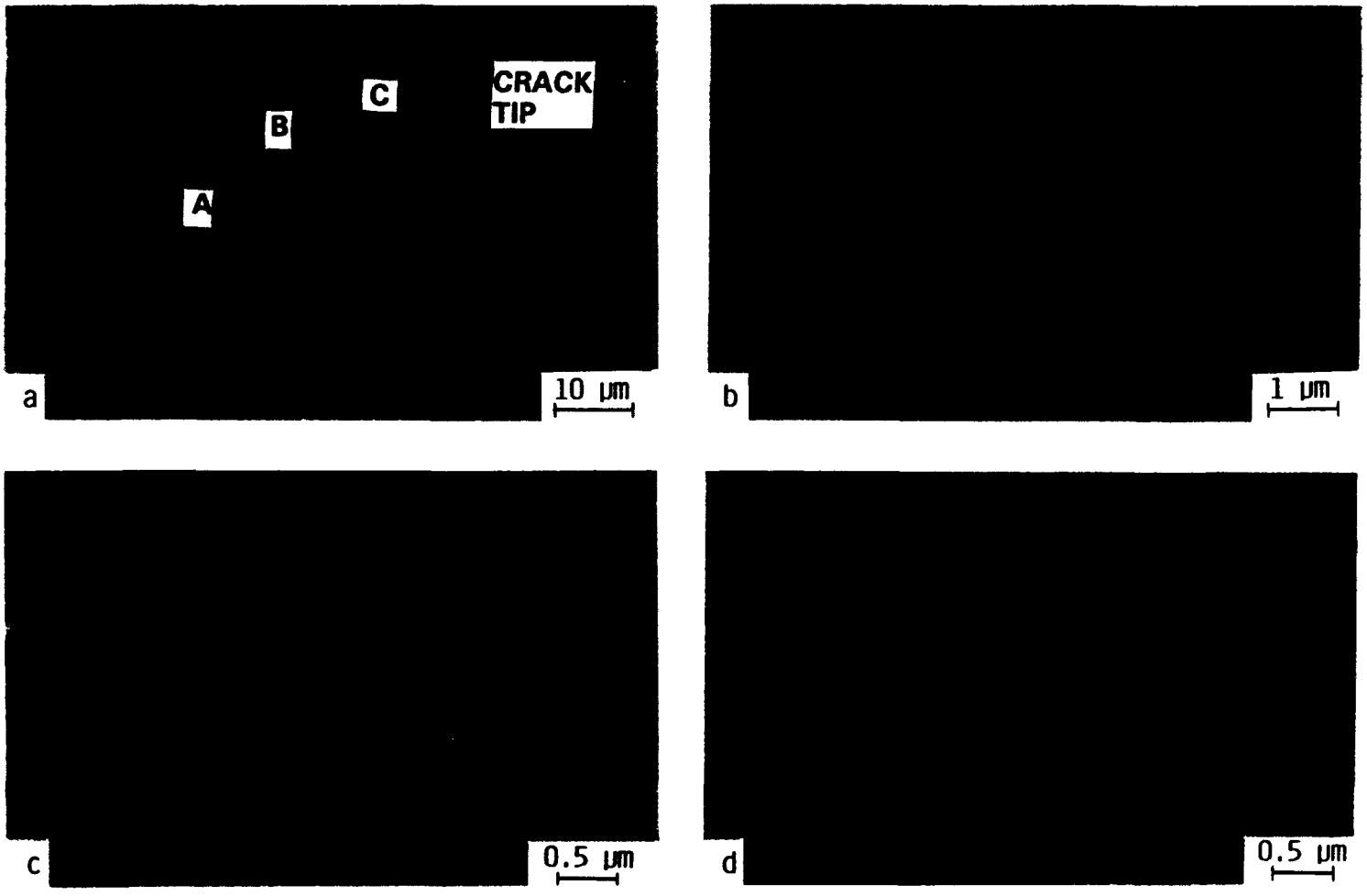

Fig. 5.5. Detailed SEM micrographs showing morphology of a single microcrack of surface length 167 μm in Al_2O_3-SiC_w, showing a) general morphology, b) evidence of crack bridging by uncracked matrix ligaments, and c,d0 crack bridging by SiC whiskers.

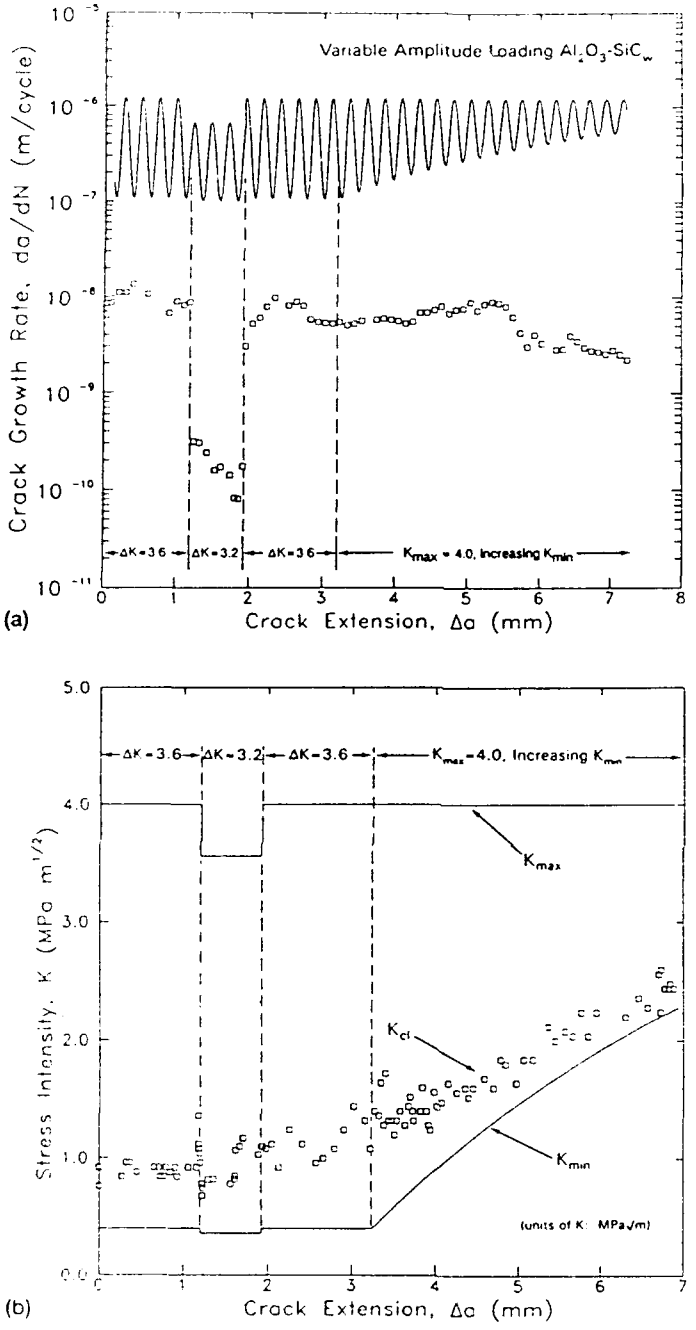

Fig. 5.6. Transient fatigue-crack growth behavior in Al_2O_3-SiC_w, showing a) variation in crack-growth rates and b) far-field crack-closure stress intensities K_{cl} following high-low, low-high and constant-K_{max}/increasing-K_{min} block-loading sequences.

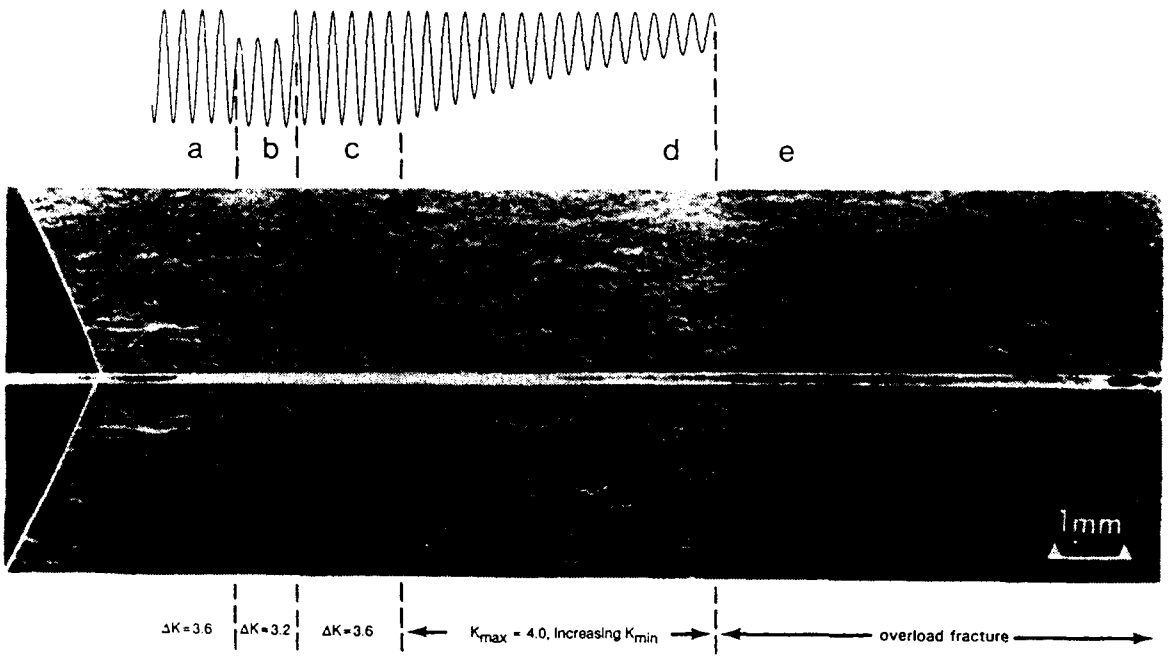

Fig. 5.7. Low magnification SEM micrograph of matching fracture surfaces in Al_2O_3-SiC_w, showing the different fractography associated with the various block-loading sequences shown in Fig. 5.8.

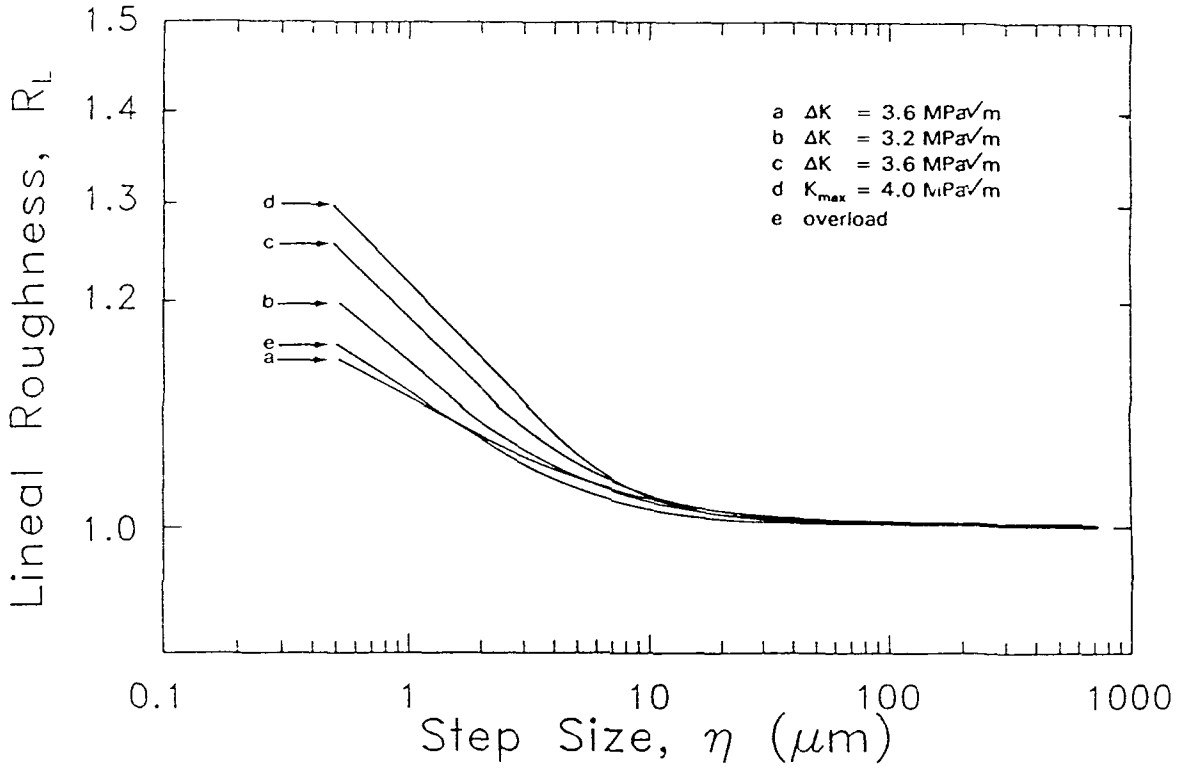

Fig. 5.8. Variation in lineal roughness R_L as a function of measuring step size η for fracture surfaces in Al_2O_3-SiC_w during variable-amplitude fatigue and overload sequences, shown in Fig. 5.8.

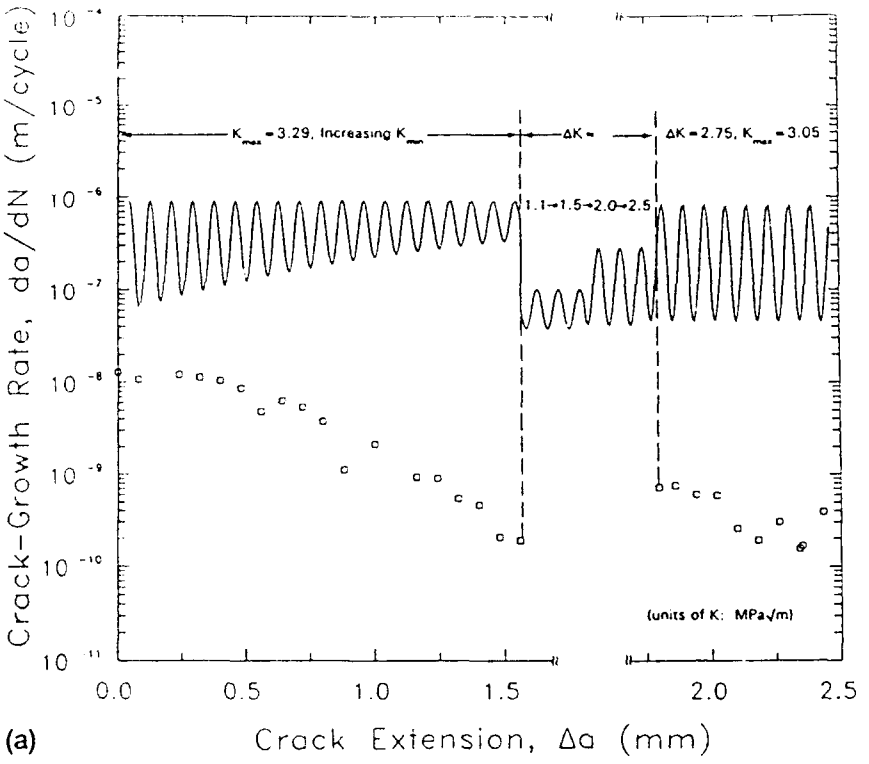

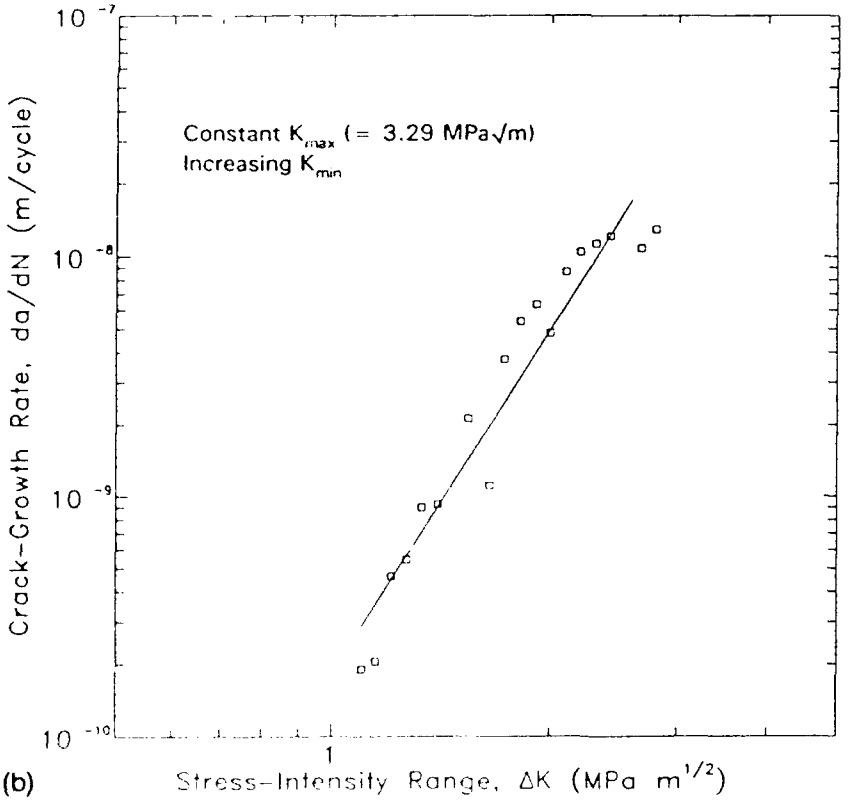

Fig. 5.9. Fatigue-crack propagation rates, da/dN, plotted as a function of (a) the crack extension for constant K_{max}/decreasing ΔK, and following load-ratio reduction sequences, and (b) the applied stress-intensity range, ΔK, for the constant-K_{max} portion of the test.

6. ACKNOWLEDGEMENTS

This work was supported by the U.S. Office of Naval Research under Grant No. N00014-89-J-1049 (R & T Project No. 431330), with Dr. S. G. Fishman as contract monitor. The authors would like to thank Drs. J. R. Porter and M. R. James of Rockwell International, Dr. R. K. Bhattacharyya of Alcoa, and United Technology for providing LAS/SiC glass-ceramic composites.

7. PROGRAM ORGANIZATION AND PERSONNEL

The work described was performed in the Department of Materials Science and Mineral Engineering, University of California in Berkeley, under the supervision of Dr. R. O. Ritchie, Professor of Materials Science, aided by research engineer Dr. R. H. Dauskardt, graduate student research assistants and undergraduate research helpers. The individual personnel are listed below.

1) Prof. R. O. Ritchie	Professor of Materials Science, University of California; Director, Center for Advanced Materials, and Deputy Director, Materials Sciences Division, Lawrence Berkeley Laboratory; Principal Investigator
2) Dr. R. H. Dauskardt	Research Engineer
3) E. Y. Luh, R. M. Petrany	Graduate Student Research Assistants
4) F. J. Pennisi	Undergraduate Engineering Aide

8. LIST OF PUBLICATIONS/REPORTS/PRESENTATIONS

8.1 Papers Published in Refereed Journals

E. Y. Luh, R. H. Dauskardt and R. O. Ritchie: "Cyclic Fatigue-Crack Growth Behavior of Short Cracks in SiC-Reinforced Lithium Aluminosilicate Glass-Ceramic Composite," J. Mater. Sci. Lett., vol. 9, 1990, pp. 719-725.

R. O. Ritchie and R. H. Dauskardt: "Cyclic Fatigue of Ceramics: A Fracture Mechanics Approach to Subcritical Crack Growth and Life Prediction," Journal of the Ceramic Society of Japan, vol. 99 (10), Oct. 1991, pp. 1047-1062.

R. H. Dauskardt, M. R. James, J. R. Porter and R. O. Ritchie: "Cyclic Fatigue-Crack Growth in SiC-Whisker-Reinforced Alumina Ceramic Composite: Long and Small-Crack Behavior," Journal of American Ceramic Society, vol. 74, 1991, in press.

8.2 Papers in Refereed Conferences

R. H. Dauskardt and R. O. Ritchie: "Cyclic Fatigue-Crack Propagation in Ceramics and Ceramic Composites," in Mechanical Behaviour of Material - VI, Proceedings of the Sixth International Conference on the Mechanical Behaviour of Materials (ICM-6), M. Jono and T. Inoue, eds., Pergamon Press, Oxford, U.K., vol. 2, 1991, pp. 325-332.

R. H. Dauskardt and R. O. Ritchie: "Cyclic Fatigue of Ceramics," in Fatigue of Advanced Materials, R. O. Ritchie, R. H. Dauskardt and B. N. Cox, eds., MCEP Ltd., Edgbaston, U.K., 1991, pp. 133-151.

8.3 Non-Refereed Publications and Published Technical Reports

R. M. Petrany, R. H. Dauskardt and R. O. Ritchie: "Cyclic Fatigue Damage in a Continuous SiC Fiber Reinforced Al_2O_3 Composite," University of California, Berkeley, Report No. UCB/R/90/N1068.

R. H. Dauskardt, Daping Yao, B. J. Dalgleish, P. F. Becher and R. O. Ritchie: "Cyclic Fatigue-Crack Propagation in a Silicon-Carbide Whisker Reinforced Alumina Composite: Role of Load Ratio," University of California, Berkeley, Report No. UCB/R/91/N1077.

8.4 Presentations

a. Invited

R. O. Ritchie, "Fatigue Crack Propagation in Ceramics," invitd presentation at the URI Winter Study Workshop on Composites, University of California, Santa Barbara, CA, Jan. 1989.

R. O. Ritchie, "Mechanisms of Subcritical Crack Growth in Ceramics and Composites: Toughening of Ceramic/Metal Interfaces," invited seminar to Sandia National Laboratories, Livermore, CA, Feb. 1989.

R. O. Ritchie and R. H. Dauskardt, "Cyclic Fatigue of Ceramics and Ceramic-Matrix Composites," invited presentation to the Engineering Foundation Conference on Advanced Structural Ceramics, Palm Coast, FL, March 1989.

R. O. Ritchie, "Micro-Mechanisms of Fracture in Structural Metals, Ceramics and Composites," invited seminar to the Materials Science and Engineering Dept., University of Washington, Seattle, WA, May 1989.

R. O. Ritchie, "Fatigue and Fracture in Composite Metals and Ceramics," invited seminar to Battelle Pacific Northwest Laboratories, Richland, WA, May 1989.

R. O. Ritchie, "Mechanisms of Fatigue-Crack Growth in Metals, Composites, Ceramics and Ceramic/Metal Interfaces," invited presentation at the Third International Conference on Fundamentals of Fracture, Irsee, F.R. Germany, June 1989.

R. O. Ritchie, "Behavior of Real Materials: Composites," invited presentation at the Physical Metallurgy Gordon Conference, Tilton, NH, Aug. 1989.

R. O. Ritchie, "Ceramic Fatigue," invited seminar to the Government Industrial Research Institute, Nagoya, Japan, Sept. 1989.

R. O. Ritchie, "Ceramics and Ceramic Composites: Fatigue and Fracture," invited seminar to Materials Research Laboratory, Industrial Technology Research Institute, Hsinchu, Taiwan, Sept. 1989.

R. O. Ritchie, "Cyclic Behavior of Ceramics and Ceramic-Matrix Composites: Long vs. Small Crack Behavior," invited seminar to Institute of Materials Science and Engineering, National Sun-Yat-Sen University, Kaoshiung, Taiwan, Sept. 1989.

R. O. Ritchie, "Fatigue and Fracture of Advanced Composite Materials," invited seminar sponsored by the Chinese Silicate Society, Beijing, PR China, Sept. 1989.

R. O. Ritchie, "Ceramic Fatigue," invited seminar to CSIRO, Clayton, Victoria, Australia, Oct. 1989.

R. O. Ritchie, "Micromechanisms of Fatigue-Crack Growth in Structural Composites," invited seminar to the Materials Research Laboratory (MRL of the Defense Science and Technology Office), Melbourne, Australia, Oct. 1989.

R. O. Ritchie, "The Susceptibility of Ceramic Materials to Fatigue Damage under Cyclic Loads," invited presentation to the 12th Annual Industrial Liaison Conference University of California, Berkeley, CA, March 1990.

R. O. Ritchie, "Mechanisms of Subcritical Cracking in Engineering Ceramics and Composites," invited Design and Manufacturing Seminar to the Department of Mechanical Engineering, University of California, Berkeley, CA, May 1990.

R. H. Dauskardt, "Cyclic Fatigue Degredation in Ceramic-Matrix Composites," invited seminar to the Rockwell International Science Center, Thousand Oaks, CA, June 1990.

R. O. Ritchie, "Cyclic Fatigue of Metal-Matrix, Glass-Matrix and Ceramic-Matrix Composites," invited seminar to Mitsubishi Komai, Yokahama, Japan, June 1990.

R. O. Ritchie, "Fatigue of Ceramic Composite Materials," invited plenary lecture at the Materials Research Meeting, C-MRS International, Beijing, China, June 1990.

R. O. Ritchie, "Cyclic Behavior of Advanced Structural Materials," invited presentation to the DARPA Meeting on *Fatigue and Reliability of Advanced Structural Materials*, La Jolla, CA, July 1990.

R. O. Ritchie, "Fatigue of Advanced Materials," invited opening plenary lecture at the Fourth International Conference on Fatigue and Fatigue Thresholds *FATIGUE '90*, Honolulu, Hawaii, July 1990.

R. O. Ritchie, "Fatigue," invited presentation at the Albrecht-Rabenau Symposium on *Contemporary Issues in Ceramic Science*, Ringberg Castle, Tegernsee, Germany, July 1990.

R. O. Ritchie, "Fatigue of Advanced Materials," invited seminar to the Department of Materials Science and Mineral Engineering, University of California, Berkeley, CA, Sept. 1990.

R. O. Ritchie, "Design of Analysis Methods for Advanced Materials," invited keynote presentation to the 6th Annual North American Welding Research Conference on *Design and Fitness for Service of Welded Structures*, Columbus, OH, Oct. 1990.

R. O. Ritchie, R. H. Dauskardt and J.-K. Shang "(Cyclic) Fatigue Crack Propagation in Ceramic-Matrix, Glass-Matrix, and Metal-Matrix Composites," invited presentation at the American Ceramic Society Conference on *Composites: Processing, Microstructure and Properties*, Orlando, FL, Nov. 1990.

R. O. Ritchie, "Micro-Mechanisms of Fatigue-Crack Growth in Structural Metals, Intermetallics, Ceramics and Composites," invited seminar to SRI International, Menlo Park, CA, March 1991.

R. O. Ritchie, "Fatigue and Fracture of Advanced Materials for Transportation Applications," invited presentation to the First International Symposium Europe-USA on *New Frontiers in Science and Engineering in an European Perspective*, Paris, France, May 1991.

R. O. Ritchie, "Ceramic Fatigue," invited presentation to Ichikawajima-Harima Heavy Industries Co. Ltd. (IHI), Tokyo, Japan, July 1991.

R. O. Ritchie, "Mechanical Fatigue Failure of Engineering Composites," invited presentation to the Industrial Products Research Institute (IPRI), Mechanical Engineering Laboratory, Tsukuba, Japan, July 1991.

R. O. Ritchie, "Elevated Temperature Fatigue Testing of Ceramics," invited presentation to the Japan Ultra-High Temperature Materials Research Center (JUTEM), Tajimi-City, Japan, July 1991.

R. O. Ritchie, "Mechanisms of Fracture and Fatigue Failure in Ceramic Materials," invited presentation to the Government Industrial Research Institute, Nagoya, Japan, July 1991.

b. Contributed

R. H. Dauskardt and R. O. Ritchie, "Cyclic Fatigue of Ceramic Materials," 41st Pacific Coast Regional Meeting of the American Ceramic Society/NICE/MRS, San Francisco, CA, Oct. 1988.

R. H. Dauskardt and R. O. Ritchie, "Cyclic Fatigue-Crack Propagation Behavior in Advanced Ceramics," presented at the 13th Annual Conference on Composites and Advanced Ceramics, Cocoa Beach, FL, Jan. 1989.

R. H. Dauskardt, R. O. Ritchie and D. B. Marshall, "Cyclic Fatigue-Crack Propagation Behavior in Ceramics," presented at the 1989 Annual Meeting of the american Ceramic Society, Indiannapolis, IN, April 1989.

R. H. Dauskardt and R. O. Ritchie, "Cyclic Fatigue-Crack Propagation in Ceramics: Long vs. Small Crack Behavior," presented at CIMTEC, the 7th World Ceramics Congress, Montecatini Terme, Italy, June 1990.

R. H. Dauskardt and R. O. Ritchie, "Cyclic Fatigue-Crack Propagation in Monolithic and Composite Ceramics: Long and Small Crack Behavior," presented at the Fourth International Conference on Fatigue and Fatigue Thresholds *FATIGUE '90*, Honolulu, Hawaii, July 1990.

8.5 Books (and sections thereof)

None

DISTRIBUTION LIST

Dr. S. G. Fishman (4)
Office of Naval Research
800 N. Quincy Street
Arlington, VA 22217-5000

Defense Technical Information Center (2)
Building 5
Cameron Station
Alexandria, VA 22304-6145

Director (1)
Naval Research Laboratory
Attn: Code 2627
Washington, D.C. 20375

Linden Clausen (1)
Office of Naval Research
University of California, Berkeley Office
Richmond Field Station
Richmond, CA 94804-0001

Sponsored Projects Office (1)
University of California at Berkeley
Berkeley, CA 94720

Office of Research Services (1)
College of Engineering
University of California at Berkeley
Berkeley, CA 94720